Neutrino Masses and Signatures of Physics Beyond the Standard Model

A THESIS

submitted for the Award of Ph.D. degree of

MOHANLAL SUKHADIA UNIVERSITY

in the

Faculty of Science

By

Subrata Khan

Under the Supervision of

Prof. Srubabati Goswami

Professor
Theoretical Physics Division
Physical Research Laboratory, Ahmedabad, India.

DEPARTMENT OF PHYSICS
FACULTY OF SCIENCE
MOHANLAL SUKHADIA UNIVERSITY
UDAIPUR (RAJ)

Year of submission: 2013

To

my parents

DECLARATION

I, **Mr. Subrata Khan**, S/o Mrs. Ivy Lata Khan and Mr. Madhai Lal Khan, resident of A3-05, DOS Housing Colony, Vastrapura, Ahmedabad 380015, hereby declare that the research work incorporated in the present thesis entitled, **"Neutrino Masses and Signatures of Physics Beyond the Standard Model"** is my own work and is original. This work (in part or in full) has not been submitted to any University for the award of a Degree or a Diploma. I have properly acknowledged the material collected from secondary sources wherever required. I solely own the responsibility for the originality of the entire content.

Date:

Subrata Khan

(Author)

CERTIFICATE

It gives me great pleasure to certify the thesis entitled, **"Neutrino Masses and Signatures of Physics Beyond the Standard Model"** by Mr. Subrata Khan under my guidance. He has completed the following requirements as per Ph.D regulations of the University.

(a) Course work as per the university rules.

(b) Residential requirements of the university.

(c) Regularly submitted six monthly progress reports.

(d) Presented his work in the departmental committee.

(e) Published minimum of one research papers in a referred research journal.

I recommend the submission of thesis.

Date:

Prof. Srubabati Goswami
(Thesis Supervisor)
Professor, THEPH,
Physical Research Laboratory,
Ahmedabad - 380 009.

Countersigned by

Head of the Department

Acknowledgements

I express my sincere and deepest gratitude to Prof. Srubabati Goswami, under the guidance of whom, the work reported in this thesis has been carried out. Her deep insight in the subject and vast experience helped me immensely in learning the subject. Discussion with her was a great pleasure as she always gave importance to my views and was always friendly and patient with me. It was a great experience to work with her and I consider myself fortunate to have her as my thesis supervisor.

I greatly acknowledge the valuable discussions with Dr. Namit Mahajan and Dr. Swapan Maji and the assistance I got from my other collaborators, Dr. Sasmita Misra, Dr. Werner Rodejohann, Prof. Sourov Roy and Dr. Atsushi Watanabe. It was a pleasing experience to work with them.

I thank Dr. D. Angom, Dr. D. Ghosh, Prof. S. Mohanty, Prof. P. K. Panigrahi, Dr. R. Rangarajan, Prof. R. Sekar for the courses they taught and many fruitful discussions. I also thank Dr. P. Konar for encouraging me.

I thank Prof. J. N. Goswami, the Director, Prof. U. Sarkar, the Dean and Prof. A. K. Singhvi and Prof. A. Joshipura, former Deans, of PRL for providing necessary facilities and encouragements to carry out research work.

I thank all the staff members of PRL computer center for providing excellent computational and internet facilities.

I also thank Subimal, Suman, Sushant for helping me with computation.

I cherish the memorable experiences with Iman, Jayati, Komal, Murli, Tapas as well as Abhishek, Arvind, Bhaswar, Bhavik, Gulab, Joydeep, Ketan, Monojit, Moumita, Neeraj, Pankaj, Prashant, Pravin, Purnendu, Rabiul, Sainath, Sandeep, Satinder, Siddhartha, Shivani, Soumya, Srinivas, Sudhanwa, Suruchi, Vimal, Zeen.

The support I got from my parents, my brothers is something beyond acknowledgement. They were always with me for whatever reason it may be and the encouragement I received from them will never fade away.

Subrata

ABSTRACT

In order to explain the origin of neutrino mass and incorporate it in the simple extension of Standard Model, heavy fields are added to the Standard Model particle spectra. Integrating out such heavy fields gives rise to effective Lagrangian containing higher-dimensional operators. The Lowest dimension of such higher dimensional operators is five. This gives an effective light neutrino mass term via the seesaw mechanism. In the context of the Type-I seesaw mechanism, the dimension five effective operator giving the light neutrino mass term arises by integrating out heavy right-handed neutrino fields. However predictions of seesaw mechanism and its implications are not quite definitive due to the presence of large number of free parameters. Thus one needs to go to scenarios where the number of free parameters are minimal.

In an attempt to find minimal scenarios we study the implications of Dirac and Majorana mass matrices with texture zeros within the type I seesaw mechanism with three right handed neutrinos. For the Dirac mass matrices we consider 5 zero textures which we show to be the most minimal form that can successfully account for low energy phenomenology. We classify the allowed textures and discuss the ramifications for leptogenesis and lepton flavor violation.

In the context of the minimal seesaw framework with only two right handed neutrinos, we discuss the implications of Dirac and Majorana mass matrices in which two properties coexist, namely, equalities among matrix elements and texture zeros. Among the large number of general possibilities, we classify the patterns at the level of the most minimal number of free parameters, consistent with the global neutrino oscillation data. The predictions of the allowed textures for mass hierarchy and effective mass governing neutrino-less double beta decay are discussed. We also explore the possibility of having non-zero CP violation for each allowed solution and possible correlation between leptogenesis and low energy CP violation.

Possibility of exploring seesaw models at present colliders leads to TeV

scale seesaw models which also triggers another important implication namely destabilization of the electroweak vacuum. We consider the minimal seesaw model in which two gauge singlet right handed neutrinos with opposite lepton numbers are added. In this model, the smallness of the neutrino mass is explained by the tiny lepton number violating coupling between one of the singlets with the standard left-handed neutrinos. This allows one to have the right handed neutrino mass at the TeV scale as well as appreciable mixing between the light and heavy states. This model is fully reconstructible in terms of the neutrino oscillation parameters apart from the overall coupling strengths. We show that the overall coupling strength (y_ν) for the Dirac type coupling between the left handed neutrino and one of the singlets can be restricted by consideration of the stability bounds on the electroweak vacuum. Incorporating this bound, the overall coupling strength of the small lepton number violating coupling can also be constrained from neutrino oscillation data. In this scenario the lepton flavor violating decays of charged leptons can be appreciable which can put further constraint on y_ν, for right-handed neutrinos at TeV scale. We discuss the combined constraints on y_ν for this scenario from the process $\mu \to e\,\gamma$ and from the consideration of vacuum stability constraints on the Higgs self coupling. We also briefly discuss the implications for neutrino less double beta decay and possible signatures of the model that can be expected at colliders.

In general, for TeV scale seesaw models, dimension-six operators which were suppressed in high scale seesaw scenarios, can have important implications apart from dimension the five operator. A linear combination of two such operators gives rise to the non-unitarity in the lepton mixing matrix, $U_{\rm PMNS}$. We discuss the origin of non-unitarity at the high scale in the context of Type-I seesaw model and derive the one loop beta function governing its evolution through renormalization group running.

List of Abbreviations

SM → Standard Model

Contents

Chapter 1

Introduction

Standard Model (SM) of Particle Physics, described by the gauge group $SU(3)_c \otimes SU(2)_L \otimes U(1)_Y$, aims to explain the fundamental particles and their interactions *viz.* electromagnetic, weak and strong interactions. The particles belong to different representations of the various symmetry group of the SM. There are three types of particles in the SM, namely - spin-$\frac{1}{2}$ fermions (quarks and leptons), spin-1 force mediating vector bosons and spin-0 Higgs boson. All the fermions have two handedness, left and right. However, in many experiments it was found that only right handed anti neutrino ($\overline{\nu_R}$) or left handed neutrino (ν_L) is involved in weak interaction. Neutrinos with the other handedness *i.e.* ν_R or $\overline{\nu_L}$ were absent, which signals violation of parity in weak interaction [1–3]. This motivated the formulation of SM to be a Chiral gauge theory *i.e.* the left handed and the right handed fermions have different gauge interactions. The left handed fermions form $SU(2)$ doublet whereas right handed fermions remain $SU(2)$ gauge singlet. Apart from this quarks have an additional $SU(3)$ color gauge symmetry and they participate in the strong interaction through gluon exchange. All other particles (except quarks and gluons) are $SU(3)_c$ singlet and hence do not participate in the strong interaction. These particles (except Higgs boson) have been discovered by experiments [4]. Recently the CMS [5] and ATLAS [6] collaboration of the LHC experiment have reported the finding of a new neutral boson with a mass in the range $124.6 - 126.6$ GeV. However the spin and parity of this particle is

yet to be determined. It is highly expected that this particle is the SM Higgs boson. If measurements of spin and parity confirms this to be Higgs boson, SM will be placed on a firm footing.

However from the theoretical point of view, there are several drawbacks of SM. First, it does not incorporate gravity. Second, upon extrapolation of the SM to high scale, the three gauge couplings do not unify. Besides there are 19 arbitrary parameters, which cannot be predicted theoretically. This includes Yukawa coupling constants which determine the fermion masses. They are free parameters of the theory and there are no predictions for them. In particular it does not include neutrino mass. Also large hierarchy among fermion masses cannot be explained in SM. Construction of unified gauge theory where fermions belong to the same(or lesser number of) multiplet(s) of the representation of the gauge group, hence having more predictivity about fermion masses, together with unification of the gauge couplings motivate physicists to construct Grand Unified Theory (GUT) with bigger gauge group. SM will be a low energy approximation of it. $SU(5)\,, SO(10)\,, E_6$ GUT are among such possibilities [7–9]. These groups can break down to SM gauge group by Spontaneous Symmetry Braking (SSB). $SU(5)$ GUT predicts the mass of the down quark and the electron to be same at GUT scale but gives different masses at electroweak scale through Renormalization Group Evolution (RGE) of the mass operators. But the unification of gauge couplings in canonical $SU(5)$ GUT is not achieved with the present precision measurements of the gauge couplings [10, 11]. The 16 dimensional representation for fermions in $SO(10)$ GUT naturally include the right handed neutrino and hence this is imensely popular for generating light neutrino masses. $SO(10)$ GUT model predicts the mass of the up quark to be same as mass of the neutrino. But this situation can be circumvented by taking two Higgs multiplet [12]. Also gauge couplings unify at some high scale within $SO(10)$ GUT due to the presence of the left-right symmetric scale.

Another problem of SM is the divergence of Higgs mass when quantum corrections are included [13]. This happens because there is no symmetry to

parameter	best fit	1σ range	3σ range
Δm^2_{21} $[10^{-5}$ eV$^2]$	7.62	7.43–7.81	7.12–8.20
$\lvert\Delta m^2_{31}\rvert$ $[10^{-3}$ eV$^2]$	2.55 2.43	$2.46 - 2.61$ $2.37 - 2.50$	$2.31 - 2.74$ $2.21 - 2.64$
$\sin^2\theta_{12}$	0.320	0.303–0.336	0.27–0.37
$\sin^2\theta_{23}$	0.613 0.600	0.573–0.635 0.569–0.626	0.36–0.68 0.37–0.67
$\sin^2\theta_{13}$	0.0246 0.0250	0.0218–0.0275 0.0223–0.0276	0.017–0.033
δ	0.80π -0.03π	$0 - 2\pi$	$0 - 2\pi$

Table 1.1: *Present best fit values,* 1σ *and* 3σ *ranges of neutrino oscillation parameters. The upper (lower) row corresponds to normal (inverted) hierarchy. Values of* Δm^2_{21} *and* $\sin^2\theta_{12}$ *are hierarchy independent.*

protect Higgs mass in SM. Consideration of SUperSYmmetry (SUSY) which puts fermions and bosons in the same multiplet, resolves this problem [14, 15]. In SUSY, bosons and fermions have same mass at high scale but after SUSY breaking (at scale $\mathcal{O}$(TeV)) masses become different [16]. In Minimal Supersymmetric extension of Standard Model (MSSM), divergence of the Higgs mass coming from the fermion loop exactly cancels the divergence coming from the loop containing its superpartner, thus giving finite mass to the Higgs bosons [17]. Also consideration of SUSY leads to the unification of the gauge couplings at $\approx 2\times10^{16}$ GeV in $SU(5)$ GUT [18,19]. Among other possibilities, people have considered the presence of extra dimension which localizes the four dimensional gauge theories in higher dimensional space-time. Consideration of extra dimension leads to many phenomenologically viable models and even the possibility of localizing gravity [20, 21].

The first experimental evidence of physics beyond the SM came from the neutrino sector [22–25]. Other drawbacks of SM are that it does not include a natural candidate for Dark Matter [26]. Also the source of CP violation in SM from the quark sector is not strong enough to successfully account the observed Baryon Asymmetry of the Universe (BAU) [26–28].

Neutrinos are massless in the SM. However results from neutrino interferometry

experiments have established that at least two of the neutrinos are massive and there is mixing between different flavors [29–35]. Quantum mechanical analysis of neutrino oscillation shows that the oscillation probability is sensitive to mass squared differences and mixing angles. Present best fit values and 3σ ranges of the mass squared differences ($\Delta m^2_{ij} \equiv m^2_i - m^2_j$) and mixing angles ($\theta_{ij}$) from the global analysis of neutrino oscillation data [36] are tabulated in Table 1.1. The relative position of the third mass eigenstate m_3 with respect to the other two is unknown, though the solar neutrino data gives $\Delta m^2_{21} > 0$ [37]. This results in two possible orderings of the neutrino masses: normal ($m_1 < m_2 < m_3$) and inverted ($m_3 < m_1 \lesssim m_2$).

An upper bound on the sum of neutrino masses also comes from cosmology. The present bound is $\sum m_i \lesssim 0.5$ eV [38–40]. However this bound can vary from 0.28 eV to 1.2 eV subject to the data set used [41, 42]. Cosmological upper bound together with measured mass squared differences in neutrino oscillation experiments imply that the absolute masses of neutrinos are orders of magnitude smaller than those of quarks and charged leptons.

The simplest extension of the SM, to include neutrino masses, could be to add right handed neutrinos and give Dirac mass to light neutrinos using SSB like other fermions. However, one will need very small Yukawa coupling to account for the small neutrino masses. A more natural mechanism to generate such small neutrino masses is the so called seesaw mechanism which needs the introduction of one or more heavy fields. At energies below their mass scales, the heavy fields get integrated out giving rise to the effective Lagrangian containing higher dimensional operators. These operators are *non-renormalizable*, and SM gauge group invariant. The lowest dimensional operator among these is the dimension-5 operator [43, 44], given by

$$\mathcal{L}_5 \sim c^{(5)}_{ij} \left(\overline{l^{\mathcal{C}}_{Li}}\, \epsilon\, \phi\right) \left(\phi^T \epsilon^T l_{Lj}\right) \tag{1.0.1}$$

where l_L and ϕ are respectively the SM lepton and Higgs doublets. $l^{\mathcal{C}}$ is defined as $l^{\mathcal{C}} = \mathcal{C}\, \bar{l}^T$, where $\mathcal{C}$ is the charge conjugation matrix. ϵ is the 2×2

anti-symmetric tensor, i, j are the generation indices. As we can see from the above expression, $c^{(5)}$ has the dimension of M^{-1}, where M is the mass of the right handed heavy field. $c^{(5)}$ can be expressed in terms of dimensionless coupling constant as $a^{(5)}/M$. This operator violates lepton number by two units and leads to Majorana masses for neutrinos. After SSB, the ϕ field acquires Vacuum Expectation Value (VEV) v and consequently neutrino mass becomes; $m_\nu \sim \frac{1}{2}\, c^{(5)} v^2$. With $v \sim 246$ GeV and $a^{(5)} \sim \mathcal{O}(1)$, to produce neutrino mass of ~ 0.5 eV, M has to be of the order of $\mathcal{O}(10^{14}$ GeV). This way of generating small neutrino masses, by integrating out the heavy singlet fermionic field is popularly called seesaw mechanism (Type-I) [45, 46].

In Type-I seesaw mechanism, the light neutrino mass matrix m_ν gets the following matrix structure at tree level

$$m_\nu = -m_D^T\, M_R^{-1} m_D \tag{1.0.2}$$

where $m_D = Y_\nu \frac{v}{\sqrt{2}}$ and Y_ν is the Dirac Yukawa coupling that couples left handed lepton doublet with the right handed heavy singlet. The Majorana mass matrix m_ν is complex symmetric and can in general be diagonalized by a unitary matrix as follows

$$U_\nu^T m_\nu\, U_\nu = D_\nu = \mathrm{diag}(m_1\,, m_2\,, m_3) \tag{1.0.3}$$

$m_1\,, m_2\,, m_3$ can be chosen real and positive. This diagonalization modifies the charged lepton current as below

$$J^{\mu+} = \frac{g_2}{\sqrt{2}}\, \overline{e_i}\, \gamma^\mu P_L\, \nu_{ei} = \frac{g_2}{\sqrt{2}}\, \overline{e_i'}\, \gamma^\mu P_L \left(U_e^\dagger\, U_\nu\right)_{ij}\, \nu'_{ej} \tag{1.0.4}$$

where $e\,, \nu_e$ are the flavor states and $e'\,, \nu'_e$ are the mass eigen states, related by $e_i = (U_e)_{ij}\; e'_j\,,\;\; \nu_{ei} = (U_\nu)_{ij}\; \nu'_{ej}$. Thus physical lepton mixing matrix is given by the Pontecorvo-Maki-Nakagawa-Sakata (PMNS) matrix, which is defined

by the product of the two unitary matrices;

$$U_{\rm PMNS} \equiv U_e^\dagger \, U_\nu \tag{1.0.5}$$

In the basis where charged-lepton mass matrix is diagonal, so that $U_e = I$, the lepton mixing matrix is given by $U_{\rm PMNS} = U_\nu$.

The next set of higher dimensional operators that arise in the theory are dimension six operators. List of different dimension six operators can be found in [47, 48]. A linear combination of two such operators is of special relevance in connection with neutrino mixings [49] and is expressed as

$$\mathcal{L}_6 \sim c_{ij}^{(6)} \left(\overline{l_{Li}}\, \epsilon\, \phi^*\right) i\partial\!\!\!/ \left(\phi^T \epsilon^T l_{Lj}\right) \tag{1.0.6}$$

This operator is of Dirac type in contrast with the Majorana type operator (1.0.1). After symmetry breaking, the right hand side of Eq. (1.0.6) becomes

$$c_{ij}^{(6)} \frac{v^2}{2} \overline{\nu_{eLi}}\, i\partial\!\!\!/\, \nu_{eLj} \tag{1.0.7}$$

which makes the coefficient of neutrino kinetic term deviate from unity by an amount of $\frac{1}{2}\, c^{(6)} v^2$. Now, in order to bring the kinetic term in its usual canonical form, the field ν_L is rescaled with a factor of $\left(1 + \frac{1}{2}\, c^{(6)} v^2\right)^{1/2}$. This also modifies the charged lepton current interaction as below [49, 50]

$$J^{\mu +} = \frac{g_2}{\sqrt{2}}\, \overline{e_i}\, \gamma^\mu P_L\, \nu_{ei} \;\longrightarrow\; \frac{g_2}{\sqrt{2}}\, \overline{e_i}\, \gamma^\mu P_L \left(\delta_{ij} - \frac{1}{4}\, c_{ij}^{(6)} v^2\right) \nu_{ej} \tag{1.0.8}$$

Now following the same procedure of basis transformation as in Eq. (1.0.4) one would obtain the lepton mixing matrix, $U_{\rm PMNS}$, as

$$U_{\rm PMNS} \;\longrightarrow\; \left(1 - \frac{1}{4}\, c^{(6)} v^2\right) U_{\rm PMNS} \tag{1.0.9}$$

$c^{(6)}$ is hermitian and unitarity of $U_{\rm PMNS}$ is no longer maintained. $c^{(6)} v^2$ can be treated as the measure of non unitarity. Because of this, the operator in Eq. (1.0.6) is called the non-unitary operator and $c^{(6)}$ is called the non-unitary

parameter. The dimension of $c^{(6)}$ is M^{-2}. With M of the order of $\mathcal{O}(10^{14}$ GeV), non-unitarity is highly suppressed.

Seesaw mechanism implies neutrinos are Majorana particles and hence lepton number symmetry is violated. Experimental verification of this comes from neutrino less double beta decay ($0\nu\beta\beta$) transition inside the nuclei, $(A\,, Z) \rightarrow (A\,, Z+2) + 2\,e^-$. Emission of two electrons and no neutrinos in the final state, is being connected to the exchange of virtual light neutrinos which is of Majorana type [51]. However presence of heavy neutrinos can act as a new contribution towards LNV process. Although the new contribution is thought to be highly suppressed due to the heavy mass scale of the singlet neutrinos but recently it was shown that the new contribution can play an important role in models with large light-heavy mixing [52–55].

The singlet neutrinos, introduced at the high scale for Type-I seesaw mechanism, also fulfil the requirements of the generation of BAU through the mechanism of leptogenesis [56, 57]. Leptogenesis is the mechanism where the heavy singlet neutrino decays into leptons, Higgs boson and their antiparticles in different manners. This leads to an overall CP asymmetry which can then be converted into Baryon asymmetry through Sphaleron process [58–61]. Thus one can connect the mechanism of light neutrino mass generation to the observed Baryon asymmetry. There is also the interesting possibility of relating the high and low energy CP violations.

Lepton Flavor Violating decay (LFV) processes *e.g.* $\mu \rightarrow e\,\gamma$ can be mediated by charged current and neutral current interactions of light neutrinos at higher orders in perturbation theory [62–64]. The branching ratio of this type of flavor violating process, when compared with process like $\mu \rightarrow e\,\overline{\nu_e}\,\nu_\mu$, turns out to be proportional to the forth power of light neutrino masses and hence is negligibly small [65]. However this effect could be enhanced in presence of heavy neutrinos through relatively large light-heavy mixing [66–68].

Study of such phenomenological consequences of seesaw mechanism needs precise knowledge of the unknown parameters in the seesaw mass matrices at high energy. Reconstruction of the seesaw mass matrices (1.0.2) from low en-

ergy observations is a challenging task as Yukawa couplings are not governed by any principle. The main problem is the mismatch in the number of parameters because in general the seesaw framework contains more parameters compared to what can be obtained from measurements at low energy and it is not possible to fix the high energy parameters entirely from low energy data [69–71]. Parameterization of the unknown Yukawa matrix (or m_D) according to Casas-Ibarra [72] cannot determine it fully. For illustration, in presence of three generation of heavy neutrinos, the total number of high energy parameter is 24 whereas measurable low energy parameters are only 9.

One possible solution is the appearance of texture zeros which was first attempted in the quark sector [73]. In general, zeros imply vanishingly small entries in the mass matrices whose origin can be traced to flavor symmetries. Consideration of texture zeros in the seesaw mass matrices provides a useful way to handle the problem of parameter mismatch since assumption of texture zeros leads to a reduction of the number of parameters and thus strengthens the predictive power of the model.

However direct testability of seesaw mechanism is way beyond the reach of present experiments. In conventional Type-I seesaw mechanism, mass scale of the heavy neutrinos is of the order of $\mathcal{O}(10^{14}$ GeV) and hence cannot be tested at present colliders. Therefore, from the point of view of testability at colliders, one needs to bring down the seesaw scale to TeV. For the canonical Type-I seesaw mechanism, this is difficult and one has to appeal to cancellations coming from flavor symmetries [74–76]. One way to circumvent this problem is provided by inverse seesaw mechanism [9, 77]. In these scenarios, mass scale of the heavy field is of the order of $\mathcal{O}(10^3$ GeV). In models with inverse seesaw mechanism, one includes additional singlet states with lepton number opposite to that of the right handed neutrinos. The Majorana mass of the singlet breaks Lepton number softly. The smallness of the neutrino mass can be related to the smallness of this parameter. For the canonical seesaw, the neutrino mass is inversely proportional to the mass of the heavy particle which determines the scale at which lepton number is violated. While in this case the neutrino mass

is proportional to the mass of the singlet characterizing the lepton number violation. Hence this is termed as inverse seesaw. This is considered to be more natural because as this parameter tends to zero, the neutrino mass also becomes zero and lepton number symmetry is reinstated. Non-unitary mixing between light and heavy particles in these class of models with inverse seesaw mechanism, can be large and can be probed at colliders [78–80].

One variant of the inverse seesaw models of the type discussed in [9, 77] is the linear seesaw model [81–83]. In these class of models, a tiny lepton number violation is incorporated through the term that couples the left-handed neutrinos and one of the singlet states. Within this scheme the minimal model consists of three left-handed neutrinos and just two singlet states. This is similar to the minimal type-I seesaw model [84–87], but in this case the two singlet states are assigned opposite lepton numbers. Thus only one of the singlets has a lepton number conserving Dirac type coupling with the left-handed states. The coupling of the other singlet with the left-handed states violate lepton number symmetry and in the limit this coupling is zero the Lagrangian acquires an extra global $U(1)$ symmetry. Therefore this should be naturally small. The smallness of the neutrino masses can now be related to the smallness of this coupling and the mass of the singlets can be at TeV leading to phenomenological consequences, same as in the inverse seesaw model.

Another important consequence of TeV scale seesaw model is significant modification towards the stability of the electroweak vacuum [88,89]. It is well known that because of quantum corrections, the Higgs self-coupling, λ, diverges for higher values of Higgs mass and goes to negative for low values of Higgs mass near Planck-scale ($M_{pl} = 1.2 \times 10^{19}$ GeV). Assuming the absence of any new physics between SM and the Planck scale, Higgs mass was found to be in the range $126 - 171$ GeV for λ(at M_{pl}) to be in the range $[0, \pi]$ [90,91]. The upper bound called the "triviality bound" essentially embodies the perturbativity of the theory. The lower bound known as the "vacuum stability bound", is obtained from the fact that a negative λ makes the potential unbounded from below and the vacuum would be unstable [92,93]. The presence of new Yukawa

couplings in seesaw models modifies the β function of Higgs self-coupling. In the conventional Type-I seesaw model, generation of small neutrino mass requires the mass scale of the singlet to be of the order of 10^{14} GeV for Dirac Yukawa Coupling $Y_\nu \sim \mathcal{O}(1)$. It was observed in [88] that the presence of this extra coupling increases the lower bound of the Higgs mass from vacuum stability constraints, gradually reaching the perturbativity bound. But, as for canonical Type-I seesaw mechanism, the window of the new physics effect (from 10^{14} GeV to Planck scale) towards the running of λ is small, electroweak vacuum is less likely to get destabilized due to its presence. Whereas for TeV scale models (with not very small $Y\nu$), as the running of Yukawa starts affecting the running of λ from TeV scale upto Planck scale, vacuum is more likely to get destabilized. Although as the mass scale of the heavy field is lowered, Y_ν has to become less in order to get $m_\nu \sim 0.5$ eV and below a certain value of the mass scale the additional contribution does not play any significant role. However from the point of view of relevance at LHC many models have been considered in the literature which can give rise to small neutrino masses with a relatively large Yukawa coupling even with the heavy field at the TeV scale. Hence in such models the effect of the Yukawa term can be significant in the running of λ [94, 95].

As mentioned earlier, the higher dimensional operators (1.0.1,1.0.6), obtained by integrating out the heavy fields, arise in the theory at relatively higher scale whereas phenomenological implication of such operators are being measured by experiments at much lower scale. RGE effects of these operators, induced due to higher order quantum corrections, needs to be incorporated for precise predictions of the model parameters and experimental verification of the model [35, 36, 96].

The dimension five operator is responsible for the neutrino masses and their mixing angles. RGE for this operator, gives rise to corrections to neutrino masses and mixing angles. RGE effect on neutrino masses and mixing angles can be large for heavy neutrino mass at a scale $\mathcal{O}\left(10^{12} - 10^{14}\text{ GeV}\right)$ and is well studied in the literature in the context of seesaw mechanism [97–110].

Dimension six operator, being Dirac type, does not contribute towards neutrino mass. It modifies the neutrino mixing parameters. Also it mediates LFV type processes. The non-unitary effect can also play a non-trivial role in relating CP violation responsible for leptogenesis with low energy CP violation [111, 112]. RGE of this operator is, however, not as widely studied. It is noteworthy to mention that the non-unitary operator, because of $\mathcal{O}(1/M^2)$ suppression, becomes significant only at TeV scale. Therefore the RG running of this operator from the TeV scale to the electro-weak symmetry breaking scale is not expected to be as large as operators which are significant at very high energy ($10^{12} - 10^{14}$ GeV). But as neutrino physics has entered the precision era, for precision calculation of neutrino mixing parameter, LFV processes, low energy CP violation, RGE of the non-unitary operator may play an important role.

In this thesis we have studied several aspects of the seesaw mechanism. In Chapter 2 we give the origin of higher dimensional operators which lead to light neutrino mass matrix and modification of the lepton mixing matrix through SSB. Then we present light neutrino mass matrices in different seesaw mechanisms and discuss the implications such as neutrino less double beta decay, leptogenesis, lepton flavor violation, modification towards vacuum stability. Chapter 3 contains phenomenological studies of Type-I seesaw mechanism. We consider texture zeros in m_D and M_R with three right handed neutrinos. We also consider minimal seesaw model with two right handed neutrinos and consider both equalities and zeros. With the reduced number of parameters, we discuss viable textures consistent with low energy data. Taking such textures, we shall make predictions for leptogenesis, low energy CP violation, lepton flavor violation, neutrino less double beta decay. In the context of Minimal Linear Seesaw Model (MLSM), we shall also constrain the parameter space of neutrino Yukawa coupling and heavy neutrino mass from the consideration of vacuum stability and LFV. In Chapter 4 we shall present the renormalization group evolution effect on higher dimensional operators. Finally we shall summarize in Chapter 5.

Chapter 2

See-saw models of neutrino masses in beyond SM scenarios

2.1 Introduction

As mentioned in Chapter 1, SM does not include a mass term for the neutrinos. The simplest extension of the SM to generate non zero masses of the light neutrinos naturally is to add heavy fields which lead to effective operators at low energy *i.e.* SM is an effective theory of a more fundamental theory *e.g.* Left-Right Symmetric model, GUT etc. Higher dimensional operators can then be added to the SM Lagrangian without disrupting the renormalizability of the theory as the fundamental model would still be renormalizable at higher energy. These operators should be SM gauge group invariant and in principle could be lepton number violating as lepton number symmetry is only an accidental symmetry in SM. Renormalizability criteria restricts the operators in the SM Lagrangian to have maximum of four mass dimension. The lowest dimension of such higher dimensional operator that could be added to the SM is dimension five. Dimension five operators was first noted down by Weinberg in 1979 in general [43, 44]. In the leptonic sector, it is given by

$$\mathcal{L}_5 = -\frac{1}{8}\frac{a^{(5)}_{ji}}{M}\left(\overline{l^{\mathcal{C}}_{Lj}}\,\epsilon\,\tau^a\,l_{Li}\right)\left(\phi^T\epsilon\,\tau^a\phi\right) + \text{h.c.} \tag{2.1.1}$$

where a_{ji} is $\mathcal{O}(1)$ and $\tau^a/2$ is the $SU(2)$ generator. This type of operator is obtained by integrating out heavy fields of mass scale M. After electroweak symmetry breaking ϕ field acquire VEV, consequently such an operator leads to the mass term for the upper component of the lepton doublet through antisymmetric combination. This is the well known seesaw mechanism. Representation of such heavy fields can be obtained by $SU(2)$ group multiplication, $2 \otimes 2 = 1 \oplus 3$. Hence there can be two possible representations of the heavy field, (i) singlet fermion/scalar and (ii) triplet fermion/scalar. Seesaw mechanism involving singlet fermion is known as Type-I seesaw [45, 46]. Seesaw mechanism mediated through triplet scalar is known as Type-II seesaw [113–117] and by triplet fermion is know as Type-III seesaw [118–120]. Seesaw mechanism cannot be mediated through singlet scaler with zero hypercharge ($Y = 0$) due to the violation of charge conservation. Although $Y = 2$ scalar would conserve charge but cannot give mass term for light neutrinos.

In seesaw models, motivated by GUT, the mass scale of the heavy fields are near the GUT scale $i.e \sim \ 10^{12} - 10^{14}$ GeV. The option to generate TeV scale seesaw is to add extra singlets, as is done in inverse seesaw, linear seesaw models. Inverse seesaw, linear seesaw mechanism provide natural scale for right handed neutrino mass to be at TeV. Below its mass scale, the heavy fields get integrated out and give rise to dimension five operator similar to Type-I seesaw as well as dimension six operator.

After SSB dimension five and dimension six operators give rise to neutrino mass matrix and non unitarity in the lepton mixing matrix respectively. The heavy neutrino introduced at high scale leads to many different phenomenological implications such as leptogenesis, lepton flavor violation, neutrino less double beta decay. Also electro weak vacuum gets destabilized in the low Higgs mass region due to the presence of neutrino Yukawa coupling.

In this Chapter we shall discuss the origin of higher dimensional operators at high energy with Feynman diagrams. We also discuss the structure of different seesaw mass matrices. Then we shall briefly present the formalism of different implications of seesaw mechanism.

2.2 Origin of higher dimensional operators

In Type-I seesaw mechanism, the additional part of the Lagrangian including the heavy neutrino field N_j to the SM Lagrangian is given by

$$\mathcal{L}_{\text{ext}} = -(Y_\nu)_{ji}\,\epsilon_{\alpha\beta}\,\phi_\beta\,\overline{N}_j P_L\,l_{\alpha i} - \frac{1}{2}M_{ji}\overline{N_j}P_R N_i^{\mathcal{C}} + \text{h.c.} \tag{2.2.1}$$

here ϕ denotes $SU(2)$ Higgs doublet with $\tilde{\phi} = \epsilon\phi^*$; ϵ is the 2×2 anti-symmetric tensor. The lepton doublet is denoted by l_i. i and j are the generation indices. For m generation light neutrinos and n generation heavy neutrinos, i and j run from 1 to m and 1 to n respectively. The Yukawa coupling Y_ν is complex-valued $m \times n$ matrix in general. After SSB one gets the Dirac mass matrix as $m_D = \frac{v}{\sqrt{2}}Y_\nu$. The Majorana mass matrix M is $n \times n$ complex symmetric matrix. The relevant part of the SM Lagrangian (required for computation in Chapter 4) is given below

$$\begin{aligned}
\mathcal{L}_{SM} = {} & i\frac{g_2}{2}\Big[\left(\partial^\mu\phi_\alpha^*\right)\sigma^a_{\alpha\beta}\phi_\beta - \phi^*_\beta\sigma^a_{\alpha\beta}\left(\partial^\mu\phi_\alpha\right)\Big]W^a_\mu + i\frac{g_1}{2}\Big[\left(\partial^\mu\phi^*_\alpha\right)\delta_{\alpha\beta}\phi_\beta \\
& - \phi^*_\beta\delta_{\alpha\beta}\left(\partial^\mu\phi_\alpha\right)\Big]B_\mu + \frac{g_2^2}{4}\phi^*_\alpha\delta_{\alpha\beta}\delta^{ab}\phi_\beta W^{a\mu}W^b_\mu + \frac{g_1g_2}{2}\phi^*_\alpha\sigma^a_{\alpha\beta}\phi_\beta W^{a\mu}B_\mu \\
& + \frac{g_1^2}{4}\phi^*_\alpha\delta_{\alpha\beta}\phi_\beta B^\mu B_\mu - \frac{\lambda}{4}\delta_{\alpha\beta}\delta_{\gamma\delta}\phi^*_\alpha\phi_\beta\phi^*_\gamma\phi_\delta - \frac{g_2}{2}\sigma^a_{\alpha\beta}\delta_{ji}\,\bar{l}_{\alpha j}\gamma^\mu P_L l_{\beta i}W^a_\mu \\
& + \frac{g_1}{2}\delta_{\alpha\beta}\delta_{ji}\,\bar{l}_{\alpha j}\gamma^\mu P_L l_{\beta i}B_\mu + g_1\,\delta_{ji}\,\bar{e_j}\gamma^\mu P_R e_i B_\mu - \frac{g_2}{2}\sigma^a_{\alpha\beta}\delta_{ji}\,\bar{q}_{\alpha j}\gamma^\mu P_L q_{\beta i}W^a_\mu \\
& - \frac{g_1}{6}\delta_{\alpha\beta}\delta_{ji}\,\bar{q}_{\alpha j}\gamma^\mu P_L q_{\beta i}B_\mu - \frac{4g_1}{3}\delta_{ji}\,\bar{u_j}\gamma^\mu P_R u_i B_\mu + \frac{2g_1}{3}\delta_{ji}\,\bar{d_j}\gamma^\mu P_R d_i B_\mu \\
& - \Big[(Y_e)_{ji}\,\delta_{\alpha\beta}\phi^*_\beta\bar{e}_j P_L l_{\alpha i} + (Y_u)_{ji}\,\epsilon_{\alpha\beta}\phi_\beta\bar{u}_j P_L q_{\alpha i} \\
& + (Y_d)_{ji}\,\delta_{\alpha\beta}\phi^*_\beta\bar{d}_j P_L q_{\alpha i} + \text{h.c}\Big]
\end{aligned} \tag{2.2.2}$$

where g_1, g_2 and B_μ, W^a_μ are gauge couplings and gauge boson fields corresponding to $U(1)$, $SU(2)$ gauge group respectively. u and d denotes up and down type quark singlets. q denotes quark doublet. Full set of Feynman rules for this model can be found in Appendix C.

2.2.1 Origin of dimension-5 operator

With the above Lagrangian (2.2.1) one can construct two possible dimension-5 Majorana type operators in the context of $l\phi \to l^{\mathcal{C}}\phi^*$ and $\bar{l}\phi^* \to \overline{l^{\mathcal{C}}}\phi$. Here we present one of them, the other one will be the same with fermion lines reversed.

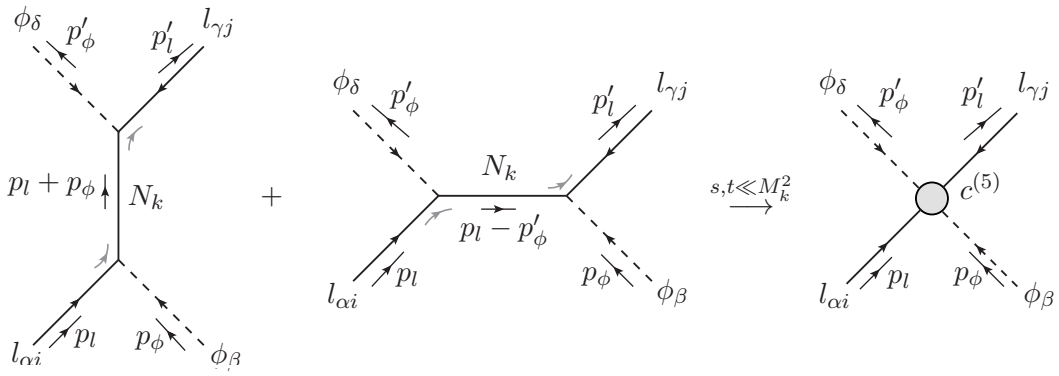

Figure 2.1: *Feynman diagram, $l\phi \to l^{\mathcal{C}}\phi^*$ mediated by heavy right handed neutrino (on the left hand side). On the right hand side, low momentum transfer approximation, leads to $c^{(5)}$ vertex.*

Tree level matching of both sides, in the limit $s, t \ll M_k^2$, gives

$$\begin{aligned} & i\left[\epsilon_{\gamma\delta}\,\epsilon_{\alpha\beta}\left(Y_\nu^T\left(M^{-1}\right)Y_\nu\right)_{ji} + \epsilon_{\gamma\beta}\,\epsilon_{\alpha\delta}\left(Y_\nu^T\left(M^{-1}\right)Y_\nu\right)_{ji}\right] P_L \\ = \; & \frac{i}{2}\,c^{(5)}_{ji}\left(\epsilon_{\gamma\delta}\,\epsilon_{\alpha\beta} + \epsilon_{\gamma\beta}\,\epsilon_{\alpha\delta}\right) P_L \end{aligned} \tag{2.2.3}$$

We identify $c^{(5)} = 2\,Y_\nu^T M^{-1} Y_\nu$. Note that $c^{(5)}$ is symmetric. Here $s = (p_l + p_\phi)^2$ and $t = \left(p_l - p'_\phi\right)^2$. So the effective dimension-5 operator (at low energy) in the Lagrangian becomes

$$\mathcal{L}^{(5)} = \frac{1}{4}\,c^{(5)}_{ji}\left(\overline{l^{\mathcal{C}}_{Lj}}\,\epsilon\,\phi\right)\left(\phi^T\epsilon^T l_{Li}\right) + \text{h.c.} \tag{2.2.4}$$

2.2.2 Origin of dimension-6 operator

In a similar way, one can construct four possible dimension-6 Dirac type operators in the context of $l\phi \to l\phi$ and $l\phi^* \to l\phi^*$, two in each cases. Here we

present one from each of them. The other two will be the same with fermion lines reversed.

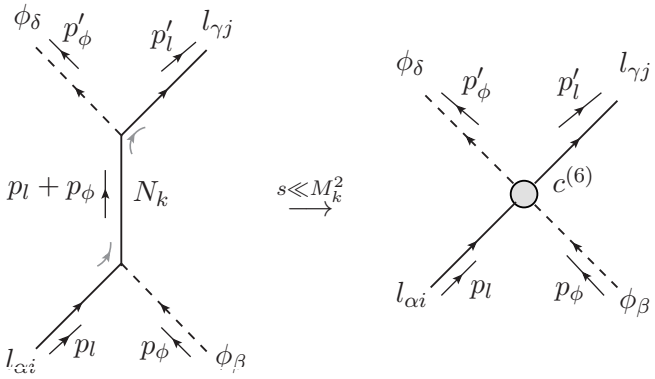

Figure 2.2: *Feynman diagram, $l\phi \to l\phi$ mediated by heavy right handed neutrino (on the left hand side). On the right hand side, low momentum transfer approximation, leads to $c^{(6)}$ vertex.*

Tree level matching of both sides, in the limit $s \ll M_k^2$, gives

$$\begin{aligned} & i \left(Y_\nu^\dagger \left(M^{-1}\right)^* M^{-1} Y_\nu\right)_{ji} \epsilon_{\gamma\delta}\, \epsilon_{\alpha\beta} \left(\not{p}_l + \not{p}_\phi\right) P_L \\ = \; & \frac{i}{2}\, c_{ji}^{(6)} \epsilon_{\gamma\delta}\, \epsilon_{\alpha\beta} \left(\not{p}_l + \not{p}_\phi\right) P_L \end{aligned} \tag{2.2.5}$$

We identify $c^{(6)} = 2\, Y_\nu^\dagger \left(M^{-1}\right)^* M^{-1} Y_\nu$. It is noteworthy that $c^{(6)}$ is Hermitian. A similarly diagram for t channel is as follows

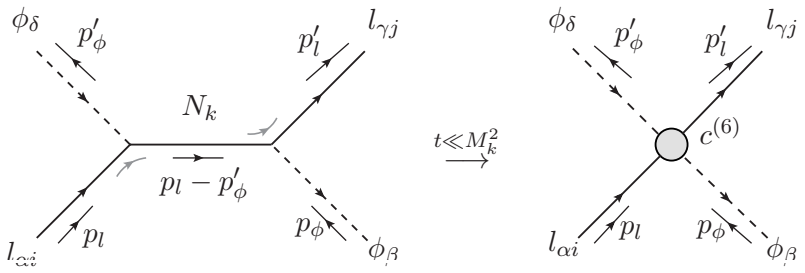

Figure 2.3: *Feynman diagram, $l\phi^* \to l\phi^*$ mediated by heavy right handed neutrino (on the left hand side). On the right hand side, low momentum transfer approximation, leads to $c^{(6)}$ vertex.*

Tree level matching of both sides, in the limit $t \ll M_k^2$, gives

$$\begin{aligned} & i \left(Y_\nu^\dagger \left(M^{-1}\right)^* M^{-1} Y_\nu\right)_{ji} \epsilon_{\gamma\beta}\, \epsilon_{\alpha\delta} \left(\not{p}_l - \not{p}'_\phi\right) P_L \\ = \quad & \frac{i}{2}\, c_{ji}^{(6)} \epsilon_{\gamma\beta}\, \epsilon_{\alpha\delta} \left(\not{p}_l - \not{p}'_\phi\right) P_L \end{aligned} \tag{2.2.6}$$

There are two other diagrams with fermion lines opposite to previous two. Note that the external scalar lines as well as the momentum dependence in s-channel and t-channel are different. For the dimension-5 operator both s-channel and t-channel contribute to the same effective vertex. But here they contribute to different vertices. The effective dimension-6 operator (at low energy) in the Lagrangian is given by

$$\mathcal{L}^{(6)} = \frac{1}{2}\, c_{ji}^{(6)} \left(\overline{l_{Lj}}\, \epsilon\, \phi^*\right) i\partial\!\!\!/ \left(\phi^T \epsilon^T l_{Li}\right) \tag{2.2.7}$$

It is noteworthy to mention that the extra 1/2 factor in $\mathcal{L}^{(5)}$ (2.2.4) is due to the Majorana nature of the dimension five operator.

2.3 Seesaw mass matrices

After SSB the Higgs field receives VEV, v, as

$$\phi \equiv \begin{pmatrix} \phi^+ \\ \phi^0 \end{pmatrix} \longrightarrow \begin{pmatrix} 0 \\ \frac{v}{\sqrt{2}} \end{pmatrix} \tag{2.3.1}$$

consequently the dimension five operator in Eq. (2.2.4) becomes

$$-\frac{1}{2} \cdot \left(-\frac{1}{4}\, c_{ji}^{(5)} v^2\right) \overline{\nu_{Lj}^{\mathcal{C}}}\ \nu_{Li} \tag{2.3.2}$$

The above expression is rearranged with *-ive* sign as fermion mass term comes with a *-ive* sign in the Lagrangian. The 1/2 factor taken out to the front as its a Majorana mass term. The light neutrino mass term is being identified as

$$m_\nu = -\frac{1}{4}\, c^{(5)} v^2 = -m_D^T\, M_R^{-1} m_D \tag{2.3.3}$$

Since is M_R very large, the mass eigenvalues are naturally suppressed. The Majorana mass matrix m_ν is symmetric and can in general be diagonalized by unitary matrix ($U_\nu = U_{PMNS}$) as in Eq. (1.0.3). Having discussed the origin of seesaw, in the next section we describe the mass matrices arising in different types of seesaw mechanism.

2.3.1 Type-I Seesaw mass matrix

After SSB the Higgs doublet receives VEV, v, as in Eq. (2.3.1). Consequently the Lagrangian in Eq. (2.2.1) becomes

$$\begin{aligned}
\mathcal{L}_{\text{Yuk}\to\text{mass}} &= -\frac{v}{\sqrt{2}}\,\overline{N_R}\,Y_\nu\,\nu_L - \frac{1}{2}\overline{N_R}M N_R^{\mathcal{C}} + \text{h.c.} \\
&= -\frac{1}{2}\left(\overline{\nu_L^{\mathcal{C}}}\,,\overline{N_R}\right)\begin{pmatrix} 0 & Y_\nu^T\frac{v}{\sqrt{2}} \\ Y_\nu\frac{v}{\sqrt{2}} & M \end{pmatrix}\begin{pmatrix}\nu_L \\ N_R^{\mathcal{C}}\end{pmatrix} + \text{h.c.} \\
&= -\frac{1}{2}\,\overline{\chi_L^{\mathcal{C}}}\,\mathcal{M}_\nu\,\chi_L + \text{h.c.} \qquad (2.3.4)
\end{aligned}$$

where χ_L is given by $\chi_L = \left(\nu_L\,, N_R^{\mathcal{C}}\right)^T$. The above expression gives the neutral lepton mass matrix, given by

$$\mathcal{M}_\nu = \begin{pmatrix} 0 & {m_D}^T \\ m_D & M \end{pmatrix} \qquad (2.3.5)$$

where $m_D = Y_\nu v/\sqrt{2}$. The neutrino mass matrix $\mathcal{M}_\nu$ can be diagonalized by a $(3+n)\times(3+n)$ unitary matrix U_0 as

$$U_0^T\,\mathcal{M}_\nu\,U_0 = \mathcal{M}_\nu^{diag} \qquad (2.3.6)$$

where $\mathcal{M}_\nu^{diag} = \text{diag}(m_1\,, m_2\,, m_3\,, M_1\,, \cdots, M_n)$ with mass eigenvalues m_i ($i = 1\,, 2\,, 3$) and M_j ($j = 1\,, \cdots, n$) for three light neutrinos and n heavy neutrinos respectively. Following standard procedure of two-step diagonalization U_0 can

be expressed as, by keeping term upto order $\mathcal{O}\left(m_D^2/M^2\right)$ [121]

$$U_0 = W\,T = \begin{pmatrix} \left(1-\frac{1}{2}\,\epsilon\right) U_\nu & m_D^\dagger (M^{-1})^* U_R \\ -M^{-1} m_D\, U_\nu & \left(1-\frac{1}{2}\,\epsilon'\right) U_R \end{pmatrix} = \begin{pmatrix} U_L & V \\ S & U_H \end{pmatrix} \tag{2.3.7}$$

W is the matrix which brings the full $(3+n)\times(3+n)$ neutrino matrix, in the block diagonal form

$$W^T \begin{pmatrix} 0 & m_D^T \\ m_D & M \end{pmatrix} W = \begin{pmatrix} m_\nu & 0 \\ 0 & m_{\rm h} \end{pmatrix}. \tag{2.3.8}$$

$T = diag(U_\nu\,, U_R)$ diagonalizes the mass matrices in the light and heavy sector appearing in the upper and lower block of the block diagonal matrix respectively. U_L in Eq.(2.3.7) corresponds to U_{PMNS} which acquires a non-unitary correction $(1-\epsilon/2)$. ϵ and ϵ' characterize the non-unitarity, given by

$$\begin{aligned} \epsilon &= m_D^\dagger \left(M^{-1}\right)^* M^{-1}\, m_D, \\ \epsilon' &= M^{-1}\, m_D\, m_D^\dagger \left(M^{-1}\right)^*. \end{aligned} \tag{2.3.9}$$

ϵ can also be obtained from Eq. (2.2.7) by giving VEV to the Higgs field as

$$\epsilon = \frac{1}{4}\, c^{(6)} v^2 \tag{2.3.10}$$

m_ν can readily be obtained from Eq.(2.3.8) as

$$m_\nu = -\,m_D^T\, M^{-1}\, m_D + \frac{1}{2}\left(m_D^T\, M^{-1}\, m_D\, \epsilon + \epsilon^*\, m_D^T\, M^{-1}\, m_D\right) \tag{2.3.11}$$

In the mass basis χ and χ' are related as follows

$$\chi_L = U_0\, \chi'_L \tag{2.3.12}$$

where un-primed are the flavor basis and primed fields are in the mass basis. Also the charged lepton current and the neutral current involving neutrino get

modified as below

$$\mathcal{L}^{cc} = \frac{g_2}{\sqrt{2}} \bar{e_L} \gamma^\mu \left[U_L \, \nu'_L + V N'^{\mathcal{C}}_R \right] W^-_\mu + \text{h.c.} \tag{2.3.13}$$

$$\begin{aligned} \mathcal{L}^{nc} &= \frac{g_2}{2\cos\theta_w} \Big[\bar{\nu}'_L \gamma^\mu U^\dagger_L U_L \nu'_L + \bar{\nu}'_L \gamma^\mu U^\dagger_L V N'^{\mathcal{C}}_R \\ &\quad + \overline{N'^{\mathcal{C}}_R} \gamma^\mu V^\dagger U_L \nu'_L + \overline{N'^{\mathcal{C}}_R} \gamma^\mu V^\dagger V N'^{\mathcal{C}}_R \Big] Z_\mu \end{aligned} \tag{2.3.14}$$

In canonical Type-I seesaw, heavy neutrino mass scale is $\mathcal{O}\,(10^{12} - 10^{14}$ GeV), as a result $M \gg m_D$ is a very good approximation. Consequently $\mathcal{O}\,(m_D^2/M^2)$ terms can be dropped out (*i.e.* $\epsilon \simeq 0$, and $\epsilon' \simeq 0$) and one can recover the conventional Type-I seesaw mass matrix (2.3.3) from Eq. (2.3.11). Also unitarity of U_L and hence U_{PMNS} is maintained.

U_{PMNS} being a 3×3 unitary matrix, can be parameterized by three 3 angles and 6 phases. Out of 6 phases, 3 phases can be removed by the redefinition of the left-handed neutrino fields. Thus 3 angles and 3 phases can affect observables if the neutrinos are Majorana particle. We follow the parameterization of the mixing matrix given by

$$\begin{aligned} U_{\text{PMNS}} &= U_{23}(\theta_{23}) U_{13}(\theta_{13}, \delta) U_{12}(\theta_{12}) P \\ &= \begin{pmatrix} c_{12}c_{13} & s_{12}c_{13} & s_{13}e^{-i\delta} \\ -s_{12}c_{23} - c_{12}s_{23}s_{13}e^{i\delta} & c_{12}c_{23} - s_{12}s_{23}s_{13}e^{i\delta} & s_{23}c_{13} \\ s_{12}s_{23} - c_{12}c_{23}s_{13}e^{i\delta} & -c_{12}s_{23} - s_{12}c_{23}s_{13}e^{i\delta} & c_{23}c_{13} \end{pmatrix} P \end{aligned} \tag{2.3.15}$$

where the U_{ij} are matrices of rotations in the ij plane by angle θ_{ij} , $s_{ij} = \sin\theta_{ij}, c_{ij} = \cos\theta_{ij}$, δ is the Dirac CP violating phase attached to $1-3$ rotation. $P\left(= \text{diag}\left(e^{i\alpha_1/2}, e^{i\alpha_2/2}, 1\right)\right)$ contains Majorana phases. Present experimental bounds on the mass squared differences and the mixing angles, from the global analysis of neutrino oscillation data, are tabulated in Table 1.1 [36]. All phases are currently unconstrained.

Reconstruction of the Yukawa coupling

The Yukawa coupling matrix (Y_ν) can be expressed in terms of low energy

parameters as below [72]

$$Y_\nu = \frac{\sqrt{2}}{v} U_R^* M_{diag}^{1/2} R m_{diag}^{1/2} U_{PMNS}^\dagger \tag{2.3.16}$$

where M_{diag} and m_{diag} are heavy neutrino and effective light neutrino mass matrix in the diagonal basis. U_R^* is a unitary matrix that diagonalizes M. R is a complex orthogonal matrix and can be parameterized as [122]

$$R = O\, e^{iA} \tag{2.3.17}$$

where O and A are real matrices. Orthogonality of R requires O to be orthogonal and A to be antisymmetric. In the quasi-degenerate light neutrino spectrum, O can be absorbed in U_{PMNS} which leads to the same physics hence O can be taken to be unity. Also in a basis where heavy neutrino mass matrix is diagonal, U_R becomes unity ($U_R = 1$). In such cases Y_ν contains less number of parameters and hence increases the predictivity of the model. However in general scenarios, such parameterization does not reduce the number of undetermined parameters.

2.3.2 Type-II and Type-III seesaw mass matrices

In Type-II seesaw mechanism, one adds $SU(2)$ triplet Higgs field to the SM particle spectra. The extended part of the Lagrangian is given by [123, 124]

$$\begin{aligned} \mathcal{L}_{\rm ext}^{\rm II} &= -(Y_\Delta^r)_{ji}\, \overline{l_{\beta j}^{\mathcal{C}}}\, \epsilon_{\beta\gamma}\, \Delta_{\gamma\alpha}^r P_L\, l_{\alpha i} + \mu_\Delta^r\, \phi_\beta\, \epsilon_{\beta\gamma}\, \Delta_{\gamma\alpha}^r\, \phi_\alpha \\ &\quad - (M_\Delta^{rs})^2\, {\rm Tr}\left[\Delta^{r\dagger}\Delta^s\right] + {\rm h.c.} \end{aligned} \tag{2.3.18}$$

where the triplet Higgs field, Δ in adjoint representation, is given by

$$\Delta = \begin{pmatrix} \frac{1}{\sqrt{2}}\Delta^+ & \Delta^{++} \\ \Delta^0 & -\frac{1}{\sqrt{2}}\Delta^+ \end{pmatrix} \tag{2.3.19}$$

$r\,, s$ are the number of triplet Higgs fields which is at least two for successful leptogenesis [125]. Apart from the above Lagrangian, the SM potential receives additional terms due to the presence of the extra Higgs field which we shall not write down explicitly. After symmetry breaking, the neutral component of Δ^r also receives VEV, $v_\Delta^r = (\mu_\Delta^r)^*\, v^2/\,(M_\Delta^r)^2$. The light neutrino mass matrix is given by

$$m_\nu = m_L = 2\,(Y_\Delta^r v_\Delta^r) \tag{2.3.20}$$

For $\mu_\Delta \sim M_\Delta \sim 10^{12} - 10^{14}$ GeV, $v_\Delta \sim v^2/M_\Delta$ which is of the form of seesaw suppression. For $\mathcal{O}(1)$ Yukawa coupling, this would naturally give the correct light neutrino mass term.

In Type-III seesaw model one adds triplet fermion in place of singlet fermion of Type-I seesaw. The additional part of the Lagrangian is given by

$$\mathcal{L}_{\rm ext}^{\rm III} = -\,(Y_\Sigma)_{ji}\,\tilde{\phi}^\dagger \overline{\Sigma}_j P_L\, l_i - \frac{1}{2}\,(M_\Sigma)_{ji}\,{\rm Tr}\left[\overline{\Sigma}_j P_R \tilde{\Sigma}_i\right] + {\rm h.c.} \tag{2.3.21}$$

where Σ and $\tilde{\Sigma}$ are given by

$$\Sigma = \begin{pmatrix} \frac{1}{\sqrt{2}}\Sigma^0 & \Sigma^+ \\ \Sigma^- & -\frac{1}{\sqrt{2}}\Sigma^0 \end{pmatrix} \qquad\qquad \tilde{\Sigma} = \epsilon\, \mathcal{C}\overline{\Sigma}^T \epsilon \tag{2.3.22}$$

$\mathcal{C}$ stands for charge conjugation. The light neutrino mass matrix is same as in Type-I seesaw mechanism with Y_ν and M replaced by Y_Σ and M_Σ respectively.

Type III seesaw mechanism can naturally be obtained in $SU(5)$ GUT model by adding $SU(2)$ triplet fermion to the 24_F dimensional representation of $SU(5)$ [118–120]. On the other hand, Type I and Type II seesaw mechanism naturally arise in $SO(10)$ GUT models. The 16 dimensional representation of $SO(10)$ in the fermionic multiplet contains one singlet right handed fermion field which can be the right handed neutrino. In $SO(10)$ GUT one needs at least two Higgs multiplet to reproduce correct masses for quarks and leptons. In the combinations $(10_H, \overline{126}_H)$ and $(120_H, \overline{126}_H)$, the singlet neutrino

receives mass from the $SU(2)_R$ triplet fields of the 126 dimensional representation of Higgs [12]. This fermion can be in the region between left-right symmetry breaking scale and GUT scale. Below its mass scale, the fermionic field gets integrated out giving rise to light neutrino mass at electro weak scale. Besides, the 126 dimensional representation of Higgs field also contains color singlet $SU(2)_L$ triplet field which naturally gives mass to light neutrino via Type-II seesaw [113–117]. In another combination $(10_H, 120_H)$, neutrino mass is obtained either through two loop radiative correction with additional $(16_H, \overline{16}_H)$ Higgs [126] or through double seesaw by adding matter fields in the adjoint representation of $SO(10)$ (45_F) with $\overline{16}_H$ Higgs [127]. Type I seesaw can also be obtained along with Type III in the $SU(5)$ model as the adjoint representation (24_F) contains a singlet too.

2.3.3 Inverse and linear seesaw mass matrices

In inverse or linear seesaw model one adds an extra singlet in addition to the right handed neutrino. The Yukawa part of the most general Lagrangian involving extra singlet states can be written as

$$\begin{aligned} -\mathcal{L} &= \overline{N}_R Y_\nu \tilde{\phi}^\dagger l_L + \overline{S} Y_S \tilde{\phi}^\dagger l_L + \overline{S} M_R N_R^c + \frac{1}{2}\overline{S}\mu S^c + \frac{1}{2}\overline{N_R} M_N N_R^c \\ &\quad + \text{h.}c. \end{aligned} \tag{2.3.23}$$

where $l_L = (\nu_x, x)_L^T$, $x = e, \mu, \tau$. l_L, N_R and S have lepton number $1, 1, -1$, respectively. After spontaneous symmetry breaking, the ϕ field acquires a vacuum expectation value $(v/\sqrt{2})$ and $Y_\nu v/\sqrt{2} = m_D$ gives rise to the Dirac mass term while the term $Y_s v/\sqrt{2} = m_S$ breaks lepton number. In the above Lagrangian lepton number violation stems from the terms with coefficients Y_s, μ and M_N and thus the symmetry of the Lagrangian is enhanced (lepton number becomes an exact symmetry) in the absence of these terms. Therefore these coefficients are expected to be naturally small (i.e. there is no *fine tuning* or *unnaturalness* in keeping these terms to be very small) according to 't Hooft's naturalness criterion.

The neutrino mass matrix in the (ν_L, N_R^c, S^c) basis can be written as

$$\mathcal{M}_\nu = \begin{pmatrix} 0 & m_D^T & m_S^T \\ m_D & M_N & M_R^T \\ m_S & M_R & \mu \end{pmatrix}. \tag{2.3.24}$$

In the literature many variants of this model have been considered.

Inverse Seesaw

The conventional inverse seesaw models assume the terms m_S and M_N in Eq. 2.3.24 to be zero. Then the mass matrix takes the form,

$$\mathcal{M}_\nu = \begin{pmatrix} 0 & m_D^T & 0 \\ m_D & 0 & M_R^T \\ 0 & M_R & \mu \end{pmatrix}. \tag{2.3.25}$$

The model is lepton number conserving in the limit μ tending to zero. The minimal inverse seesaw model considered in the literature [128] consists of $3\nu_L + 2N_R + 2S$. The model with $3\nu_L + 1N_R + 1S$ is a 5×5 matrix with rank 3. Thus there are two zero eigenvalues of this matrix which is not consistent with low energy phenomenology. The model consisting of $3\nu_L + 2N_R + 1S$ is a 6×6 matrix with rank 5. Thus there is one zero eigenvalue. However, this belongs to the (N_R, S) block and hence this scenario is not considered if one assumes that there are no light singlets. In Eq. (2.3.25) the Majorana mass term of N_R is not considered. In principle this can be included [129, 130], although this does not change the structure of the effective light neutrino mass matrix at the leading order [131, 132].

Linear Seesaw

In the so called linear seesaw models [81–83] one retains the $\nu - S$ term in the Lagrangian through the Yukawa coupling matrix Y_s and makes the μ and the M_N term to be zero. In these models lepton number violation stems from the

term containing Y_s. The corresponding mass matrix is,

$$\mathcal{M}_\nu = \begin{pmatrix} 0 & m_D^T & m_S^T \\ m_D & 0 & M_R \\ m_S & M_R^T & 0 \end{pmatrix}. \tag{2.3.26}$$

In the limit $M_R >> m_D, m_S$ the above mass matrix can be diagonalized using the seesaw approximation and in the leading order the effective light neutrino mass matrix m_{light} can be expressed as

$$m_\nu = m_D^T {M_R}^{-1} m_S + m_S^T {M_R}^{-1} m_D. \tag{2.3.27}$$

Since this contains only one power of the Dirac mass term it is called linear seesaw.

One can make an order of magnitude estimate of the various terms to check the conditions required to get $m_\nu \sim 0.1$ eV. Assuming typical values $m_D \sim 100$ GeV (Yukawa coupling strength $Y_\nu \sim \mathcal{O}(1)$, $v \sim 100$ GeV) and $M_R = 1$ TeV one needs $Y_s \sim 10^{-11}$. In the heavy sector we get two degenerate neutrinos of mass $\sim$ TeV. The minimal model consists of adding just two singlet states N_R and S. The rank of the 3+1+1 mass matrix is 4 corresponding to one zero mass eigenvalue. The Majorana mass term M_N can also be included which would lift the degeneracy between the heavy states, However, the contribution of this term to the light neutrino mass matrix is sub-dominant [131, 132].

Inverse + Linear Seesaw

It is also possible to keep both the terms m_s and μ in the Lagrangian. Then in the limit $M_R >> m_D, m_S$ and in the leading order the effective light neutrino mass matrix m_{light} can be expressed as

$$m_\nu = -m_D^T \frac{\mu}{M_R^2} m_D + m_D^T \frac{1}{M_R} m_S + m_S^T \frac{1}{M_R} m_D. \tag{2.3.28}$$

In this case, for $M_R \sim$ TeV, one needs $\mu \sim 10^{-8}$ GeV and $Y_s \sim 10^{-11}$. As discussed earlier Minimal Linear Seesaw Model (MLSM) contains one N and

one S. This feature makes the model fully reconstructible from the low energy parameter (as we shall see later) and draws special attention for prediction. The full mass matrix can be recasted as,

$$\mathcal{M}_\nu = \begin{pmatrix} 0 & {m'_D}^T \\ m'_D & M \end{pmatrix} \tag{2.3.29}$$

where $m'^T_D = (m^T_D, m^T_S)$ and M is given by

$$M = \begin{pmatrix} 0 & M_R \\ M_R & 0 \end{pmatrix} \tag{2.3.30}$$

The eigenvalues (M_1, M_2) are obtained as $(-M_R, M_R)$ corresponding to degenerate neutrinos with opposite CP parities. The negative sign in the mass eigenvalues can be absorbed in the phases of the diagonalizing matrix U_R giving,

$$U_R = \frac{1}{\sqrt{2}} \begin{pmatrix} i & 1 \\ -i & 1 \end{pmatrix} \tag{2.3.31}$$

In this model, the mass and gauge eigenstates are related as in Eq. (2.3.12). For convenience, we write is as follows

$$\begin{pmatrix} \nu_L & \nu^c \end{pmatrix} = U_L \begin{pmatrix} {\nu_L}' & \nu^{c\prime} \end{pmatrix} \tag{2.3.32}$$

where,

$$\nu^c = \begin{pmatrix} N^c_R & S^c \end{pmatrix} \tag{2.3.33}$$

The leptonic part of the charged current interaction in the mass basis (2.3.13) can be re-expressed as,

$$\mathcal{L}_{\rm CC} = \frac{g}{\sqrt{2}} \left[\overline{\ell'}_{\alpha\, L}\, \gamma_\mu\, U^\dagger_e \{ (U_L)_{\alpha i} \nu'_{Li} + (V)_{\alpha j} N^c_{Rj} \} W^\mu \right] + \text{h.c.} \tag{2.3.34}$$

The PMNS matrix is defined as in Eq. (1.0.5)

$$U_{\rm PMNS} = U_e^\dagger \left(1 - \frac{1}{2}\epsilon\right) U_L \tag{2.3.35}$$

where U_e is the unitary matrix which takes the left-handed charged lepton fields to their mass basis. In a basis, where charged lepton mass matrix is diagonal, U_e is being taken as unity. For TeV scale seesaw model $M \sim \mathcal{O}(\text{TeV})$ and hence ϵ can not be neglected. As a result, U_{PMNS} becomes non-unitary and the correction to unitarity is proportional to $\epsilon/2$.

Inverse seesaw mechanism naturally arises in E_6 GUT [9]. The 27 dimensional representation of E_6 under $(SO(10), SU(5))$ subgroups contains an extra singlet fermion which can give rise to light neutrino masses through inverse seesaw mechanism.

2.3.3.1 Reconstruction of the Yukawa coupling

In this subsection, we demonstrate how the Yukawa coupling matrices of the MLSM can be reconstructed apart from an overall constant. m_ν for this case, Eq. (2.3.27), can also be expressed in terms of two independent vectors

$$Y_\nu \equiv y_\nu \hat{\mathbf{a}}; \quad Y_S \equiv y_s \hat{\mathbf{b}} \tag{2.3.36}$$

where $\hat{\mathbf{a}}$ and $\hat{\mathbf{b}}$ are complex vectors with unit norm. y_ν and y_s are the norms of the Yukawa matrices Y_ν and Y_S, respectively. This feature allows one to completely reconstruct the Yukawa matrices Y_ν and Y_S in terms of the oscillation parameters as [133],

- Normal Hierarchy (NH): $(m_1 < m_2 < m_3)$

$$\begin{aligned} Y_\nu &= \frac{y_\nu}{\sqrt{2}} \left(\sqrt{1+\rho}\, U_3^\dagger + \sqrt{1-\rho}\, U_2^\dagger\right) \\ Y_S &= \frac{y_s}{\sqrt{2}} \left(\sqrt{1+\rho}\, U_3^\dagger - \sqrt{1-\rho}\, U_2^\dagger\right) \end{aligned} \tag{2.3.37}$$

with ρ given by,

$$\rho = \frac{\sqrt{1+r} - \sqrt{r}}{\sqrt{1+r} + \sqrt{r}} \tag{2.3.38}$$

U_i's are the columns of the unitary matrix U that diagonalizes the light neutrino mass matrix (m_{light}) above and r is the ratio of the solar and atmospheric mass squared differences.

$$r = \frac{\Delta m^2_{\odot}}{\Delta m^2_{atm}} \tag{2.3.39}$$

where $\Delta m^2_{\odot}$ denotes the solar mass square difference (Δm^2_{21}) and Δm^2_{atm} denotes the atmospheric mass square difference ($|\Delta m^2_{32}|$ for NH, $|\Delta m^2_{31}|$ for IH).

- For inverted Hierarchy (IH): $(m_3 << m_2 \approx m_1)$

$$\begin{aligned} Y_\nu &= \frac{y_\nu}{\sqrt{2}} \left(\sqrt{1+\rho}\, U_2^\dagger + \sqrt{1-\rho}\, U_1^\dagger \right) \\ Y_S &= \frac{y_s}{\sqrt{2}} \left(\sqrt{1+\rho}\, U_2^\dagger - \sqrt{1-\rho}\, U_1^\dagger \right) \end{aligned} \tag{2.3.40}$$

with

$$\rho = \frac{\sqrt{1+r} - 1}{\sqrt{1+r} + 1}. \tag{2.3.41}$$

For Inverse + Linear seesaw, the Yukawa couplings can also be reconstructed but with two unknown parameters. The parameter μ in Eq. (2.3.28) will introduce an extra unknown parameter in Y_S in addition to y_s, as mentioned in [133].

2.3.4 SUSY seesaw

In SUSY theories light neutrino gets mass in a similar manner as in extended SM. R-parity (introduced to evade proton decay) conserving MSSM does not include a neutrino mass term. Addition of heavy neutrino superfield to the

MSSM, modifies the MSSM superpotential in the following manner

$$\mathcal{W}_{\nu\text{MSSM}} = \mathcal{W}_{\text{MSSM}} + \mathcal{W}_{\text{new}} \tag{2.3.42}$$

$\mathcal{W}_{\text{new}}$ is given by

$$\mathcal{W}_{\text{new}} = -\left(Y_\nu\right)_{ji} \mathcal{L}_j \cdot \mathcal{H}_u \mathcal{N}^c_{Ri} - \frac{1}{2} M_{ji} \mathcal{N}^c_{Rj} \mathcal{N}^c_{Ri} \tag{2.3.43}$$

where $\mathcal{N}^c_R$ is left handed. Fields are written in curly notation to denote superfields. The light neutrino mass matrix is same as in extended SM except the Dirac mass term for neutrino in νMSSM gets modified as $m_D = Y_\nu \frac{v_u}{\sqrt{2}}$, where v_u is the VEV for the up-type ($Y = +1$) Higgs doublet, H_u, given by

$$v_u = v \sin\beta \qquad \text{where} \quad \beta = \tan^{-1}\left(\frac{v_u}{v_l}\right) \tag{2.3.44}$$

v_l is the VEV of the down type ($Y = -1$) Higgs doublet, H_d.

2.4 Implications of Seesaw mechanism

In this section we shall briefly discuss the phenomenological implications of the right handed fermion field introduced in Type-I seesaw mechanism.

2.4.1 CP Violation and Leptogenesis

In the neutrino oscillations, CP violation may be observed in the difference between the appearance probabilities $P(\nu_\alpha \to \nu_\beta) - P(\bar{\nu}_\alpha \to \bar{\nu}_\beta)$ with $\alpha \neq \beta$. The difference is proportional to the leptonic version of the Jarlskog invariant [134]

$$J_{CP} = \text{Im}\left\{U_{e1}\, U_{\mu 2}\, U^*_{e2}\, U^*_{\mu 1}\right\} \tag{2.4.1}$$

A promising channel for the discovery of CP violation is $P(\nu_\mu \to \nu_e) - P(\bar{\nu}_\mu \to \bar{\nu}_e)$ in long-baseline experiments such as T2K and NOνA [135].

In order to have CP violation, the mass matrices — or the Yukawa sector of the Lagrangian — must have at least one complex phase which is not absorbed by field redefinitions. To ascertain if there exists such phase degrees of freedom, it is convenient to evaluate the weak basis invariant quantities [136–138]

$$I_l = \mathrm{Tr}\left[m_\nu m_\nu^\dagger, m_l m_l^\dagger\right]^3, \tag{2.4.2}$$

$$I_{h'} = \mathrm{Im}\left(\mathrm{Tr}\left[h' H M^* h'^* M\right]\right) \tag{2.4.3}$$

where m_l is the charged-lepton mass matrix and $h' \equiv m_D^\dagger m_D$, $H \equiv M^\dagger M$. The necessary conditions for successful leptogenesis and the observation of CP violation in oscillation experiments are $I_h \neq 0$ and $I_l \neq 0$ respectively. It is to be noted that in general in models with three right handed neutrinos there are three weak basis invariants that can be related to CP violation responsible for leptogenesis [136–138]. However for models with two right handed neutrinos these three are not independent and are proportional to each other. The other weak basis invariants obtained by substituting $m_D^\dagger m_l m_l^\dagger m_D$ in place of h' in $I_{h'}$ are not related to leptogenesis as shown in [136–138]. Therefore it is sufficient to consider only $I_{h'}$ to check if the CP violation at high energy is related to leptogenesis or not. The low-energy invariant I_l is related to J_{CP} as [136–138]

$$I_l = -6i\Delta_{\mu e}\Delta_{\tau\mu}\Delta_{\tau e}\Delta m^2_{21}\Delta m^2_{31}\Delta m^2_{32} J_{CP} \tag{2.4.4}$$

where $\Delta_{\gamma\beta} = (m_\gamma^2 - m_\beta^2)$, with $\gamma, \beta = e, \mu, \tau$ and Δm^2_{ij} are the light neutrino mass squared differences defined earlier. Using Eq. (2.4.2) and Eq. (2.4.4) one would obtain

$$J_{CP} = -\frac{\mathrm{Im}\left\{h_{12}\, h_{23}\, h_{31}\right\}}{\Delta m^2_{21}\, \Delta m^2_{31}\, \Delta m^2_{32}} \tag{2.4.5}$$

where $h = m_\nu\, m_\nu^\dagger$. With the parameterization of Eq. (2.3.16) and using Eq. (2.4.1), one has

$$J_{CP} = \frac{1}{8}\, \sin 2\theta_{12}\, \sin 2\theta_{23}\, \sin 2\theta_{13}\, \cos\theta_{13}\, \sin\delta \tag{2.4.6}$$

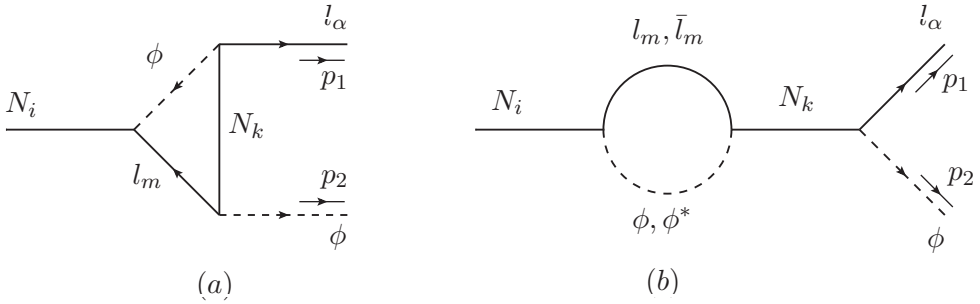

Figure 2.4: *Diagrams contributing to the (a: vertex, b: wave function) CP asymmetry in the heavy neutrino decay.*

Another place where CP violation in the lepton sector plays an important role is leptogenesis, even though in general the low and high energy CP violations can be completely uncorrelated. Let us consider the decay of one heavy right-handed neutrino N_i into Higgs and lepton doublets governed by the Lagrangian (2.2.1). The CP asymmetry generates through the interference between tree level and one loop heavy Majorana neutrino decay diagrams (Fig. 2.4).
The CP asymmetry is given by [56]:

$$\begin{aligned}
\varepsilon_i &= \sum_\alpha \varepsilon_i^\alpha \equiv \frac{\sum\limits_\alpha \Big[\Gamma(N_i \to \phi\, l_\alpha) - \Gamma(N_i \to \phi^\dagger\, \bar{l}_\alpha)\Big]}{\sum\limits_\beta \Big[\Gamma(N_i \to \phi\, l_\beta) + \Gamma(N_i \to \phi^\dagger\, \bar{l}_\beta)\Big]} \\
&= \frac{1}{4\pi\, v^2}\, \frac{1}{(\tilde{m}_D^*\, \tilde{m}_D^T)_{ii}} \sum_{j\neq i} \sum_\alpha \left(\mathcal{I}_{ij}^\alpha\, f\left(M_j^2/M_i^2\right) + \mathcal{J}_{ij}^\alpha\, \frac{1}{1 - M_j^2/M_i^2} \right) \qquad (2.4.7) \\
&= \frac{1}{4\pi\, v^2}\, \frac{1}{(\tilde{m}_D^*\, \tilde{m}_D^T)_{ii}} \sum_{j\neq i} \mathrm{Im}\left[\left(\tilde{m}_D^*\, \tilde{m}_D^T\right)_{ij}^2 \right] f\left(M_j^2/M_i^2\right) \qquad (2.4.8)
\end{aligned}$$

where

$$\begin{aligned}
\mathcal{I}_{ij}^\alpha &= \mathrm{Im}\Big[\big(\tilde{m}_D^*\big)_{i\alpha} \big(\tilde{m}_D^T\big)_{\alpha j} \big(\tilde{m}_D^* \tilde{m}_D^T\big)_{ij} \Big] \\
\mathcal{J}_{ij}^\alpha &= \mathrm{Im}\Big[\big(\tilde{m}_D^*\big)_{i\alpha} \big(\tilde{m}_D^T\big)_{\alpha j} \big(\tilde{m}_D^* \tilde{m}_D^T\big)_{ji} \Big] \qquad (2.4.9)
\end{aligned}$$

$$f(x) = \begin{cases} \sqrt{x}\left[1 + \frac{1}{1-x} - (1+x)\ln\left(\frac{1+x}{x}\right)\right] & \text{SM} \\ \sqrt{x}\left[\frac{2}{1-x} - \ln\left(\frac{1+x}{x}\right)\right] & \text{MSSM} \end{cases} \qquad (2.4.10)$$

Here ε_i^α describes the decay asymmetry of the right-handed neutrino of mass M_i into leptons of flavor $\alpha = e, \mu, \tau$. In MSSM there will be additional diagrams with particles in the loops replaced by their superpartners and in the expression of CP asymmetry, v^2 should be replaced by v_u^2.

If the rest-mass of the lightest heavy neutrino is much lighter than the other two, i.e. $M_1 \ll M_{2,3}$, the lepton asymmetry is dominated by the decay of this lightest of the heavy neutrinos. In this case $f(M_j^2/M_1^2) \simeq -3\, M_1/M_j$. Moreover, only the first term proportional to $\mathcal{I}_{1j}^\alpha$ in Eq. (2.4.7) is relevant then since the second term proportional to $\mathcal{J}_{ij}^\alpha$ is suppressed by an additional power of M_1/M_j. The second term in Eq. (2.4.7) vanishes when one sums over flavors to obtain the flavor independent decay asymmetry. It is to be noted that in the decay mode, the right-handed neutrino mass matrix is diagonal ($M^{\rm diag} = U_R^T M U_R$). So $\tilde{m}_D$ is given by $\tilde{m}_D = U_R^T m_D$.

Baryon Asymmetry of the Universe

Final lepton asymmetry can be obtained by solving the Boltzmann equation. In lepton asymmetry, the effective mass parameters which are responsible for the wash-out are important. The wash-out of every decay asymmetry ε_i^α is governed by an effective mass

$$\tilde{m}_i^\alpha = \frac{(\tilde{m}_D^*)_{i\alpha}\,(\tilde{m}_D^T)_{\alpha i}}{M_i}\,. \tag{2.4.11}$$

The above implies no summation over i. The summation of $\tilde{m}_i^\alpha$ over the flavor index α yields $\tilde{m}_i$, which is the relevant parameter for the wash-out of ε_i. One needs to insert the effective masses in the resultant lepton asymmetry η_L, given by

$$\eta_L \simeq \frac{1}{g_*} \sum_i \kappa_i \varepsilon_i \tag{2.4.12}$$

where κ_i are the factor which represent wash-out effect calculated by solving the Boltzmann equations, and g_* is the number of relativistic degrees of freedom. The wash-out effect strongly depends on the effective mass $\tilde{m}_i =$

$(\tilde{m}_D \tilde{m}_D^\dagger)_{ii}/M_i$. If the right-handed neutrinos are strongly coupled to the thermal bath $\tilde{m}_i \gtrsim 10^3\,\text{eV}$, an approximate analytic expression for the factor κ_i is available [139, 140]

$$\kappa_i \simeq 0.3 \left(\frac{10^{-3}\,\text{eV}}{\tilde{m}_i}\right) \left(\ln \frac{\tilde{m}_i}{10^{-3}\,\text{eV}}\right)^{-0.6}. \tag{2.4.13}$$

Finally a part of lepton asymmetry is converted to the baryon asymmetry, η_B, by the sphaleron processes in thermal equilibrium and leads to the relation $\eta_B = -28/51\,\eta_L$ in the SM [57].

2.4.2 Lepton Flavor Violation

Lepton flavor violating decay process, $\mu \to e\,\gamma$ can be mediated through light neutrino. Branching ratio is given by

$$\text{Br}\,(\mu \to e\,\gamma) = \frac{\Gamma\,(\mu \to e\,\gamma)}{\Gamma\,(\mu \to e\,\overline{\nu_e}\,\nu_\mu)} \tag{2.4.14}$$

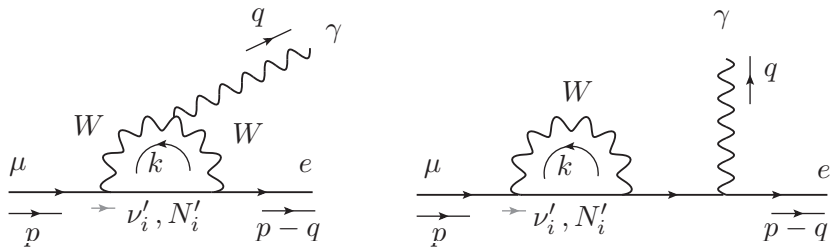

Figure 2.5: *Representative diagrams contributing to the LFV process.*

In unitary gauge, there is another diagram similar to the second one with the photon connected to the μ line. However in $R\,\xi$ gauge there will be other diagrams containing goldstone bosons [65].

Branching ratio (proportional to m_i^4/m_W^4) is tiny ($\sim \mathcal{O}(10^{-40})$) if mediated through light neutrinos only. Hence it cannot be probed through experiment. In presence of heavy fermion, branching ratio is given by [68]

$$\text{Br}\,(\mu \to e\,\gamma) = \frac{3\alpha}{8\pi} \left| V_{ei} V_{i\mu}^\dagger f(x) \right|^2, \tag{2.4.15}$$

where

$$x = \left(\frac{M_i^2}{m_W^2}\right), \qquad f(x) = \frac{x\,(1 - 6x + 3x^2 + 2x^3 - 6x^2\ln x)}{2(1-x)^4} \tag{2.4.16}$$

$f(x)$ is a slowly varying function of x ranging from 0 to 1 for x between 0 to infinity. The light-heavy mixing matrix V is define in Eq. (2.3.7). Through large light-heavy mixing, branching ratio can be enhanced significantly.

In the seesaw extended MSSM, there are additional diagrams containing super particles in the loops. Expression for the decay width of $\mu \to e\,\gamma$ is some what lengthy and can be found in [141–143]. For canonical seesaw, the mass scale of the heavy neutrino is $\mathcal{O}\,(10^{12}$ GeV), and hence the SM seesaw contribution (2.4.15) is negligible. However for MSSM seesaw even with $M_R \sim 10^{12}$ GeV, the LFV processes can be enhanced significantly through the non diagonal term of the slepton mass matrix. In order to avoid very large branching ratio for LFV processes, one assume universal minimal super gravity conditions *i.e.* all the scalars have same mass at the gravitational scale $\left(M_X = M_{pl}/\sqrt{8\pi}\right)$. RGE form M_X to M_R would induce small non diagonal elements to the slepton mass matrix, thus can give the branching ratio for $\mu \to e\,\gamma$ below the present experimental lower bound (2.4×10^{-12}) [144]. Branching ratio is given by [143]

$$\begin{aligned} \mathrm{BR}(\mu \to e\,\gamma) &= c \times \left|\left(m_{\tilde{l}}^2\right)_{e\mu}\right|^2 \\ &\simeq c' \times \left|(\tilde{m}_D\, L\, \tilde{m}_D^\dagger)_{e\mu}\right|^2 \end{aligned} \tag{2.4.17}$$

where $m_{\tilde{l}}$ is the slepton mass matrix. $c\,, c'$ are constants containing loop factors, scalar and gaugino masses, universal trilinear gauge couplings, tanβ. L is diagonal matrix, given by

$$L_{kl} = \ln\frac{M_X}{M_k}\,\delta_{kl}, \tag{2.4.18}$$

M_k being the mass of the k^{th} heavy neutrino.

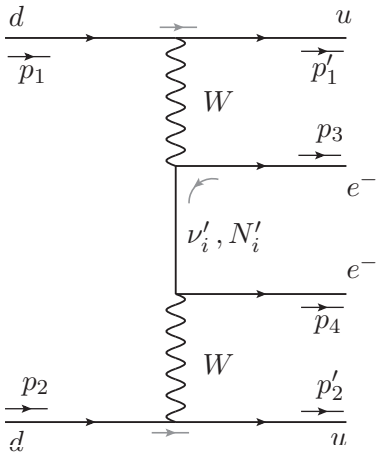

Figure 2.6: *Typical diagram contributing to the* $0\nu\beta\beta$ *process.*

2.4.3 Neutrino less Double Beta decay

Usual beta decay contains neutrino in the final state. But in principle double beta decay can take place without any neutrino in the final state due to Majorana nature of neutrinos as depicted in Fig. 2.6.

The half life for neutrino-less double beta decay in presence of heavy singlets is given by [54, 55]

$$T^{-1}_{(1/2)} = G\frac{|\mathcal{M}_\nu|^2}{m_e^2}\,|m_{ee}|^2 \tag{2.4.19}$$

where m_e is the electron mass, m_{ee} is the effective mass governing neutrino less double beta decay. It is given by

$$m_{ee} = U^2_{L_{e\,i}}\,m_i + \langle\, p^2\rangle \frac{V^2_{e\,i}}{M_i} \tag{2.4.20}$$

First term is the usual light neutrino contribution. The second term is the additional contribution due to heavy neutrino and is suppressed for heavy neutrino mass scale $\mathcal{O}\,(10^{12}$ GeV). $\langle\, p^2\rangle$ is given by [145]

$$\langle\, p^2\rangle = -\,m_e m_p \frac{\mathcal{M}_N}{\mathcal{M}_\nu}, \tag{2.4.21}$$

$\mathcal{M}_\nu$ and $\mathcal{M}_N$ denote the nuclear matrix elements corresponding to light and

heavy neutrino exchange respectively. m_p is the proton mass. The typical values of the parameters are [54] $G = 7.93 \times 10^{-15}$ yr^{-1}, $\mathcal{M}_N = 363 \pm 44$, $\mathcal{M}_\nu = 5.24 \pm 0.52$, $\langle p^2 \rangle = -(182 \text{ MeV})^2$. V is defined in Eq. (2.3.7).

2.4.4 Stability of the electro weak vacuum

2.4.4.1 Vacuum stability in SM

The tree-level potential of the Higgs field in the the Standard Model(SM) is given as

$$V(\Phi) = \lambda \left(\phi^\dagger \phi\right)^2 - m^2 \phi^\dagger \phi. \tag{2.4.22}$$

The physical Higgs mass is defined as $m_h^2 = 2\lambda\, v^2$. Higgs quartic coupling, λ, receives quantum corrections from higher order loop diagrams. As a result it runs with renormalization scale, μ. The Renormalization Group (RG) equation for the Higgs quartic coupling λ can be expressed in general as

$$\mu \frac{d\lambda}{d\mu} = \sum_i \frac{{\beta_\lambda}^{(i)}}{(16\pi^2)^i} \tag{2.4.23}$$

where i denotes the i^{th} loop. The β function of λ in SM upto 1 loop is given as,

$$\beta_\lambda^{(1)} = 24\lambda^2 - \left(\frac{9}{5} g_1^2 + 9 g_2^2\right) \lambda + \frac{27}{200} g_1^4 + \frac{9}{20} g_1^2 g_2^2 + \frac{9}{8} g_2^4 + 4 T_1 \lambda - 2 Y_1 \tag{2.4.24}$$

where,

$$T_1 = \text{Tr}\left[3 {Y_u}^\dagger Y_u + 3 {Y_d}^\dagger Y_d + {Y_l}^\dagger Y_l\right] \tag{2.4.25}$$

$$Y_1 = \text{Tr}\left[3 ({Y_u}^\dagger Y_u)^2 + 3 ({Y_d}^\dagger Y_d)^2 + ({Y_l}^\dagger Y_l)^2\right] \tag{2.4.26}$$

In the above equations, g_i denote the gauge couplings with $i = 1, 2, 3$ corresponding to $U(1)$, $SU(2)$ and $SU(3)$ gauge groups respectively. The above equations include the Grand Unified Theory (GUT) modified coupling for the U(1). Y_f with $f = u, d, l$ represent the Yukawa coupling matrices for the up quarks, down quarks and the charged leptons. The running behavior is con-

trolled mainly by the top Yukawa coupling Y_t which drives λ towards more negative values in the low Higgs mass region. The running of the top Yukawa is governed by the following equations

$$\beta_{Y_u}^{(1)} = Y_u \left[\frac{3}{2} Y_u{}^\dagger Y_u + \frac{3}{2} Y_d{}^\dagger Y_d + T - \left(\frac{17}{20} g_1^2 + \frac{9}{4} g_2^2 + 8 g_3^2 \right) \right]. \tag{2.4.27}$$

where u stands for up quark family. Two loop RG Equations for λ, the Yukawa and the gauge couplings are used for numerical analysis [146–150] and can be found in Appendix B. As discussed earlier the constraints from vacuum stability and perturbativity, limits Higgs mass in the range 126-171 GeV. Therefore if the scalar particle observed by the CMS [5] and ATLAS [6] collaboration is assumed to be the Higgs Boson then the reported mass is near the lower bound obtained from vacuum stability condition.

Considering the one loop effective potential for the Higgs field, the effective Higgs quartic coupling $\tilde{\lambda}$, for sufficiently large value of the Higgs field ϕ, is given by* [151, 152]

$$\begin{aligned} \tilde{\lambda} \;=\; & \lambda - \frac{1}{32\pi^2} \left[\frac{3}{8} \left(\frac{3}{5} g_1^2 + g_2^2 \right)^2 \left(\frac{1}{3} - \ln \frac{\left(\frac{3}{5} g_1^2 + g_2^2 \right)}{4} \right) \right. \\ & \left. + 6 Y_t^4 \left(\ln \frac{Y_t^2}{2} - 1 \right) + \frac{3}{4} g_2^4 \left(\frac{1}{3} - \ln \frac{g_2^2}{4} \right) \right] \end{aligned} \tag{2.4.28}$$

In Fig. 2.7, we plot the running of λ and $\tilde{\lambda}$ as functions of the renormalization scale for illustrative values of Higgs mass (m_h), top mass (m_t) and strong coupling constant ($\alpha_s = g_3^2/4\pi$). The allowed range of values of m_t (173.2 ± 0.9 GeV) is taken from [153] and that of α_s (0.1184 ± 0.0007) is taken from [154]. The Higgs mass has been varied between $124.6 - 126.6$ GeV, as obtained by ATLAS and CMS.

We have included the corrections to incorporate the mismatch between the top pole mass and $\overline{MS}$ renormalized coupling. This is given as [91],

$$Y_t(m_t) = \frac{\sqrt{2} m_t}{v} (1 + \delta_t(m_t)) \tag{2.4.29}$$

*Contribution of heavy neutrinos towards the effective potential has not been considered.

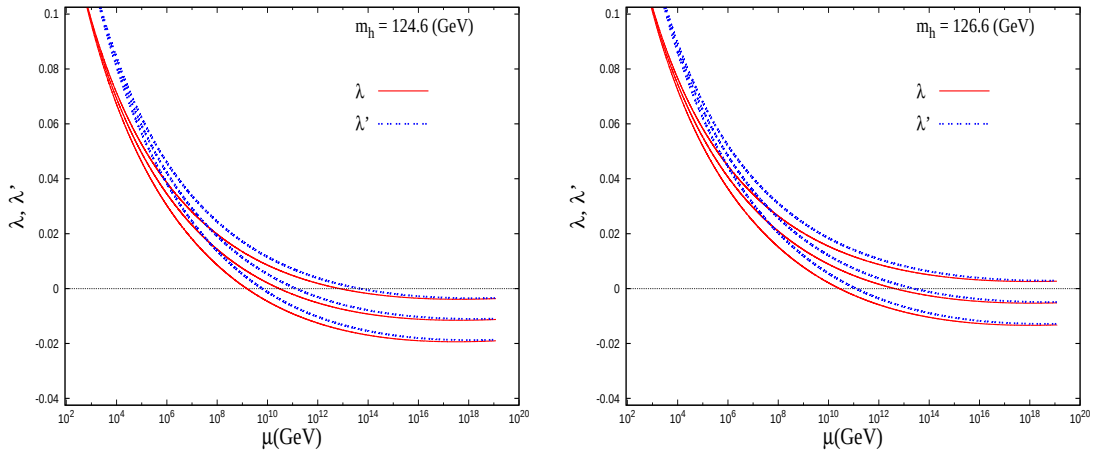

Figure 2.7: *Variation of* λ *and* $\tilde{\lambda}$ (*denoted by* λ' *in the figure*) *with the renormalization scale for fixed values of the parameters* $(m_h\,, m_t\,, \alpha_s)$. *The upper, middle and lower curves are drawn with the set of parameters* (m_t, α_s)=$\{(172.3\,\text{GeV}\,, 0.1191)$, $(173.2\,\text{GeV}\,, 0.1184)$, $(174.1\,\text{GeV}\,, 0.1177)\}$ *respectively.*

$\delta_t(m_t)$ denotes the matching correction at top pole mass and can be found in Appendix B.4. We include the QCD corrections upto three loop [155] while electroweak corrections are taken upto one loop [156]. We also include suitable matching conditions for $\overline{MS}$ renormalized λ and the Higgs mass at $\mu = m_t$ [157].

$$\lambda(m_t) = \frac{m_h^2}{2\,v^2}(1 + \delta_h(m_t)) \tag{2.4.30}$$

$\delta_h(m_t)$ can by found in Appendix B.4. The threshold effect due to the top mass is included. The plots demonstrate

(i) $\tilde{\lambda} - \lambda$ remains +ive upto Planck scale.

(ii) Higher values of top mass drives λ and $\tilde{\lambda}$ towards more negative values at a lower renormalization scale.

(iii) The uncertainty in the value of the strong coupling constant α_s also affects the running of λ and $\tilde{\lambda}$ in a direction opposite to the top mass effect. Higher values of α_s aids in keeping λ and $\tilde{\lambda}$ positive.

The plots corroborate the fact that for lower values of Higgs mass in the range reported by ATLAS and CMS, the stability of the vacuum till the Planck scale may be retained only for certain choices of the parameters (m_t, α_s). For instance for $m_h = 124.6$ GeV, $\tilde{\lambda} = 0$ is achieved around $10^{10} - 10^{14}$ GeV for 1σ

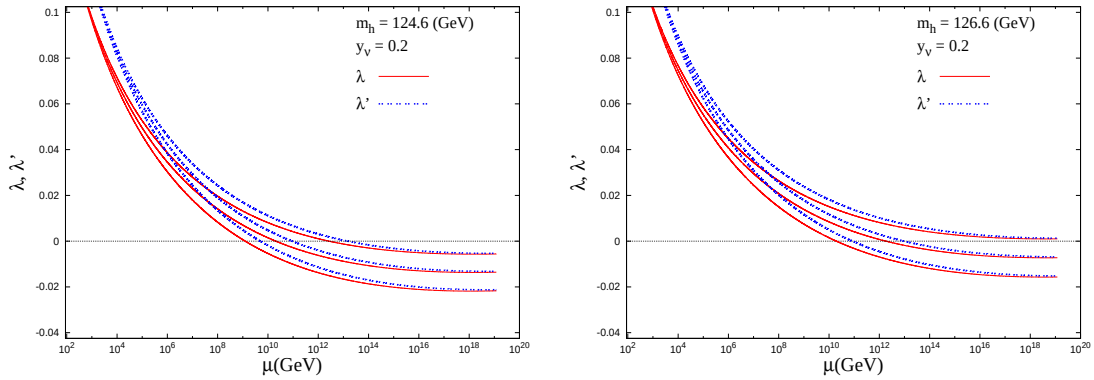

Figure 2.8: *Variation of* λ *and* $\tilde{\lambda}$ (*denoted by* λ' *in the figure*) *with* μ *for fixed values of the parameters* $(m_h\,, m_t\,, \alpha_s)$ including the Dirac Yukawa coupling y_ν. *The upper, middle and lower curves are drawn with the set of parameters* (m_t, α_s)=$\{(172.3\,\text{GeV}\,, 0.1191),\ (173.2\,\text{GeV}\,, 0.1184),\ (174.1\,\text{GeV}\,, 0.1177)\}$ *respectively.*

range variation in the values of m_t and α_s. A non-negative $\tilde{\lambda}$ till the Planck Scale is achieved only for the mass of the top (α_s) near its lowest (highest) range with higher Higgs mass.

2.4.4.2 Vacuum stability in presence of heavy neutrino

In seesaw models, the presence of heavy neutrino Yukawa coupling modifies the beta function of λ through T_1 and Y_1. Modified T_1 and Y_1 are given by [158]

$$T_1 = \text{Tr}\left[3Y_u{}^\dagger Y_u + 3Y_d{}^\dagger Y_d + Y_l{}^\dagger Y_l + Y_\nu{}^\dagger Y_\nu\right] \tag{2.4.31}$$

$$Y_1 = \text{Tr}\left[3(Y_u{}^\dagger Y_u)^2 + 3(Y_d{}^\dagger Y_d)^2 + (Y_l{}^\dagger Y_l)^2 + (Y_\nu{}^\dagger Y_\nu)^2\right] \tag{2.4.32}$$

As can be seen from the above expressions, the Y_ν dependence of $\beta_\lambda^{(1)}$ is similar to the top Yukawa, hence in the low Higgs mass region it will drive λ towards more negative value near Planck scale. In Fig. 2.8 we show the effect of inclusion of heavy neutrino Yukawa term on the running of λ and $\tilde{\lambda}$ in the context of minimal linear seesaw model. As expected, λ and $\tilde{\lambda}$ become negative at a lower renormalization scale in presence of the seesaw term.

Chapter 3

Phenomenology of See-saw models

3.1 Introduction

In the Type-I seesaw approximation the light neutrino mass matrix at the tree level is given by

$$m_\nu = -\, m_D^T\, M_R^{-1} m_D \tag{3.1.1}$$

Diagonalizing the above mass matrix one would obtain mass eigen values for light neutrinos and mixing angles for the generation mixing of neutrinos*. As mentioned earlier, for Type I seesaw in presence of three heavy singlet fermionic fields, there are 24 unknown parameters on the right hand side of Eq. (3.1.1). In general M_R being complex symmetric, contains 12 parameters among which 3 phases can be absorbed by redefining 3 heavy neutrino fields. m_D being a complex matrix contains 18 parameters among which 3 phases can be absorbed by redefining 3 light neutrino fields. m_ν being complex symmetric contains only 9 parameters which can be measured in experiments; three masses, three mixing angles and three phases among which only 5 have been measured in

*Seesaw arises naturally at high scale whereas observations are made at low scale. One would expect modification due to RG effect [159]. However for hierarchical neutrinos this effect is small in SM [103, 106].

experiments so far. There exists two types of parameter mismatch, measurable parameters which is 9 and measured parameters so far which is 5. The other one being the total number of parameters at high energy which is 24 and measurable parameters at low energy which is 9. This parameter mismatch leads to arbitrariness in the study of phenomenological consequences of the seesaw mechanism.

As mentioned earlier, putting zeros in the mass matrices m_ν, reduces the number of parameters in the low energy neutrino mass matrix and thus increases the predictivity of the model. It has been shown in the literature that the maximum number of zeros that can be accommodated in the three generation low energy neutrino mass matrix is two [160] in order to reproduce measured mass squared differences and mixing angles. Implications of two texture zeros in the low energy Majorana mass matrix have been studied in [160–173] and one texture zero have been studied in [174–176]. Texture zeros in both the charged lepton and neutrino mass matrices have been studied in [177–182].

Within the framework of seesaw mechanism it is often considered more natural to consider texture zeros appearing in the Yukawa coupling matrix m_D and/or the right-handed Majorana mass matrix M_R [86, 87, 161, 183–191]. In particular, it has been shown in [190] that if M_R is diagonal and if one assumes that all light neutrino states are massive then the maximum number of zeros that can be accommodated in m_D is four. The phenomenology of those cases is studied in detail in [191].

The minimal Type-I seesaw model consists of two right handed neutrino which is motivated from the fact that results from oscillation experiments allow one light neutrino state to be massless [192–194]. For two generation heavy right handed neutrino, the total number of high energy parameter is 13. Thus even though the number of high energy parameters gets reduced, still it is higher than the number of measurable low energy parameters. Texture zeros can be imposed in m_D and M_R to reduce the number of parameters. Besides, one can assume equality among the different elements of the mass matrices.

This was considered in [195] in the context of light neutrino mass matrix. To reduce the number of parameters further and hence enhance the predictivity of the model, one can impose equality among matrix elements together with texture zeros which was considered in [196] in the context of light neutrino mass matrix. Another interesting consequence of two generation right handed neutrino is that for a specific texture of the right handed neutrino mass matrix, Yukawa couplings are fully determined in terms of the low energy parameters apart from an overall constant. Coincidentally, the above mentioned specific texture of the right handed neutrino mass matrix also arises in the context of minimal flavor violation [133]. The assumption of texture zeros makes it possible to make predictions for leptogenesis, LFV, neutrino less double beta decay.

Another consequence of seesaw mechanism is that the presence of new Yukawa coupling drives Higgs self coupling, λ, towards a more negative value in the low Higgs mass region. The imposition of the condition $\lambda(M_{Pl}) = 0$, enables one to put constraint on the Yukawa coupling strength if the Higgs mass is known [88,89,94,95]. Also as light heavy mixing is large, Lepton Flavor Violating (LFV) decays can be appreciable. Using the experimental bound on the branching ratio of LFV type processes, one can further constrain the Yukawa coupling in the region where heavy neutrino mass is around TeV. This constrained Yukawa couplings can be used further to study the collider signals of heavy neutrino.

In this chapter we discuss three specific type of textures and their phenomenological implications in the context of Type-I seesaw. The first one is adding three right handed heavy neutrino to the SM. We show that if we relax the condition that all light neutrinos are massive and allow one light neutrino state to be massless then the maximum number of zeros allowed in m_D is five. We demonstrate that even with a diagonal M_R one can obtain allowed textures consistent with low energy observations for m_D with 5 zeros. We further relax the assumption of a diagonal M_R and consider off-diagonal non-singular M_R in order to avoid light right-handed (sterile) neutrinos. We find that the

maximum number of zeros that is possible for M_R is four and only three such matrices have a non-vanishing determinant. Interestingly these matrices obey $L_\mu - L_\tau$, $L_e - L_\tau$ and $L_e - L_\mu$ flavor symmetry. We investigate if it is possible to have allowed textures assuming the above forms for M_R and m_D with 5 zeros. The allowed textures can be used to study the implications for LFV and leptogenesis for the allowed textures surviving the constraints from low energy phenomenology. We also comment on more than 5 zeros in m_D. Next we have considered two generation of right handed neutrinos and imposed equality and texture zero together. We obtained viable textures and studied low and high energy phenomenology for those textures. Finally in the context of minimal linear seesaw mechanism, we have constrained both Yukawa couplings and mass scale of the right handed neutrinos from the consideration of vacuum stability, LFV and measured neutrino masses. We have also commented on possible collider signature of the model.

3.2 Allowed Textures and their Phenomenology

In the context of the type I seesaw mechanism, the mass matrix for the left handed neutrinos, obtained through seesaw diagonalization, depends on the Dirac type Yukawa coupling matrix of the neutrinos (m_D) as well as on the bare Majorana mass matrix (M) of the heavy right handed neutrinos. After putting zeros in the mass matrices and equalities among the mass matrices we shall use the following criteria to classify allowed textures. The low energy neutrino mass matrix m_ν

(i) contains no vanishing entry (general case)

(ii) contains two vanishing entries [160]

(iii) contains one vanishing entry [174]

After evaluating the low energy neutrino mass matrix from m_D and M_R containing zero entries, invalid cases can easily be ruled out almost at first sight.

First of all, the rank of m_ν should be at least two. The resulting m_ν

will have zeros in most of the cases. From the 15 possible two zero textures[†] only seven are found to be consistent with the data [160]. With the recent global analysis of oscillation data, these seven textures are still allowed in the 3σ ranges of the oscillation parameters [36, 198]. Although in 1σ region of parameter space some textures are disfavored [173]. In our analysis, we proceed with 3σ range of the parameters. The allowed patterns of the two zero texture are characterized by the simultaneous vanishing of the ee- and $e\mu$- (with 1σ value of oscillation parameter [198], only this one remains viable), the ee- and $e\tau$-, the $e\mu$- and $\mu\mu$-, the $e\tau$- and $\mu\mu$-, the $e\tau$- and $\tau\tau$-, the $e\mu$- and $\tau\tau$, and finally the $\mu\mu$- and $\tau\tau$-entries. The first two possibilities are only possible for a normal hierarchy, the latter five only for quasi-degenerate neutrinos. In particular, if e.g. one neutrino mass is zero then it is not allowed that $(m_\nu)_{\mu\mu} = (m_\nu)_{\tau\tau} = 0$. If the $\mu\tau$ entry of m_ν is zero, then no other entry is allowed to vanish. Regarding the presence of only one zero entry in m_ν, an important information is that if the determinant of m_ν vanishes, then the $\mu\tau$ element can not be zero [174].

The above mentioned properties of texture zeros in the light neutrino mass matrix will be used to distinguish the allowed possibilities from the disallowed ones. However in presence of no zero in the light neutrino mass matrix, one needs to look for some relations among the matrix elements to make predictions.

Finally, we would like to mention that we do not take into account the fine-tuned possibility that the low energy texture zeros are resulting from cancellation of terms [74].

3.2.1 5 zero in m_D with diagonal M_R and 4 zero in M_R

In this section, we consider 5 zeros in m_D in presence of three heavy right handed neutrinos. This is more minimal than the 4 zero m_D case considered in [190] and is allowed if we include solutions with one of the light neutrino mass as zero.

[†]If neutrinos are Dirac particles then up to five zero entries are allowed in m_ν [197].

3.2.1.1 M_R more minimal than diagonal

Heavy neutrino mass matrices in diagonal form contain three independent zeros. More minimal form of M_R can be chosen as following, non-singular matrices with four independent zeros:

$$M_R = \begin{pmatrix} M_1 & 0 & 0 \\ 0 & 0 & M_2 \\ 0 & M_2 & 0 \end{pmatrix}, \quad \begin{pmatrix} 0 & 0 & M_2 \\ 0 & M_1 & 0 \\ M_2 & 0 & 0 \end{pmatrix}, \quad \begin{pmatrix} 0 & M_2 & 0 \\ M_2 & 0 & 0 \\ 0 & 0 & M_1 \end{pmatrix}. \quad (3.2.1)$$

These forms correspond to flavor symmetries $L_\mu - L_\tau$, $L_e - L_\tau$ and $L_e - L_\mu$, respectively. Majorana (and thus symmetric) matrices with 5 or more zeros are all singular, lead to light sterile neutrinos and will not be studied here. As we shall see, an exactly diagonal M_R leads to allowed forms of m_ν with single zero entries. Using the above textures of M_R will give typically two simultaneously vanishing entries in m_ν.

With m_D being non-symmetric 3×3 matrix in general, there are $N = {}^9C_n$ possibilities to place n zero entries in it. We therefore have e.g. $N = 126, 84$ and 36 if $n = 5$, 6 and 7. With our analysis aiming at 5 zero textures in m_D and with the four forms of M_R, there are in total 504 candidates. Most of them can be ruled out by the arguments given in Section 3.2.1.3.

3.2.1.2 Diagonal M_R

If M_R is diagonal then we find in total 12 allowed cases, all of which generate a vanishing determinant for m_ν:

(i) six of them have a vanishing $e\mu$ entry in m_ν,

(ii) another six contain a vanishing $e\tau$ element.

These two cases are displayed in Tables 3.1 and 3.2. Let us first discuss the neutrino mixing phenomenology. The 12 cases are specified by a vanishing element in m_ν and $m_1 = 0$ or $m_3 = 0$, depending on whether a normal or inverted hierarchy is present. In case of $(m_\nu)_{e\mu} = 0$ it has been shown that in

m_D	leptogenesis	wash-out
$\begin{pmatrix} 0 & 0 & 0 \\ 0 & b_2 & c_2 \\ a_3 & 0 & c_3\, e^{i\gamma_3} \end{pmatrix}$	$\mathcal{I}^{\tau}_{23} = c_2^2\, c_3^2\, \sin 2\gamma_3$	$\tilde{m}^{\tau}_2 = \frac{c_2^2}{M_2}$
$\begin{pmatrix} 0 & 0 & 0 \\ a_2 & 0 & c_2 \\ 0 & b_3 & c_3\, e^{i\gamma_3} \end{pmatrix}$	$\mathcal{I}^{\tau}_{23} = c_2^2\, c_3^2\, \sin 2\gamma_3$	$\tilde{m}^{\tau}_2 = \frac{c_2^2}{M_2}$
$\begin{pmatrix} a_1 & 0 & c_1 \\ 0 & 0 & 0 \\ 0 & b_3 & c_3\, e^{i\gamma_3} \end{pmatrix}$	$\mathcal{I}^{\tau}_{13} = c_1^2\, c_3^2\, \sin 2\gamma_3$	$\tilde{m}^{\tau}_1 = \frac{c_1^2}{M_1}$
$\begin{pmatrix} 0 & b_1 & c_1 \\ 0 & 0 & 0 \\ a_3 & 0 & c_3\, e^{i\gamma_3} \end{pmatrix}$	$\mathcal{I}^{\tau}_{13} = c_1^2\, c_3^2\, \sin 2\gamma_3$	$\tilde{m}^{\tau}_1 = \frac{c_1^2}{M_1}$
$\begin{pmatrix} 0 & b_1 & c_1 \\ a_2 & 0 & c_2\, e^{i\gamma_2} \\ 0 & 0 & 0 \end{pmatrix}$	$\mathcal{I}^{\tau}_{12} = c_1^2\, c_2^2\, \sin 2\gamma_2$	$\tilde{m}^{\tau}_1 = \frac{c_1^2}{M_1}$
$\begin{pmatrix} a_1 & 0 & c_1 \\ 0 & b_2 & c_2\, e^{i\gamma_2} \\ 0 & 0 & 0 \end{pmatrix}$	$\mathcal{I}^{\tau}_{12} = c_1^2\, c_2^2\, \sin 2\gamma_2$	$\tilde{m}^{\tau}_1 = \frac{c_1^2}{M_1}$

Table 3.1: *The Dirac mass matrix, the non-zero expressions relevant for leptogenesis and the corresponding wash-out actors. All these cases give m_ν with one vanishing eigenvalue and $(m_\nu)_{e\mu} = 0$. The right-handed neutrino mass matrix is always diagonal.*

general θ_{13} must necessarily be non-zero [174]. If $m_1 = 0$ then one finds from the condition $(m_\nu)_{e\mu} = 0$ that

$$
\begin{aligned}
|U_{e3}| \;&\simeq\; \frac{m_2\, \cos\theta_{12}\, \cot\theta_{23}}{\sqrt{\Delta m^2_{\rm atm}/\sin^2\theta_{12} - 2\sqrt{\Delta m^2_{\rm atm}\Delta m^2_{\odot}}\,\cos 2\alpha}} \\
&\simeq\; \begin{cases} 0.057 - 0.077 & \text{at } 1\sigma \\ 0.050 - 0.132 & \text{at } 3\sigma \end{cases}
\end{aligned}
\tag{3.2.2}
$$

The numerical range of $|U_{e3}|$ is obtained by using the exact expression for $(m_\nu)_{e\mu}$ and varying the neutrino parameters in their currently allowed 1σ and 3σ ranges. From Table 1.1, we see that the present 1σ bound on $\sin\theta_{13}$ is $0.1476-0.1658$ (for NH), $0.1493-0.1661$ (for IH) and 3σ bound is $0.130-0.182$ [36]. This implies that the above texture is severely constrained even in the 3σ range.

m_D	Leptogenesis	washout
$\begin{pmatrix} 0 & 0 & 0 \\ 0 & b_2 & c_2 \\ a_3 & b_3\, e^{i\beta_3} & 0 \end{pmatrix}$	$\mathcal{I}^{\mu}_{23} = b_2^2\, b_3^2\, \sin 2\beta_3$	$\tilde{m}_2^{\mu} = \frac{b_2^2}{M_2}$
$\begin{pmatrix} 0 & 0 & 0 \\ a_2 & b_2 & 0 \\ 0 & b_3\, e^{i\beta_3} & c_3 \end{pmatrix}$	$\mathcal{I}^{\mu}_{23} = b_2^2\, b_3^2\, \sin 2\beta_3$	$\tilde{m}_2^{\mu} = \frac{b_2^2}{M_2}$
$\begin{pmatrix} 0 & b_1 & c_1 \\ 0 & 0 & 0 \\ a_3 & b_3\, e^{i\beta_3} & 0 \end{pmatrix}$	$\mathcal{I}^{\mu}_{13} = b_1^2\, b_3^2\, \sin 2\beta_3$	$\tilde{m}_1^{\mu} = \frac{b_1^2}{M_1}$
$\begin{pmatrix} a_1 & b_1 & 0 \\ 0 & 0 & 0 \\ 0 & b_3\, e^{i\beta_3} & c_3 \end{pmatrix}$	$\mathcal{I}^{\mu}_{13} = b_1^2\, b_3^2\, \sin 2\beta_3$	$\tilde{m}_1^{\mu} = \frac{b_1^2}{M1}$
$\begin{pmatrix} 0 & b_1 & c_1 \\ a_2 & b_2\, e^{i\beta_2} & 0 \\ 0 & 0 & 0 \end{pmatrix}$	$\mathcal{I}^{\mu}_{12} = b_1^2\, b_2^2\, \sin 2\beta_2$	$\tilde{m}_1^{\mu} = \frac{b_1^2}{M_1}$
$\begin{pmatrix} a_1 & b_1 & 0 \\ 0 & b_2\, e^{i\beta_2} & c_2 \\ 0 & 0 & 0 \end{pmatrix}$	$\mathcal{I}^{\mu}_{12} = b_1^2\, b_2^2\, \sin 2\beta_2$	$\tilde{m}_1^{\mu} = \frac{b_1^2}{M_1}$

Table 3.2: *The Dirac mass matrix, the non-zero expressions relevant for leptogenesis and the corresponding wash-out factors. All these cases give m_ν with one vanishing eigenvalue and $(m_\nu)_{e\tau} = 0$. The right-handed neutrino mass matrix is always diagonal.*

In an inverted hierarchy, with $m_3 = 0$ and $m_2 \simeq m_1$ we find

$$|U_{e3}| \simeq \frac{\sin 2\theta_{12}\, \sin\alpha}{\sqrt{1 - \sin^2 2\theta_{12}\, \sin^2\alpha}}\, \cot\theta_{23} \tag{3.2.3}$$

While in principle $|U_{e3}|$ can be sizable according to this equation, it turns out [174] that the vanishing of the $e\mu$-element implies also that $|\sin\alpha| \ll 1$. In fact, expanding in terms of $|U_{e3}|$ one finds up to first order that

$$\begin{aligned}(m_\nu)_{e\mu} \;=\; & \left(m_2\, e^{2i\alpha} - m_1\right) \cos\theta_{12}\, \sin\theta_{12}\, \cos\theta_{23} + e^{i\delta}\, \sin\theta_{23} \left(e^{2i\beta}\, m_3 \right. \\ & \left. - \sin^2\theta_{12}\, m_2\, e^{2i\alpha} - \cos^2\theta_{12}\, m_1\right)\, |U_{e3}| \end{aligned} \tag{3.2.4}$$

We see that for $m_2 \simeq m_1 \gg m_3$ the phase should be such that $e^{2i\alpha} \simeq 1$ for $(m_\nu)_{e\mu} = 0$. This value implies for the effective mass for neutrino less double beta decay that $\langle m_{ee}\rangle \simeq \sqrt{\Delta m^2_{\rm atm}}\, \cos^2\theta_{13}$, i.e., there are no cancellations.

We find numerically a lower value of $|U_{e3}| \gtrsim 0.005$ when the 3σ ranges of the oscillation parameters are used, whereas for the 1σ ranges we get $|U_{e3}| \gtrsim 0.082$.

If the $e\tau$-entry of m_ν is zero, then similar expressions as Eqs. (3.2.2) and (3.2.3) are obtained, with $\cot\theta_{23}$ replaced by $\tan\theta_{23}$. Numerically, we obtain the value for $|U_{e3}|$ for normal hierarchy, as below

$$|U_{e3}| \;\simeq\; \begin{cases} 0.088 - 0.116 & \text{at } 1\sigma \\ 0.056 - 0.145 & \text{at } 3\sigma \end{cases} \tag{3.2.5}$$

For inverted hierarchy, the 1σ and 3σ lower bound on $|U_{e3}|$ is approximately 0.017 and 0.009 respectively.

Turning to leptogenesis, we see from Tables 3.1, 3.2 that for all 12 cases there is only one physical phase present. In addition, there is always only one flavored $\mathcal{I}^\alpha_{1j}$ present (which is equal to the unflavored $\mathcal{I}_{1j}$) and the corresponding wash-out parameter $\tilde{m}^\alpha_1$ (which is equal to the unflavored $\tilde{m}_1$) is non-zero. For some cases, m_D is such that the heavy neutrino with mass M_1 decouples. In such situations, we have calculated the corresponding quantities for the second neutrino, i.e. $\mathcal{I}^\alpha_{2j}$ and $\tilde{m}^\alpha_2$. As indicated, all $\mathcal{J}^\alpha_{1j}$ are zero. All 12 possibilities can accommodate successful leptogenesis.

We have checked that for the cases with a vanishing $e\mu$ or $e\tau$ element in m_ν the invariant $J_{\rm CP}$ from Eq. (2.4.1), responsible for low energy CP violation in oscillations is non-zero and is proportional to the same phase factor as in $\mathcal{I}_{ij}$. For instance, if we consider

$$m_D = \begin{pmatrix} 0 & 0 & 0 \\ 0 & b_2 & c_2 \\ a_3 & 0 & c_3\, e^{i\gamma_3} \end{pmatrix} \tag{3.2.6}$$

which gives m_ν with $m_{e\mu} = 0$ for a diagonal M_R, then the only non-zero $\mathcal{I}_{ij}$ that we get is

$$\mathcal{I}^\tau_{23} = c_2^2\, c_3^2\, \sin 2\gamma_3 \tag{3.2.7}$$

to be compared with

$$J_{\rm CP} = a_3^2\, b_2^2\, c_2^2\, c_3^2\, (a_3^2\, (b_2^2 + c_2^2) + b_2^2\, c_3^2)\, M_2^3\, M_3^3\, \sin 2\gamma_3 \tag{3.2.8}$$

Thus we see that $\mathcal{I}_{ij}^{\tau}$ and $J_{\rm CP}$ contain the same phase factor $\sin 2\gamma_3$. Hence, the Dirac CP phase is always identical to the high-energy "leptogenesis phase". This conclusion is true for all the textures in Tables 3.1 and 3.2. Let us note that in the case of 4 zero textures [190, 191] there always was an ambiguity in what regards the one-to-one identification of low and high energy CP phases with each other. This is not the case for 5 zero textures.

Regarding LFV, in case the $e\mu$ entry of m_ν vanishes, $(m_D\, L\, m_D^\dagger)_{12}$ is also zero, where L is given by Eq. (2.4.18). Hence, $\mu \to e\gamma$ will not be detected if the only source of LFV is the supersymmetric seesaw with universal minimal super gravity conditions studied here. The remaining, in general non-zero branching ratios turn out to be proportional to the respective elements of m_ν. Considering the first matrix in Table 3.1. The low energy mass matrix is

$$m_\nu = -\begin{pmatrix} \frac{a_3^2}{M_3} & 0 & \frac{a_3\, c_3\, e^{i\gamma_3}}{M_3} \\ \cdot & \frac{b_2^2}{M_2} & \frac{b_2\, c_2}{M_2} \\ \cdot & \cdot & \frac{c_2^2}{M_2} + \frac{c_3^2\, e^{i\gamma_3}}{M_3} \end{pmatrix} \tag{3.2.9}$$

and for LFV we find

$$|(m_D\, L\, m_D^\dagger)_{13}|^2 = a_3^2\, c_3^2\, L_3^2\ , \quad |(m_D\, L\, m_D^\dagger)_{23}|^2 = b_2^2\, c_2^2\, L_2^2 \tag{3.2.10}$$

Hence, $\mathrm{BR}(\tau \to e\gamma) \propto |(m_\nu)_{e\tau}|^2$ and $\mathrm{BR}(\tau \to \mu\gamma) \propto |(m_\nu)_{\mu\tau}|^2$. The ratio of $\mathrm{BR}(\tau \to e\gamma)$ and $\mathrm{BR}(\tau \to \mu\gamma)$ can however not be predicted in general because the a priori unknown heavy neutrino masses enter this ratio directly and via the factors L_i. The qualitatively same situation is encountered for a vanishing $e\tau$ entry of m_ν, in which case $\mathrm{BR}(\tau \to e\gamma)$ is zero and the other branching ratios are proportional to the respective elements of m_ν, but with different dependence on the heavy masses.

3.2.1.3 Non-diagonal M_R

If M_R takes on the non-diagonal four zero textures in Eq. (3.2.1) then we can generate two zero textures in m_ν. However, only four of the seven allowed two zero textures can be obtained. For each of the three possibilities $L_e - L_\mu$, $L_e - L_\tau$ and $L_\mu - L_\tau$, at first sight 8 potentially successful cases survive:

- for every non-diagonal form of M_R there are two cases with a vanishing ee and $e\mu$ entry in m_ν. They have the additional property

$$\begin{aligned} &|(m_\nu)_{\mu\mu}\,(m_\nu)_{\tau\tau}| = |(m_\nu)^2_{\mu\tau}| \quad \text{and} \\ &\arg\left\{(m_\nu)_{\mu\mu}\,(m_\nu)_{\tau\tau}\,\left((m_\nu)^*_{\mu\tau}\right)^2\right\} = 0 \end{aligned} \tag{3.2.11}$$

- for every non-diagonal form of M_R there are two cases with a vanishing ee and $e\tau$ entry in m_ν. They have the same property given in Eq. (3.2.11);

- for every non-diagonal form of M_R there are two cases with a vanishing $e\mu$ and $\mu\mu$ entry in m_ν. They have the additional property

$$\begin{aligned} &|(m_\nu)_{ee}\,(m_\nu)_{\tau\tau}| = |(m_\nu)^2_{e\tau}| \quad \text{and} \\ &\arg\left\{(m_\nu)_{ee}\,(m_\nu)_{\tau\tau}\,\left((m_\nu)^*_{e\tau}\right)^2\right\} = 0 \end{aligned} \tag{3.2.12}$$

- for every non-diagonal form of M_R there are two cases with a vanishing $e\tau$ and $\tau\tau$ entry in m_ν. They are subject to the condition

$$\begin{aligned} &|(m_\nu)_{ee}\,(m_\nu)_{\mu\mu}| = |(m_\nu)^2_{e\mu}| \quad \text{and} \\ &\arg\left\{(m_\nu)_{ee}\,(m_\nu)_{\mu\mu}\,\left((m_\nu)^*_{e\mu}\right)^2\right\} = 0 \end{aligned} \tag{3.2.13}$$

All 24 m_ν have a non-vanishing determinant, hence no neutrino mass is zero. They also share the property of a zero invariant $J_{\rm CP}$, i.e., in the parameterization of the PMNS matrix applied here the CP phase δ is zero or π. However, it is known [160,162–168] that if $(m_\nu)_{e\mu} = (m_\nu)_{\mu\mu} = 0$ or if $(m_\nu)_{e\tau} = (m_\nu)_{\tau\tau} = 0$, the CP phase should be large because the small ratio of solar and atmospheric

Δm^2 is proportional to $\cos\delta$. Hence, these 12 cases can be disregarded at once.

In the cases with $(m_\nu)_{ee} = (m_\nu)_{e\mu} = 0$ and $(m_\nu)_{ee} = (m_\nu)_{e\tau} = 0$, it is extremely cumbersome to try to obtain analytical estimates from these equations. However, we have checked numerically that no point in the allowed parameter space can simultaneously satisfy the two zero texture conditions and conditions Eq. (3.2.11) [199]. The reason for this lies in a class of the two zero textures which require hierarchical neutrino masses, whereas the additional conditions imply larger neutrino masses.

3.2.1.4 Dirac Mass Matrices with more than five Zeros

Finally, in this Subsection we shortly discuss Dirac mass matrices with more than five zero entries.

Among the 9 elements of m_D which are in general complex the first non-trivial case with maximal number of zeros is 8. This implies 2 heavy neutrinos are completely decoupled from the light neutrinos and it is well known that one cannot explain the low energy phenomenology successfully with only one heavy neutrino coupled to the system.

If m_D contains seven zeros, then we find no valid m_ν for the four minimal forms of M_R under study. In fact we have checked that the above statement is true for the most general form of M_R if m_D contains 7 zeros. One can group the ${}^7C_9 = 36$ possible forms of m_D, in 3 categories. Their respective structures are

$$m_D = \begin{pmatrix} 0 & 0 & 0 \\ 0 & 0 & X \\ 0 & 0 & X \end{pmatrix} \quad , \quad \begin{pmatrix} 0 & 0 & 0 \\ 0 & 0 & 0 \\ 0 & X & X \end{pmatrix} \quad , \quad \begin{pmatrix} 0 & 0 & 0 \\ 0 & X & 0 \\ 0 & 0 & X \end{pmatrix} \tag{3.2.14}$$

The first two matrices will lead, irrespective of M_R, in the seesaw mechanism to at least two vanishing eigenvalues in m_ν and are thus ruled out in general. The third one can give two non-vanishing eigenvalues but the final m_ν contains more than 2 zeros for the minimal forms of M_R considered in Section 3.2.1.1 as well as for diagonal M_R.

For the case of 6 zeros in m_D, the possible types of patterns are

$$\begin{pmatrix} 0 & 0 & X \\ 0 & 0 & X \\ 0 & 0 & X \end{pmatrix} , \quad \begin{pmatrix} X & 0 & 0 \\ 0 & X & 0 \\ 0 & 0 & X \end{pmatrix} , \quad \begin{pmatrix} 0 & 0 & 0 \\ 0 & 0 & 0 \\ X & X & X \end{pmatrix} , \quad \begin{pmatrix} X & 0 & 0 \\ 0 & X & 0 \\ X & 0 & 0 \end{pmatrix} \quad (3.2.15)$$

For m_D's of the first and third form two eigenvalues of m_ν are zero for a general M_R. Hence these forms of m_D are ruled out in general. For m_D's of the second type none of the eigenvalues of m_ν are zero and these cannot be ruled out for a general M_R. But, for the 4 types of M_R that considered in Section 3.2.1.1, the resultant m_ν contains more than 2 zeros and hence are ruled out. For the m_D's of the fourth type one eigenvalue of m_ν is zero but it contains more than 2 zeros in the flavor basis for a general M_R and therefore are not allowed.

Thus we conclude that in the context of texture zero, the 5 zero textures in m_D with diagonal M_R correspond to scenarios with a minimal number of free parameters. In total, considering zeros in m_D and M, we have a seesaw scenario with 8 zero entries.

3.2.2 Hybrid Scenario

In this section, we consider the minimal seesaw model with two right-handed neutrinos. In this choice there are less number of free parameters. Thus the mass matrices get simple forms and rich predictions compared to the standard three heavy neutrino models. In this scenario the Dirac mass matrix m_D and the Majorana mass matrix M will be 2×3 and 2×2 matrices respectively. In this framework, the rank of the induced matrix m_ν becomes at most 2, so that at least one neutrino remains massless.

3.2.2.1 The equalities among matrix elements

Before going to the study of coexistence of the equalities and vanishing elements in the mass matrices, we outline the handling of the equalities among mass matrix elements and discuss the situation where only equalities are im-

posed on the neutrino mass matrices.

In both Dirac and Majorana mass matrices, the matrix elements are in general complex valued. We impose the equalities among the matrix elements such that these are applicable not only to the absolute values of the matrix elements but also to the phases. We shall comment on the un-removable phases of the matrix elements and CP violation of certain textures later.

We start with the classification of the general possibilities of the Dirac mass matrix. It should be noted that, here and in what follows, the textures of m_D are specified by the positions of the matrix elements which are connected with the other elements by equalities. At the stage of enumerating general possibilities, the locations of the vanishing elements specify the "identity" of the textures. For example, the equation $(m_D)_{11} = (m_D)_{12}$ symbolizes the texture

$$m_D = \begin{pmatrix} a & a & b \\ c & d & e \end{pmatrix} . \tag{3.2.16}$$

Since there are 6 matrix elements in the Dirac mass matrix m_D, we can impose equality relations between matrix elements up to 5. According to the above criterion of texture identity, it turns out that each case contains the general possibilities of

- 1 equality : 15 patterns,
- 2 equalities : 65 patterns,
- 3 equalities : 90 patterns,
- 4 equalities : 31 patterns,
- 5 equalities : 1 patterns.

The case of 3 equalities provides the largest varieties of textures, whereas the 5 equalities case means all matrix elements are equal so that only one possible form is available in this case. 5 equalities in m_D will give an effective light neutrino mass matrix of rank 1 thus we exclude 5 equalities in m_D at once.

Next let us discuss the Majorana mass matrix M. We take M as a 2×2 complex symmetric matrix, which means that there are 3 independent matrix elements in M_R. Therefore M_R can accommodate at most 2 equalities. However, 2 equalities in M imply a vanishing determinant. With such an M, there appears a state which does not receive seesaw suppression in mass. Here, we do not consider such spectrum and in what follows we shall simply exclude the cases where M has two equalities. The three alternatives for M (or M^{-1}) with 1 equality are:

$$M^{-1} = \begin{pmatrix} A & B \\ B & A \end{pmatrix}, \quad \begin{pmatrix} A & A \\ A & B \end{pmatrix}, \quad \begin{pmatrix} A & B \\ B & B \end{pmatrix}. \tag{3.2.17}$$

In 2×2 case, the equalities in M are directly connected to the equalities in M^{-1}. We shall examine these three textures as general possibilities in the following discussions. It is noteworthy that for the three textures in (3.2.17), all the matrix elements cannot be made real by re-definition of the right-handed neutrino fields. Thus, although 1 equality relation reduces the number of the free parameters by one, it does not reduce the number of the phases which can be rotated away from the Lagrangian. This is different from the case of texture zeros. If we impose 1 zero texture in M, there is no un-removable phase in the matrix.

Now we are in the stage to study the combination of m_D and M_R according to the total number of equalities to be distributed in them. First of all, it is easy to see that the case of total 7 or 6 equalities cannot be viable because they would either need 5 equalities in m_D or 2 equalities in M_R or both together.

The next possibility is of total 5 equalities. In this case, there is only one option that satisfy the selection criteria namely,

- 4 equalities in m_D and 1 equality in M

For this case, from the 7 representatives of m_D in Appendix A.4 and 3 patterns

of (3.2.17), we have

$$
\begin{aligned}
m_D &= \begin{pmatrix} a & a & a \\ a & a & b \end{pmatrix}, \begin{pmatrix} a & a & a \\ a & b & b \end{pmatrix}, \begin{pmatrix} a & a & b \\ a & b & a \end{pmatrix}, \begin{pmatrix} a & a & b \\ a & b & b \end{pmatrix}, \begin{pmatrix} a & a & b \\ b & b & a \end{pmatrix}, \\
M^{-1} &= \begin{pmatrix} A & B \\ B & A \end{pmatrix}, \begin{pmatrix} A & A \\ A & B \end{pmatrix}, \begin{pmatrix} A & B \\ B & B \end{pmatrix}. \qquad (3.2.18)
\end{aligned}
$$

In Eq. (3.2.18), we have dropped the two Dirac mass matrices containing rows that are not independent of each other. With these forms of m_D, we obtain m_ν which has only one massive state because we can rotate the right-handed fields in such a way that only one right-handed neutrino is coupled with the left-handed neutrinos. We can therefore exclude these two cases from the viable possibilities.

In Eq. (3.2.18), the Dirac mass matrices presented are the "representatives", from which all possible forms of m_D are generated. Thus (3.2.18) actually contains large number of the combinations. For instance, corresponding to the first m_D in (3.2.18), there are 5 other associated forms. Accordingly, it is to be understood that there are 6×3 combinations of m_D and M for the first m_D presented in Eq. (3.2.18). However, not all of these combinations are independent. They contain the combinations which are associated with each other by the permutation of the two right-handed neutrinos. Thus, it is sufficient to consider the column exchanges of each m_D in (3.2.18).

Finally, we comment on the case of total 4 equalities. There are two possible options to be considered, for distributing 4 equalities in m_D and M_R.

- 4 equalities in m_D and 0 equality in M
- 3 equalities in m_D and 1 equality in M

These two cases cannot be excluded a priori and we regard them as general possibilities for total 4 equalities:

$$
m_D = \begin{pmatrix} a & a & a \\ a & a & b \end{pmatrix}, \begin{pmatrix} a & a & a \\ a & b & b \end{pmatrix}, \begin{pmatrix} a & a & b \\ a & a & b \end{pmatrix}, \begin{pmatrix} a & a & b \\ a & b & a \end{pmatrix}, \qquad (3.2.19)
$$

$$\begin{pmatrix} a & a & a \\ b & b & b \end{pmatrix}, \begin{pmatrix} a & a & b \\ a & b & b \end{pmatrix}, \begin{pmatrix} a & a & b \\ b & b & a \end{pmatrix},$$
$$M^{-1} = \begin{pmatrix} A & B \\ B & C \end{pmatrix}, \tag{3.2.20}$$

and

$$m_D = \begin{pmatrix} a & a & a \\ b & b & c \end{pmatrix}, \begin{pmatrix} a & a & b \\ a & b & c \end{pmatrix}, \begin{pmatrix} a & a & b \\ a & c & b \end{pmatrix}, \begin{pmatrix} a & a & c \\ a & b & b \end{pmatrix}, \begin{pmatrix} a & a & b \\ b & c & a \end{pmatrix},$$
$$\begin{pmatrix} a & a & c \\ b & b & a \end{pmatrix}, \begin{pmatrix} a & a & a \\ a & b & c \end{pmatrix}, \begin{pmatrix} a & a & b \\ a & a & c \end{pmatrix}, \begin{pmatrix} a & a & b \\ a & c & a \end{pmatrix}, \begin{pmatrix} a & b & c \\ a & b & c \end{pmatrix},$$
$$\begin{pmatrix} a & a & c \\ b & b & c \end{pmatrix}, \begin{pmatrix} a & b & c \\ b & a & c \end{pmatrix}, \begin{pmatrix} a & a & c \\ c & b & b \end{pmatrix}, \begin{pmatrix} a & b & c \\ c & a & b \end{pmatrix} \tag{3.2.21}$$

$$M^{-1} = \begin{pmatrix} A & B \\ B & A \end{pmatrix}, \begin{pmatrix} A & A \\ A & B \end{pmatrix}, \begin{pmatrix} A & B \\ B & B \end{pmatrix}. \tag{3.2.22}$$

We note that there are at most 2 un-removable phases in the above textures (3.2.20) and (3.2.22). However, with a vanishing matrix element, the number of the un-removable phases is reduced to one.

3.2.2.2 Hybrid textures

The hybrid textures are the matrices in which vanishing elements and equalities among elements coexist. The procedure adopted to impose the equalities and texture zeros on the mass matrices is as follows. We impose texture zeros on the mass matrices after introducing the equalities among the matrix elements. For instance if we consider the following m_D and put $b = 0$ we get,

$$\begin{pmatrix} a & a & b \\ b & b & a \end{pmatrix} \rightarrow \begin{pmatrix} a & a & 0 \\ 0 & 0 & a \end{pmatrix}. \tag{3.2.23}$$

	m_D	M^{-1}	$m_\nu \left(a' = a\sqrt{A}\,, b' = b\sqrt{A}\right)$
I	$\begin{pmatrix} b & a & a \\ a & b & 0 \end{pmatrix}$	$\begin{pmatrix} 0 & A \\ A & A \end{pmatrix}$	$\begin{pmatrix} a'(a'+2b') & a'^2+a'b'+b'^2 & a'^2 \\ a'^2+a'b'+b'^2 & b'(2a'+b') & a'b' \\ a'^2 & a'b' & 0 \end{pmatrix}$
II	$\begin{pmatrix} a & b & a \\ 0 & a & b \end{pmatrix}$	$\begin{pmatrix} A & 0 \\ 0 & A \end{pmatrix}$	$\begin{pmatrix} a'^2 & a'b' & a'^2 \\ a'b' & a'^2+b'^2 & 2a'b' \\ a'^2 & 2a'b' & a'^2+b'^2 \end{pmatrix}$
III	$\begin{pmatrix} a & a & b \\ 0 & b & a \end{pmatrix}$	$\begin{pmatrix} 0 & A \\ A & 0 \end{pmatrix}$	$\begin{pmatrix} 0 & a'b' & a'^2 \\ a'b' & 2a'b' & a'^2+b'^2 \\ a'^2 & a'^2+b'^2 & 2a'b' \end{pmatrix}$
IV	$\begin{pmatrix} 0 & a & b \\ a & b & 0 \end{pmatrix}$	$\begin{pmatrix} A & A \\ A & 0 \end{pmatrix}$	$\begin{pmatrix} 0 & a'^2 & a'b' \\ a'^2 & a'^2+2a'b' & a'b'+b'^2 \\ a'b' & a'b'+b'^2 & b'^2 \end{pmatrix}$

Table 3.3: *Viable textures of m_D and M^{-1} with corresponding m_ν.*

The resultant texture belongs to 4 equalities and 1 zero. It is noteworthy that we do not impose texture zeros on each entry, but rather force the parameter b to be zero. On the other hand, if we consider the following m_D and put $b = 0$ and $c = 0$ we get,

$$\begin{pmatrix} a & a & c \\ b & b & a \end{pmatrix} \rightarrow \begin{pmatrix} a & a & 0 \\ 0 & 0 & a \end{pmatrix}. \tag{3.2.24}$$

Thus, after putting the zeros, the resultant matrix is the same in both cases though Eq. (3.2.24) is obtained by setting two different parameters to be zero. In that sense (3.2.24) belongs to 3 equalities and 2 zeros denoting the fact that the zeros have originated from different parameters. Such a classification is justified because strictly speaking, when we impose texture zeros then it does not imply exact zero element but some matrix element which is anomalously small compared to the other elements[‡]. Therefore in the most general scenario the two matrices can belong to different categories although the total number of reductions remain the same. However, it is to be noted that we have treated a zero as an exact zero and from this viewpoint both (3.2.23) and (3.2.24) will give identical results for the predictions of masses and mixing angles. Therefore

[‡]From the viewpoint of model building it is difficult to obtain exact zeros for instance due to quantum corrections.

once we consider the case of 4 equalities and 1 zero we need not redo the calculations for 3 equalities and 2 zeros. Generalizing the above we can say that in our calculations when we put more than one zero in any of the matrices, it eventually increases the number of equalities of that matrix and reduce the number of zeros. Thus m equalities and n zeros already gets considered under $m+1$ equalities and $n-1$ zeros. One can continue this reduction till $n=2$. Thus maximum number of zeros in any reduction is 2, distributed as one zero in m_D and one zero in M.

The maximum possible number of reductions that one can get in minimal seesaw model is 7. The parameter reductions can be distributed as equalities and zeros according to the following tables (for total 7 and 6 reduction cases):

Total 7 reductions

equality	zero	results
7	0	×
6	1	×
5	2	×

Total 6 reductions

equality	zero	results
6	0	×
5	1	×
4	2	√

In the tables, the symbol "√" means there are textures which are compatible to the current oscillation data, and the symbol "×" means there is no such viable one in each case. The general textures in each case are created, for example, by imposing the zero elements on (3.2.22). By thorough examinations of all possibilities, we find four almost viable textures in 4 equalities + 2 zero case, listed in Table 3.3. Besides there are two textures in the 5 equalities + 1 zero case with vanishing θ_{13} and other parameters in the experimental range, but discarded by the result of reactor experiments [200–202]. The total number of textures that we analyzed in the above two categories were 456. On the other hand, no viable solution exists at the level of 7 reductions.

In Table 3.4 we present numerical values of the five oscillation parameters, the averaged neutrino mass $\langle m_{ee}\rangle$ governing neutrino-less double beta ($0\nu2\beta$) decay, the neutrino mass m_β probed in tritium beta decay and the mass ordering for the four allowed textures. We also indicate whether the

	I($\eta=-0.1$)	II($\eta=-0.28$)	III($\eta=0.25$)	IV($\eta=-0.15$)
Δm^2_{21} [10^{-5}eV^2]	7.62	8.20	8.2	7.12
$\lvert\Delta m^2_{31}\rvert$ [10^{-3}eV^2]	2.40	2.30	2.30	2.74
$\sin^2\theta_{12}$	0.33(0.31)	0.23(0.35)	0.24(0.35)	0.30(0.28)
$\sin^2\theta_{23}$	0.54(0.56)	0.52(0.54)	0.51(0.46)	0.58(0.60)
$\sin^2\theta_{13}$	0.039(0.022)	0.05(0.029)	0.042(0.31)	0.046(0.028)
$\langle m_{ee}\rangle$ [eV]	0.017(0.019)	0.004(0.005)	0	0(0.004)
m_β [eV]	0.049	0.012(0.01)	0.011(0.01)	0.01(0.01)
Normal hierarchy	$\times$	$\surd$	$\surd$	$\surd$
Inverted hierarchy	$\surd$	$\times$	$\times$	$\times$
I_l	$\neq 0$	$\neq 0$	$\neq 0$	$\neq 0$
I_h	0	0	0	$\neq 0$

Table 3.4: *Representative values (values for the perturbed (η) cases are presented inside the brackets) of the five oscillation parameters for the allowed solutions. We also present the mass m_β probed in β-decay and the effective mass $\langle m_{ee}\rangle$ governing neutrino less double beta decay. In the items for the mass ordering, the symbol "$\surd$" means each texture accommodates the corresponding mass patterns, and "$\times$" means it does not. The last two items show finiteness of the invariant measures for the CP violation [136–138] at low and high energy respectively.*

basis-independent measures of low and high energy CP violation are zero or non-zero. In obtaining the values of the mixing angles we take the mass squared differences from their allowed 3σ ranges of Table 1.1 and check if the values of all the 3 mixing angles lie within the allowed range or not. In the items for the mass ordering, the symbol "$\surd$" means each texture is consistent with the corresponding mass orderings, and "$\times$" means it is not. The textures I is consistent with the inverted hierarchy while II, III and IV accommodate the normal hierarchy.

The resultant mass matrices after seesaw diagonalization for case I has $(m_\nu)_{\tau\tau}$ =0. In principle this texture can be analyzed as in Section 3.2.1.2, [174]. But, as this texture (so also the other three) contains only two independent parameters, definite predictions can be made for them by equating the two non zero eigen values with two mass squared differences. The two nonzero eigenvalues of the resultant matrix m_ν (for texture I), obtained after seesaw diagonalization, are

$$\lambda_\pm = \frac{1}{2}\left(a'^2 + 4a'b' + b'^2 \pm \sqrt{9a'^4 + 8a'^3b' + 14a'^2b'^2 + 8a'b'^3 + 5b'^4}\right) \quad (3.2.25)$$

where $a' \equiv a\sqrt{A}$ and $b' \equiv b\sqrt{A}$. Identifying these as $\lambda_- = -\sqrt{|\Delta m^2_{31}| + \Delta m^2_{21}}$ and $\lambda_+ = \sqrt{|\Delta m^2_{31}|}$ the parameters a' and b' are fixed in terms of the two mass differences. These can be expressed in powers of r (ratio of the mass squared differences as in Eq. 2.3.39) as,

$$\begin{aligned} a' &\simeq \left(|\Delta m^2_{31}|\right)^{1/4} \left(0.848 + 0.116\, r + \mathcal{O}(r^2)\right), \\ b' &\simeq -\left(|\Delta m^2_{31}|\right)^{1/4} \left(0.227 + 0.201\, r + \mathcal{O}(r^2)\right). \end{aligned} \tag{3.2.26}$$

All nonzero values of the mixing angles can be described as functions of the mass differences as,

$$\sin\theta_{12} \simeq 0.57 + 0.01\, r, \tag{3.2.27}$$

$$\sin\theta_{23} \simeq 0.73 + 0.04\, r, \tag{3.2.28}$$

$$\sin\theta_{13} \simeq 0.19 + 0.15\, r. \tag{3.2.29}$$

This texture gives a relatively large θ_{13}. It is to be noted that for the texture I, the possible ranges of the mixing angles are narrow; the values $\sin\theta_{ij}$'s vary at most a few percent. The solution I is consistent with IH and $m_3 = 0$. This texture was allowed in the 3σ ranges of oscillation parameter according to [203]. The effective mass governing neutrino-less double beta decay for this case can be approximated as [204]

$$\langle m_{ee}\rangle = \sqrt{\Delta m^2_{31}}\sqrt{1 - \sin^2 2\theta_{12}\sin^2 2\alpha} \tag{3.2.30}$$

where α denotes the Majorana Phase. The values of $\langle m_{ee}\rangle$ presented in Table 3.4 are obtained by using the above expression with $\alpha = \pi/4$.

Texture II does not contain any zero in the effective light neutrino mass matrix which make the solution rather cumbersome. In Table 3.4 we present representative values for the prediction of this texture. For the solution III and IV the element $(m_\nu)_{ee}$ in the resultant light neutrino mass matrix is vanishing. This predicts the effective mass governing neutrino-less double beta decay to be zero.

	$m_D\,(\eta)$	$m_\nu\ \left(a'=a\sqrt{A}\,, b'=b\sqrt{A}\right)$
I	$\begin{pmatrix} b & a & a\,(1+\eta) \\ a & b & 0 \end{pmatrix}$	$\begin{pmatrix} a'\,(a'+2b') & a'^2+a'b'+b'^2 & a'^2\,(1+\eta) \\ a'^2+a'b'+b'^2 & b'\,(2a'+b') & a'b'\,(1+\eta) \\ a'^2\,(1+\eta) & a'b'\,(1+\eta) & 0 \end{pmatrix}$
II	$\begin{pmatrix} a & b & a \\ a\eta & a & b \end{pmatrix}$	$\begin{pmatrix} a'^2 & a'\,(b'+a'\eta) & a'\,(a'+b'\eta) \\ a'\,(b'+a'\eta) & a'^2+b'^2 & 2a'b' \\ a'\,(a'+b'\eta) & 2a'b' & a'^2+b'^2 \end{pmatrix}$
III	$\begin{pmatrix} a & a & b\,(1+\eta) \\ 0 & b & a \end{pmatrix}$	$\begin{pmatrix} 0 & a'b' & a'^2 \\ a'b' & 2a'b' & a'^2+b'^2\,(1+\eta) \\ a'^2 & a'^2+b'^2\,(1+\eta) & 2a'b'\,(1+\eta) \end{pmatrix}$
IV	$\begin{pmatrix} a\eta & a & b \\ a & b & a\eta \end{pmatrix}$	$\begin{pmatrix} 2a'b'\eta & a'^2+b'\,(a'+b')\,\eta & b'\,(a'+b'\eta) \\ a'^2+b'\,(a'+b')\,\eta & a'\,(a'+2b') & b'^2+a'\,(a'\eta+b') \\ b'\,(a'+b'\eta) & b'^2+a'\,(a'\eta+b') & b'\,(b'+2a'\eta) \end{pmatrix}$

Table 3.5: *The allowed textures of m_D with small perturbation (η) in the equalities/zeros along with the corresponding m_ν. M^{-1} remains the same as in Table 3.3.*

In general for NH in the limit $m_1 \to 0$ the expression for $\langle m_{ee}\rangle$ is [204],

$$\langle m_{ee}\rangle = \sqrt{\Delta m^2_{32}}|\sqrt{r}\sin^2\theta_{12} + \sin^2\theta_{13}e^{-2i(\alpha+\delta)}| \tag{3.2.31}$$

where δ is the Dirac CP violating phase. Assuming the phase factor to be -1, the solar and reactor angles correlate with r as $\sin^2\theta_{13}/\sin^2\theta_{12} = \sqrt{r}$. For the current allowed values of θ_{12} and r, this relation implies large θ_{13}.

Besides these 4 combinations, the patterns obtained by permuting 2-3 column of m_D for each combination in the above list will also be compatible with the data. This is because the 2-3 column exchange keeps θ_{23} close to $\pi/4$ without disturbing the good agreement of θ_{12} with the data. The predicted θ_{13} also remains the same. Although such 4 counterparts are independent textures, we present only 4 textures in the table because physical predictions of the 4 counterparts are almost the same as the original ones.

At this level of minimality, patterns other than these 8 textures are not consistent with the 3σ ranges of parameters [203].

However, in view of the recent global analysis of the neutrino oscillation data [36,198], we see that the predicted value of the reactor angle (presented in

Table 3.4) falls outside the 3σ range. Thus we conclude that at the level of six reductions, there are no allowed solutions incorporating the present precision measurement of θ_{13} and one should explore the lower level of reductions (*i.e.* total of 5 reductions). In five reductions, number of independent parameters are three whereas number of equations to constrain them is two. Thus the predictive power gets reduced. But for the textures of six reductions whose solutions lie near the vicinity of the 3σ ranges of the present precision data, a small perturbation can bring the solutions inside the 3σ regions. As an illustration, we consider applying small perturbation to disturb the equalities or elevate the zeros. Some representative cases are presented inside the brackets, (), of Table 3.4. It is noteworthy to mention that these perturbations are proportional to a or b, hence does not introduce any new phase in the mass matrix consequently the CP violating behavior at low and high energy of these textures remains similar as before.

We note that the neutrino mass m_β probed by direct searches in tritium β-decay experiments for IH (in the limit $m_3 \to 0$) is given as [204]

$$m_\beta = \sqrt{\Delta m^2_{31}} \tag{3.2.32}$$

For NH in the limit $m_1 \to 0$, m_β can be expressed as [204]

$$m_\beta = \sqrt{\sin^2\theta_{12}\Delta m^2_{21} + \sin^2\theta_{13}\Delta m^2_{31}} \tag{3.2.33}$$

In Table 3.4 we present the values of m_β for the four allowed patterns. For all the scenarios m_β is below the sensitivity (0.2 eV) of KATRIN experiment [205, 206].

The texture forms should be assumed at some high-energy scale where the right-handed neutrinos are not decoupled from the theory. Since the see-saw scale is expected to be around 10^{14} GeV for $\mathcal{O}(1)$ Yukawa couplings, extrapolation to the low energy scale by Renormalization Group (RG) equations is necessary. However, within the SM, the RG effects on the neutrino parameters are appreciable only if the light neutrino spectrum is quasi-

degenerate [97,99,103,106,107,207,208]. In the seesaw scenario with two heavy neutrinos, we necessarily have one massless neutrino and hence a hierarchical spectrum. Thus the RG effects are not strong enough to disfavor an allowed texture or allow a disfavored texture within the present setup. Also the two heavy neutrinos are almost degenerate, so threshold effect is absent.

3.2.2.3 CP violation at high and low-energy scales

Besides the predictions for the oscillation parameters and the $0\nu2\beta$ decay, distinctive features of each texture also appear in CP violating phenomena. In this section, we discuss leptogenesis [59] and CP violation at the neutrino oscillation for the almost allowed hybrid textures. Here we deal with non-flavored leptogenesis [209–211].

In Table 3.4, we demonstrate whether I_l and I_h are zero or non-zero for each of the solutions. All the solutions allow I_l to be non-vanishing in general indicating the possibility of observing CP violation at low energy. As for the high-energy CP violation, the textures I, II, and III give $I_h = 0$ while solutions IV give $I_h \neq 0$. Thus, only the texture IV accommodates non-vanishing values for both I_l and I_h so that there can be a correlation between low and high energy CP violation. In what follows we consider in detail the prediction of this interesting solution for leptogenesis and explore the correlation between CP violation at high and low-energy scales in the limit $\eta \to 0$.

The relation between leptogenesis and CP violation at low energy stems from the fact that there is only one physical phase in the neutrino mass matrices, and the one phase controls both the baryon to photon ratio η_B and the invariant measure $J_{\rm CP}$. Without loss of generality, one may take

$$m_D = x \begin{pmatrix} 0 & |a|e^{i\varphi} & |b| \\ |a|e^{i\varphi} & |b| & 0 \end{pmatrix}, \quad M_R^{-1} = \begin{pmatrix} |A| & |A| \\ |A| & 0 \end{pmatrix}. \tag{3.2.34}$$

The phase of the element A and b have been absorbed into the right-handed neutrino fields. With this phase convention, η_B and $J_{\rm CP}$ are given as the function of the phase φ with the condition that $\eta_B = J_{\rm CP} = 0$ at $\varphi = 0$.

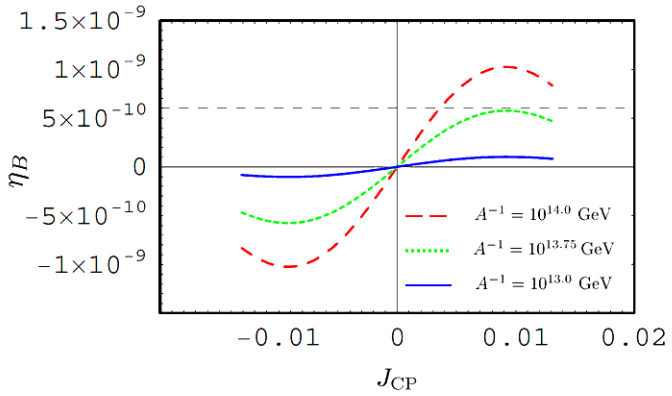

Figure 3.1: *The baryon-to-photon ratio η_B as a function of the Jarlskog invariant $J_{\rm CP}$. The Horizontal dashed line shows $\eta_B = 6 \times 10^{-10}$ suggested by the WMAP observation.*

Fig. 3.1 shows the parametric plot of η_B and $J_{\rm CP}$ as a function of the phase φ. The dashed(red), dotted(green) and solid(blue) curves are the cases of the heavy mass scales $A^{-1} = 10^{14.0}$, $10^{13.75}$ and $10^{13.0}\,$GeV respectively. The other parameters are determined so that the data in Table 1.1 are satisfied. From Fig. 3.1, it is seen that the absolute value of the baryon asymmetry $|\eta_B|$ is increased as the right-handed neutrino scale is increased with a fixed value of $J_{\rm CP}$. The observed baryon asymmetry is achievable only if the scale A^{-1} is larger than $\simeq 10^{13.75}\,{\rm GeV} = 5.6 \times 10^{13}$ GeV which corresponds to the right-handed neutrino masses $M_1 = 3.5 \times 10^{13}\,{\rm GeV}$ and $M_2 = 9.1 \times 10^{13}\,{\rm GeV}$. For a fixed successful number of the baryon asymmetry η_B, there is a correlation between the invariant $J_{\rm CP}$ and the right-handed neutrino scale A^{-1}. For $A^{-1} > 10^{13.75}\,{\rm GeV}$, the relation is represented by

$$J_{\rm CP} \sim 0.01 \left(\frac{10^{13.75}\,{\rm GeV}}{A^{-1}} \right)^2 . \tag{3.2.35}$$

Thus low energy CP violation can be correlated with the mass scale of the right handed neutrino. The texture IV predicts measurable CP violation at future oscillation experiments if the right-handed neutrino scale is around $5.6 \times 10^{13} \lesssim A^{-1} \lesssim 7 \times 10^{13}\,{\rm GeV}$.

3.3 Stability of electroweak vacuum in presence of heavy fields

In this section, we discuss the effect of neutrino Yukawa coupling on the stability of electroweak vacuum. As mentioned in Chapter 2.4.4.2, the electroweak vacuum is likely to get destabilized due to the presence of this new Yukawa term. Requirement of the stability of the electroweak vacuum puts constraints on the Yukawa couplings of seesaw model. We take minimal linear seesaw model (MLSM) for this study as this model is fully reconstructible. Moreover, as we shall see, the assumption of small lepton number violation leads to a simplification in the beta function of λ, thus allowing one to obtain constraint on the overall Yukawa coupling strength.

3.3.1 Vacuum Stability in the Minimal Linear Seesaw Model

The MLSM contains two degenerate singlet neutrinos at TeV scale (2.3.30). Presence of these fields modify the SM Renormalization Group Equations for the Yukawa couplings and the Higgs self coupling, for scale higher than the mass of the singlets. Including the corrections due to the neutrino Yukawa couplings upto one loop, the modified β function governing the running of λ is given as,

$$\beta'^{(1)}_{\lambda} = \beta^{(1)}_{\lambda} + 4\mathrm{Tr}(Y_\nu'^{\dagger} Y'_\nu)\lambda - 2\mathrm{Tr}[(Y_\nu'^{\dagger} Y'_\nu)^2] \tag{3.3.1}$$

where $Y'^{T}_{\nu} = \left(Y^{T}_{\nu},\, Y^{T}_{S}\right)$. The one loop β functions corresponding to the Yukawa couplings Y_u, Y_d and Y_e also acquire additional factors containing $Y_\nu'^{\dagger} Y'_\nu$ [158]. Finally, one needs to include the RG running of the coupling Y'_ν which is governed by the following equation [158]:

$$16\pi^2 \mu \frac{dY'_\nu}{d\mu} = Y'_\nu \left[\frac{3}{2} Y_\nu'^{\dagger} Y'_\nu - \frac{3}{2} Y_e^{\dagger} Y_e + T_1 - \frac{9}{20} g_1^2 - \frac{9}{4} g_2^2\right] \tag{3.3.2}$$

In this case the quantity T_1 is given by, same as in Eq. 2.4.31,

$$T_1 = \text{Tr}\left[3Y_u^\dagger Y_u + 3Y_d^\dagger Y_d + Y_e^\dagger Y_e + Y_\nu'^\dagger Y_\nu'\right] \tag{3.3.3}$$

RG equation for neutrino Yukawa coupling is taken upto one loop.

The Y_ν' dependence of the beta function of λ is in terms of $\text{Tr}\left[Y_\nu'^\dagger Y_\nu'\right]$ and $\text{Tr}\left[(Y_\nu'^\dagger Y_\nu')^2\right]$ only. From the parameterization of Y_ν and Y_S (2.3.37,2.3.40), we find

$$\text{Tr}\left[Y_\nu'^\dagger Y_\nu'\right] = y_\nu^2 + y_s^2 \simeq y_\nu^2, \tag{3.3.4}$$

$$\text{Tr}\left[Y_\nu'^\dagger Y_\nu' Y_\nu'^\dagger Y_\nu'\right] = y_\nu^4 + 2y_\nu^2 y_s^2 \rho^2 + y_s^4 \simeq y_\nu^4 \tag{3.3.5}$$

since $y_s << y_\nu$. The exact equalities in the above expressions are also held without the parameterization of Eq. (2.3.37,2.3.40). However ρ remains undetermined. Also small y_s makes the trace terms single parameter dependent. Thus β_λ contains only one unknown parameter (*i.e.* y_ν) whereas for Type-I seesaw, all the unknown parameters enter into the expression of β_λ.

Also we can see from Eq. (3.3.4,3.3.5) that the trace terms do not depend on the neutrino oscillation parameters. In addition, under the approximation of $y_s << y_\nu$, there is no dependence on mass hierarchy as well (only ρ depends on hierarchy). In Fig. 2.8 we show the effect of inclusion of this term on the running of λ.

In Fig. 3.2 we give the plot of the allowed region of y_ν as a function of the Higgs mass for fixed values of top mass and the strong coupling constant. The two curves with the same line type(color) that are close to each other correspond to the condition $\tilde{\lambda}(M_{pl}) = 0$ (the upper curve) and $\lambda(M_{pl}) = 0$ (the lower curve). The region below the curves satisfy the condition of vacuum stability. $y_\nu = 0$ corresponds to the SM. The first panel is for $m_t = 172.6$ GeV. For this value of top mass, only a small allowed region in y_ν is obtained for Higgs mass > 126.3 GeV and $\alpha_s = 0.1191$, considering the condition $\tilde{\lambda}(M_{pl}) = 0$. From this we obtain an upper bound $y_\nu \lesssim 0.16$. The 2$^{\text{nd}}$ panel corresponds to a lower value of $m_t = 172.3$ GeV. In this case we obtain the upper bound

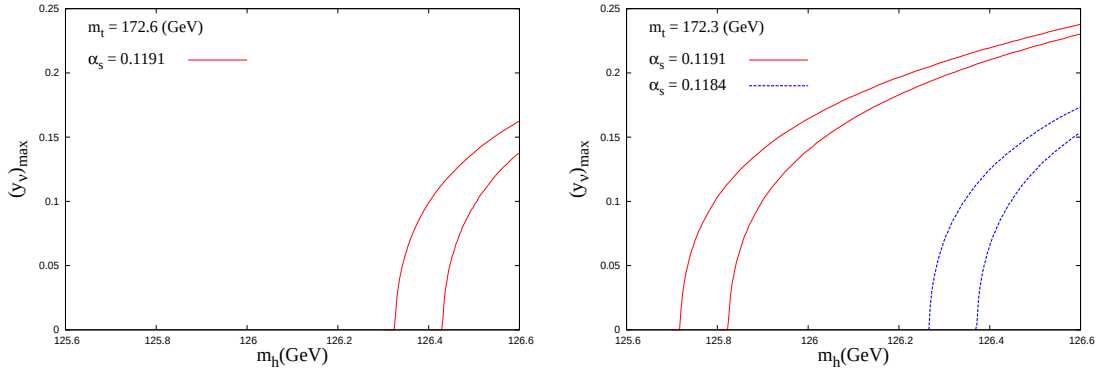

Figure 3.2: *The allowed region of y_ν with varying Higgs mass. The region below the curves is allowed. Among the two same type (color) lines, the upper line corresponds to $\tilde{\lambda}(M_{pl}) \geq 0$ and the lower line corresponds to $\lambda(M_{pl}) \geq 0$.*

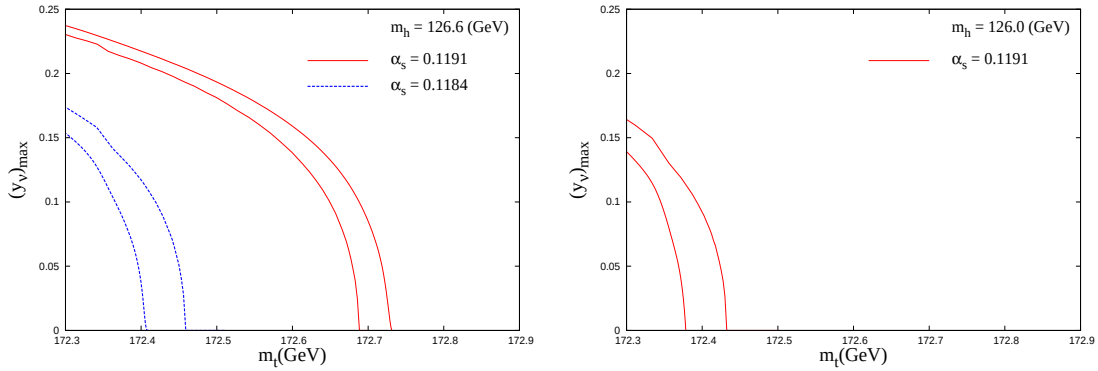

Figure 3.3: *Same as in Fig. 3.2 with varying top mass.*

$y_\nu \lesssim 0.24$ for $\alpha_s = 0.1191$. This bound is obtained for a Higgs mass of 126.6 GeV. For lower values of Higgs mass, the allowed y_ν values are correspondingly lower. Fig. 3.3 shows the variation of y_ν with m_t for fixed values of Higgs mass. Again larger values of m_h and α_s and smaller values of m_t admit a larger allowed range of y_ν. Fig. 3.4 show the variation of y_ν with α_s. In general, larger allowed regions are obtained for higher values of Higgs mass, lower values of top mass and higher values of α_s. From the above figures we obtain overall upper bound on the value of y_ν as [212]

$$y_\nu \lesssim 0.24 \tag{3.3.6}$$

The above plots are obtained by keeping M_R fixed at 1 TeV.

In Fig. 3.5 we show how the upper bound on y_ν depends on the scale of

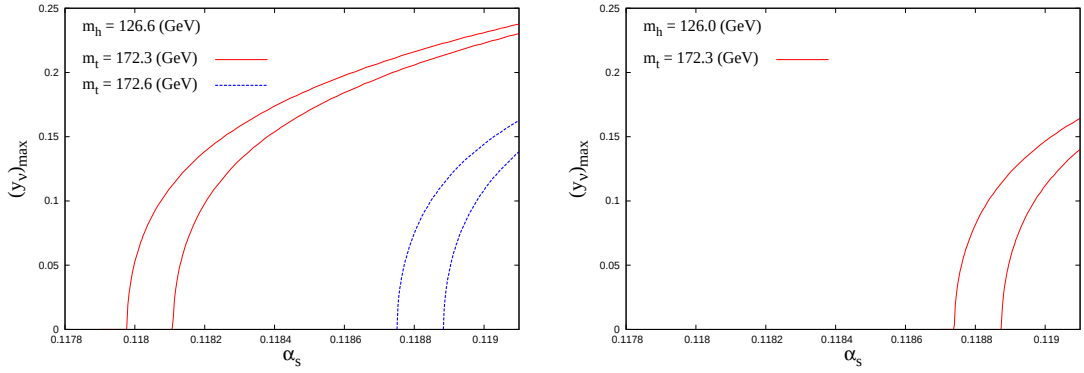

Figure 3.4: *Same as in Fig. 3.2 with varying strong coupling constant.*

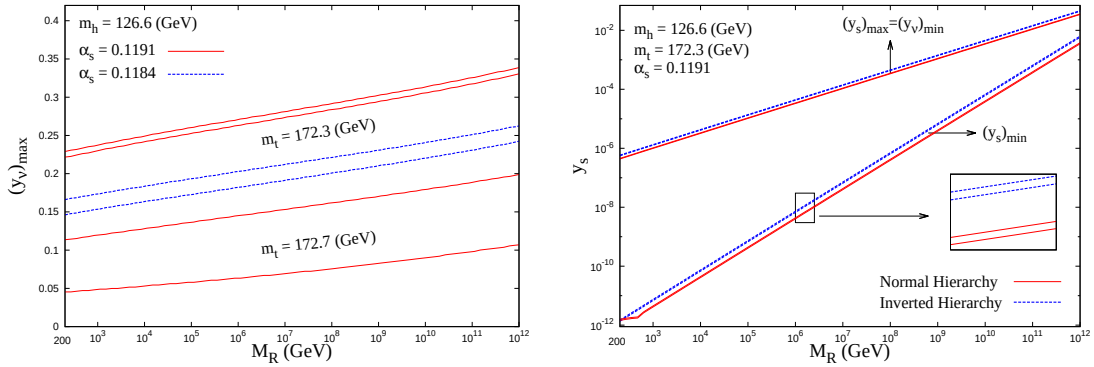

Figure 3.5: *The left-panel shows the upper bound on y_ν as a function of the right-handed neutrino mass from consideration of vacuum stability. The upper set of lines are for $m_t = 172.3$ GeV (with two different values of α_s) and the lower lines are for $m_t = 172.7$ GeV (with single value of α_s). The red (green) solid (dashed) line in the right panel shows the upper limit on y_s (same as the lower limit of y_ν) obtained from the measured value of $\sqrt{\Delta m^2_{atm}}$ for NH (IH). Also shown are the lower bound on y_s from vacuum stability and neutrino masses. See text for details .*

M_R. We see that variation of M_R within a few TeV (which is our range of current interest) would not change the bound on y_ν drastically. In fact this trend continues even if M_R is increased to higher values. At $M_R = 10^{12}$ GeV, the upper bound on y_ν obtained is [212],

$$y_\nu \lesssim 0.34 \tag{3.3.7}$$

It is noteworthy to mention that for higher values of M_R, y_s needs to be increased to keep the neutrino mass in the desired range. Beyond 10^{12} GeV the contribution from the y_s term starts getting significant and hence this needs to be included in the RG evolution.

3.3.2 Constraints from Neutrino Mass

In the linear seesaw model lepton number breaking is introduced by the term m_S while the term m_D conserves lepton number. Since the absence of the term m_S enhances the symmetry of the Lagrangian it is natural to assume that the lepton number violating term is much smaller than the lepton number conserving term. This consideration puts an absolute upper bound on y_s which is

$$(y_s)_{max} \leq y_\nu \tag{3.3.8}$$

This also defines a lower limit on y_ν since for smaller values of y_s, y_ν has to be higher so that the relation $y_\nu y_s v^2/M_R \sim m_\nu$ is satisfied. Thus the above equation can be made to imply a stronger statement which is

$$(y_s)_{max} \leq (y_\nu)_{min} \tag{3.3.9}$$

On the other hand, the upper bound on y_ν at each M_R, as obtained from the vacuum stability condition can be used to obtain a lower bound on y_s, again from the standpoint of producing correct neutrino masses. From these considerations it is possible to set a lower bound on y_ν and lower and upper bounds on y_s for both NH and IH. The right panel in Fig. 3.5 displays these bounds on

y_s as a function of M_R incorporating the constraints on neutrino mass squared differences from oscillation data for NH and IH. The mass eigenvalues in NH can be expressed as,

$$m_1 = 0, \quad m_2 = \frac{y_\nu y_s v^2}{2M_R}(1-\rho), \quad m_3 = \frac{y_\nu y_s v^2}{2M_R}(1+\rho) \quad (NH) \tag{3.3.10}$$

where m_2 and m_3 are related to the mass squared differences ($\Delta m^2_{ji} = m^2_j - m^2_i$) as,

$$\begin{aligned} m_2 &= \sqrt{\Delta m^2_{21}} = \sqrt{\Delta m^2_\odot} \\ m_3 &= \sqrt{\Delta m^2_{32} + \Delta m^2_{21}} = \sqrt{\Delta m^2_{atm} + \Delta m^2_\odot} \end{aligned} \tag{3.3.11}$$

This gives us the following equations for NH:

$$\frac{\sqrt{\Delta m^2_\odot}}{(1-\rho)} = \frac{\sqrt{\Delta m^2_{atm}}}{(2\sqrt{\rho})} = \frac{y_\nu y_s v^2}{2M_R} \tag{3.3.12}$$

Taking $\rho \approx 1 - 2\sqrt{r}$ for NH, the above equations give a single equation:

$$y_\nu y_s \approx M_R \sqrt{\Delta m^2_{atm}}/v^2 \tag{3.3.13}$$

Using Eq. (3.3.9) and Eq. (3.3.10) in Eq. (3.3.13) one gets (with $(y_s)_{max} = (y_\nu)_{min}$),

$$(y_s)_{max} \approx \sqrt{M_R}(\Delta m^2_{atm})^{1/4}/v \tag{3.3.14}$$

This defines the upper bound on y_s (or the lower bound on y_ν) for each M_R. The solid (red) line in the right panel in Fig. 3.5 displays these bounds as a function of M_R. The plot is obtained using the exact Eq. (3.3.12) and The uncertainty in the values of $\Delta m^2_\odot$ and Δm^2_{atm} gives a thin band which is displayed in the inset. On the other hand since we know $(y_\nu)_{max}$ at each M_R from consideration of vacuum stability, the above equation gives us a lower bound on y_s as

$$y_s \gtrsim \frac{M_R \sqrt{\Delta m^2_{atm}}}{v^2 (y_\nu)_{max}}. \tag{3.3.15}$$

This is also shown in Fig. 3.5.

For IH the mass eigenvalues are given as,

$$m_3 = 0, \quad m_1 = \frac{y_\nu y_s v^2}{2M_R}(1-\rho), \quad m_2 = \frac{y_\nu y_s v^2}{2M_R}(1+\rho) \tag{3.3.16}$$

The absolute masses can be expressed in terms of mass squared differences as,

$$m_1 = \sqrt{\Delta m^2_{13}} = \sqrt{\Delta m^2_{atm}}, \quad m_2 = \sqrt{\Delta m^2_{\odot} + \Delta m^2_{atm}} \tag{3.3.17}$$

and we get,

$$\frac{\sqrt{\Delta m^2_{atm}}}{(1-\rho)} = \frac{\sqrt{\Delta m^2_{\odot}}}{(2\sqrt{\rho})} = \frac{y_\nu y_s v^2}{2M_R}. \tag{3.3.18}$$

Taking $\rho \approx r/4$ for IH, we get a single equation

$$y_\nu y_s \approx 2M_R\sqrt{\Delta m^2_{atm}}/v^2. \tag{3.3.19}$$

Again this gives an upper bound on y_s which is the same as the lower bound on y_ν. This is shown in the right panel of Fig. 3.5 by the dashed (green) line. Similarly one can also use this equation and Similarly one can use the upper bound on y_ν obtained from vacuum stability condition to put a lower bound on y_s which is displayed in Fig. 3.5.

The bounds on y_s for $M_R = 1$ TeV :

$$(4.6 - 5.0) \times 10^{-12} < y_s < (1.05 - 1.09) \times 10^{-6} \qquad \text{NH} \tag{3.3.20}$$

$$(7.6 - 8.3) \times 10^{-12} < y_s < (1.35 - 1.4) \times 10^{-6} \qquad \text{IH} \tag{3.3.21}$$

Thus using constraints from vacuum stability and neutrino masses, one can determine the range of the unknown coupling parameters y_ν and y_s.

3.3.3 Constraints from Lepton Flavor Violation

As mentioned in Chapter 2.4.2, that LFV processes are suppressed in high scale seesaw model. However in TeV scale seesaw models, since lepton number

Branching Ratios	Experimental constraints
$\mathrm{Br}(\mu \to e\gamma)$	$< 2.4 \times 10^{-12}$
$\mathrm{Br}(\tau \to e\gamma)$	$< 3.3 \times 10^{-8}$
$\mathrm{Br}(\tau \to \mu\gamma)$	$< 4.4 \times 10^{-8}$
$\mathrm{Br}(\mu \to 3e)$	$< 1.0 \times 10^{-12}$
$\mathrm{Br}(\tau \to 3e)$	$< 2.7 \times 10^{-8}$
$\mathrm{Br}(\tau \to 3\mu)$	$< 2.1 \times 10^{-8}$
$\mathrm{Br}(\tau \to e\mu\mu)$	$< 1.7 \times 10^{-8}$
$\mathrm{Br}(\tau \to ee\mu)$	$< 1.5 \times 10^{-8}$

Table 3.6: Various experimental constraints from charged lepton flavor violating decays [4].

violation (LNV) is separated from the scale of lepton flavor violation (LFV), this may not be the case [53, 213]. It is well known that LNV is due to the dimension 5 operator whereas the LFV can be related to the dimension 6 operator. In general, the flavor structure of the coupling strengths of these operators are not correlated. However, in MLSM such a relation can be established from the hypothesis of minimal flavor violation [214].

In this section we consider the branching ratios of LFV decays in MLSM. In view of the recent measurement of θ_{13} the branching ratios now can be studied in terms of the CP phases. In addition, from the experimental upper limits on LFV processes one can obtain constraints on the parameter y_ν/M_R as a function of the CP phases. When combined with the upper bound on y_ν from vacuum stability as a function of M_R, the parameter space can be further constrained. Table 3.6 lists the experimental constraints coming from the charged lepton flavor violating decays [4].

In this section we shall concentrate only on the constraints coming from $\mu \to e\gamma$ channel since this is the most constraining as can be seen from Table 3.6 [§].

Branching ratio for the process, $\mu \to e\gamma$ is given in Eq. (2.4.15). The current experimental constraint on this is obtained by MEG Collaboration [144] (see, Table 3.6). Using the parameterization of Y_ν and Y_S in Eq.(2.3.37) and (2.3.40),

[§]Although the $\mu \to 3e$ conversion in nuclei has a better constraint, the sensitivities are lowered by the uncertainties in nuclear form factors [215, 216].

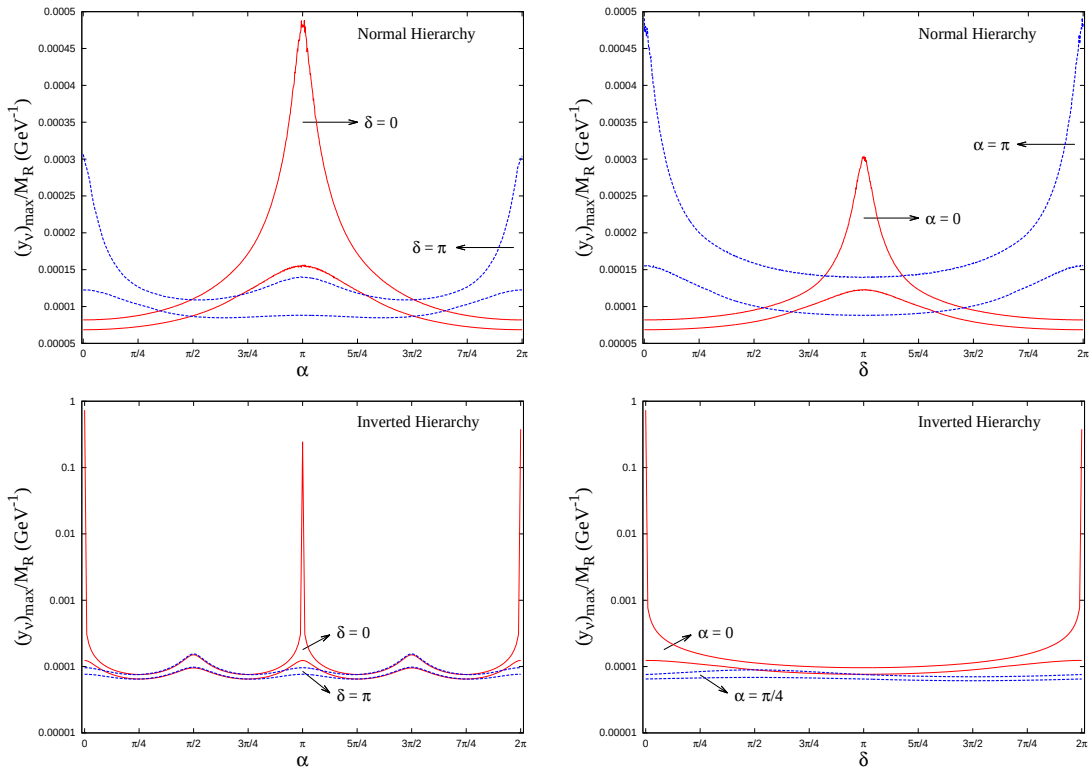

Figure 3.6: *The upper panels show the allowed regions of y_ν/M_R vs the CP phases α and δ for NH while the lower panels are for IH. The area below each curve is consistent with the experimental upper bound on the rate of $\mu \to e\gamma$. The two lines of the same type (color) correspond to the maximum and minimum value of the upper bound obtained by varying the oscillation parameters over their 3σ range.*

we obtain, for normal hierarchy

$$\begin{aligned} \mathrm{Br}\left(\mu \to e\gamma\right) &= \frac{3\alpha}{8\pi}\frac{y_\nu^4 v^4}{4M_R^4} f^2(x)\left(\sqrt{r}s_{12}^2 + 2\,r^{(1/4)}s_{13}s_{12}c_{(\alpha+\delta)}\right)s_{23}^2 \\ &\quad + \mathcal{O}\left(y_s, (\sqrt{r}, s_{13})^2\right) \end{aligned} \tag{3.3.22}$$

In the above expressions and in subsequent part, we have used the following notations

$$\begin{aligned} s_{ij} &= \sin\theta_{ij}, \quad c_{ij} = \cos\theta_{ij}, \quad c_{\alpha+\delta} = \cos(\alpha+\delta), \quad s2_{ij} = \sin 2\theta_{ij}, \\ c2_{ij} &= \cos 2\theta_{ij}, \quad s4_{ij} = \sin 4\theta_{ij}, \quad c4_{ij} = \cos 4\theta_{ij}, \quad c2_\alpha = \cos 2\alpha, \\ c4_\alpha &= \cos 4\alpha \quad \text{etc.} \end{aligned} \tag{3.3.23}$$

The above equation (3.3.22) in conjunction to the upper bound on the $\mathrm{Br}(\mu \to$

$e\gamma$) can be used to put an upper bound on y_ν/M_R as,

$$y_\nu/M_R < \left[\frac{2.4\times10^{-10}}{3\alpha v^4 f^2(x) G^{NH}(r,\theta_{ij},\alpha,\delta)}\right]^{1/4}. \tag{3.3.24}$$

Here, the factor $G^{NH}(r,\theta_{ij},\alpha,\delta)$ contains the oscillation parameters. The upper bound on y_ν/M_R varies in a range depending on the values of the CP phases. The minimum value of the upper bound occurs at $\alpha+\delta=0$ while the maximum occurs at $\alpha+\delta=\pi$. This is reflected in the top panels in Fig. 3.6 where we display the allowed values of y_ν/M_R as a function of the CP phases[¶]. The left most panel displays the variation of the upper bound in y_ν/M_R as a function of the Majorana phase α. The solid(red) line corresponds to the Dirac phase $\delta=0$ while the dashed (green) line is for $\delta=\pi$. The other oscillation parameters are marginalized over the 3σ range in Table 1.1 to give the maximum and minimum value of the upper bound on y_ν/M_R. For other values of oscillation parameters the upper bound would lie somewhere between these two values. From the figure it can be inferred that the maximum value of the upper bound on y_ν/M_R is

$$y_\nu/M_R \lesssim 0.00049(\text{GeV}^{-1}), \tag{3.3.25}$$

which occurs for $\delta=0$ and $\alpha=\pi$ for NH.

For IH, the branching ratio can be expressed as,

$$\begin{aligned}\text{Br}\,(\mu\to e\gamma) \;=\; & \frac{3\alpha}{8\pi}\frac{y_\nu^4 v^4}{4M_R^4} f^2\left(\frac{M_R^2}{m_W^2}\right)\frac{1}{16}\left[\left(3-c4_\alpha+2c2_\alpha^2 c4_{12}\right)c_{23}^2(1-s_{13})\right.\\ & \left.-\,2s_{13}\left(2s_\delta s2_\alpha(1+c2_\alpha s2_{12})+c2_\alpha c_\delta(2c2_{12}+c2_\alpha s4_{12})\right)s2_{23}\right]\\ & +\,\mathcal{O}\left(y_s,(\sqrt{r},s_{13})^2\right)\end{aligned} \tag{3.3.26}$$

From this one can again get an upper bound on y_ν/M_R. This is displayed in the lower panels in Fig. 3.6. As in NH, the value of the upper bound for IH

[¶]In this plot we have taken $f(x)$ to be unity. For $M_R=200$ GeV, there will be a multiplicative factor ~ 1.3. As M_R increases, this factor tends to become unity. In Fig. 3.7, we have included the exact value of $f(x)$ at each M_R.

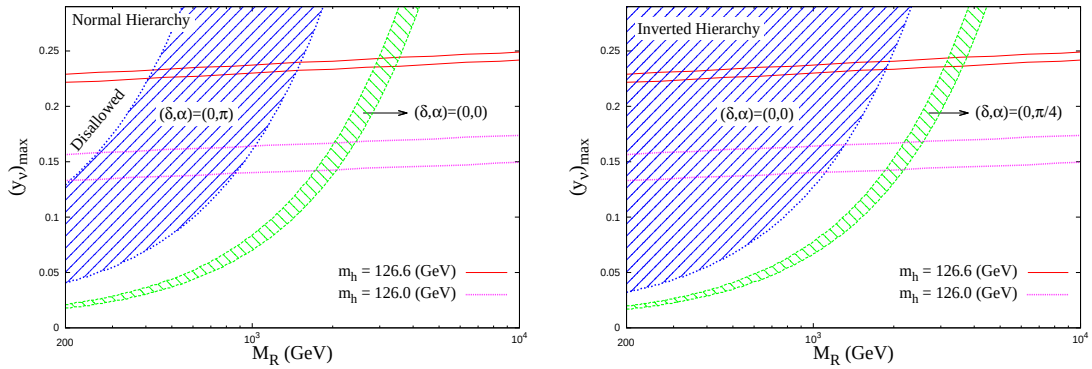

Figure 3.7: The allowed regions of y_ν^{max} as a function of M_R from the combined constraints of $Br(\mu \to e\gamma)$ and vacuum stability. The area to the right of the curved lines are allowed from experimental bound on $Br(\mu \to e\gamma)$ while the area below the slanting lines are allowed from the constraint on vacuum stability. The vacuum stability bound shown here correspond to $m_t = 172.3$ GeV and $\alpha_s = 0.1191$. The two (very) close line corresponding to $m_h = 126.6$ GeV is due to $\tilde{\lambda}(M_{pl}) = 0$ (upper one) and $\lambda(M_{pl}) = 0$ (lower one). Similarly for $m_h = 126.0$ GeV. .

also depends on the CP phases. The maximum allowed value in this case is

$$y_\nu/M_R \lesssim 0.7(\text{GeV}^{-1}), \tag{3.3.27}$$

which occurs for $\delta = 0, \alpha = 0$ as can be seen from the figure. The lines of same line type (color) corresponds to the upper bounds including the uncertainties in the masses and mixing parameters.

The maximum value of y_ν/M_R obtained from experimental bound on BR($\mu \to e\,\gamma$) (Table 3.6) and Eq. (3.3.22), can be used to retrieve the maximum value of y_ν for each M_R. This is shown in Fig. 3.7. Note that while extracting the bound on y_ν for a particular M_R from the figure, one has to be careful to ensure that the perturbativity bound on y_ν ($\lesssim 1$) is not violated. We also superimpose the bounds obtained from consideration of vacuum stability in this figure. The area to the left of the shaded bands is disallowed from the constraint on the branching ratio $\mu \to e\gamma$. These bands are obtained for fixed values of the CP phases (δ, α). The band for each combination of CP phase is obtained by varying the oscillation parameters in their current 3σ range. The area below the slanting lines are allowed from the constraint on vacuum stability. The figure shows that the constraints from Br($\mu \to e\gamma$) can some-

times further constrain the value of y_ν as obtained from vacuum stability. For instance for $M_R = 200$ GeV and NH the constraint from $\mathrm{Br}(\mu \to e\gamma)$ restricts y_ν to be ≤ 0.13 for values of CP phases $(\delta, \alpha) = (0, \pi)$. For $(\delta, \alpha) = (0, 0)$ the maximum allowed value of y_ν is lower. For other combinations of CP phases the bands lie anywhere inside or between the two shaded regions. Thus if we consider all possible values of CP phases then only the region marked disallowed is not compatible with the constraints from $\mathrm{Br}(\mu \to e\gamma)$ for NH though it was consistent with vacuum stability constraints.

For IH and $(\delta, \alpha) = (0, 0)$, the hatched region extends all the way upto $M_R = 200$ GeV and there is no significant constraint from $\mu \to e\gamma$ given the present uncertainty on the neutrino oscillation parameters. However for the green hatched region corresponding to $(\delta, \alpha) = (0, \pi/4)$ the region to its left is disfavored and y_ν^{max} is constrained to lower values as compared to the bound from vacuum stability. But if we consider all possible values of CP phases then this area becomes allowed. Hence we conclude that, given the present uncertainty of oscillation parameters and the CP phases, no improvement over the vacuum stability bound can be obtained on $(y_\nu)_{max}$ from $\mathrm{Br}(\mu \to e\gamma)$ for IH [212].

We note in passing that in these type of models the Higgs boson can decay to two neutrinos of which one is heavy and the other one is light, as long as the heavy neutrino is lighter than the Higgs boson. This has been studied in the context of inverse seesaw models and constraints were put on the Yukawa coupling y_ν to be $y_\nu \lesssim 0.02$ for $M_R \lesssim 120$ GeV from the experimental data on the channel $h \to WW^* \to \ell\ell\nu\nu$ [78–80, 217]. For larger masses of the heavy neutrino current Higgs searches do not provide any constraint on the parameter space.

On the other hand, the search for heavy singlet neutrinos at LEP by the L3 collaboration in the decay channel $N \to eW$ showed no evidence of such a singlet neutrino in the mass range between 80 GeV ($|V_{\alpha i}|^2 \lesssim 2 \times 10^{-3}$) and 205 GeV ($|V_{\alpha i}|^2 \lesssim 1$) [218]. $V_{\alpha i}$ is the mixing parameter between the heavy and light neutrino. Heavy singlet neutrinos in the mass range from 3 GeV up

to the Z-boson mass (m_Z) has also been excluded by LEP experiments from Z-boson decay upto $|V_{\alpha i}|^2 \sim 10^{-5}$ [219–221]. In the light of these experimental observations we have chosen the parameter M_R to be greater than or equal to 200 GeV in this study.

3.3.4 Inclusion of NNLO correction

It is to be noted that the premise of our analysis is the assumption that there exists a region in the parameter space in which electroweak vacuum in the SM is stable upto the Planck scale. In view of the low mass of the Higgs candidate measured at LHC, many refined analysis appeared in the literature recently [222–224] examining this point critically from different angles. In particular, the authors of [222] incorporate the next to next to leading order (NNLO) correction to the matching of $\overline{MS}$ Higgs self coupling, λ, and Higgs mass. This excludes the stability of the electroweak vacuum within the SM upto the Planck scale at 2σ CL. for $M_H < 126$ GeV. However, this value crucially depend on the ranges of the top quark mass m_t chosen in the analysis. Reference [222] considered the range $m_t = 173.1 \pm 0.7$ GeV.

Here we incorporate the NNLO corrections to the matching of $\overline{MS}$ λ and Higgs mass [222]. We have also included $\mathcal{O}(\alpha\,\alpha_s)$ correction to the matching of top Yukawa and top pole mass [225]. This correction is comparable to QCD correction. Expression for this can be found in Appendix B.4. In the following we include RG equations upto three loop for λ, Y_t as well as the three gauge couplings [226, 227]. Expressions for three loop beta functions can be found in Appendix B. Also the effective Higgs self coupling is taken upto two loop [152].

$$\begin{aligned}\delta^{(2)}\lambda_{\text{eff}} &= \frac{Y_t^4}{(16\pi^2)^2}\left[g_3^2\left\{24\left(\ln\frac{\mathrm{Y_t^2}}{2}\right)^2 - 64\ln\frac{\mathrm{Y_t^2}}{2} + 72\right\} - \frac{3}{2}Y_t^2\left\{3\left(\ln\frac{\mathrm{Y_t^2}}{2}\right)^2\right.\right. \\ &\quad \left.\left. - 16\ln\frac{\mathrm{Y_t^2}}{2} + 23 + \frac{\pi^2}{3}\right\}\right] \qquad (3.3.28)\end{aligned}$$

We find the that in the 1σ range of parameter space of m_t and α_s, $\tilde{\lambda} \geq 0$ condition is highly constrained upto Planck scale. At the level of 2σ range of

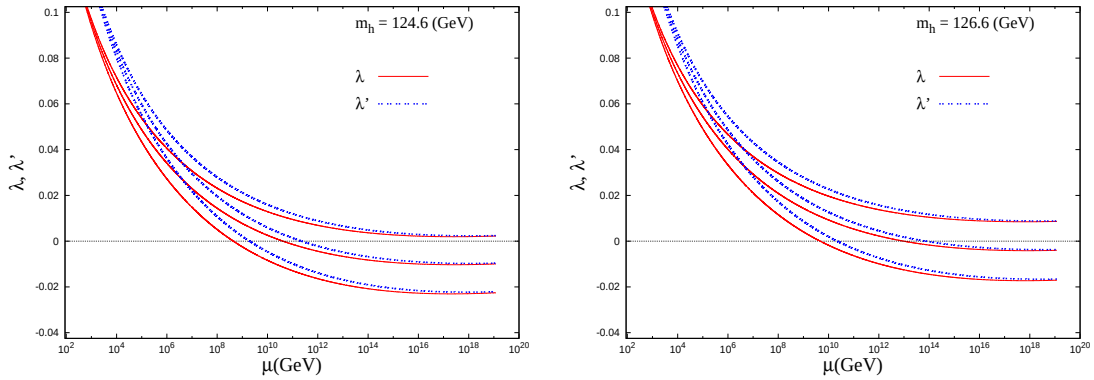

Figure 3.8: *Variation of* λ *and* $\tilde{\lambda}$ (*denoted by* λ' *in the figure*) *with the renormalization scale for fixed values of the parameters* $(m_h\,, m_t\,, \alpha_s)$. *The upper, middle and lower curves are drawn with the set of parameter* (m_t, α_s)=$\{(171.7\,\text{GeV}\,, 0.1198), (173.1\,\text{GeV}\,, 0.1184), (174.5\,\text{GeV}\,, 0.1170)\}$ *respectively.*

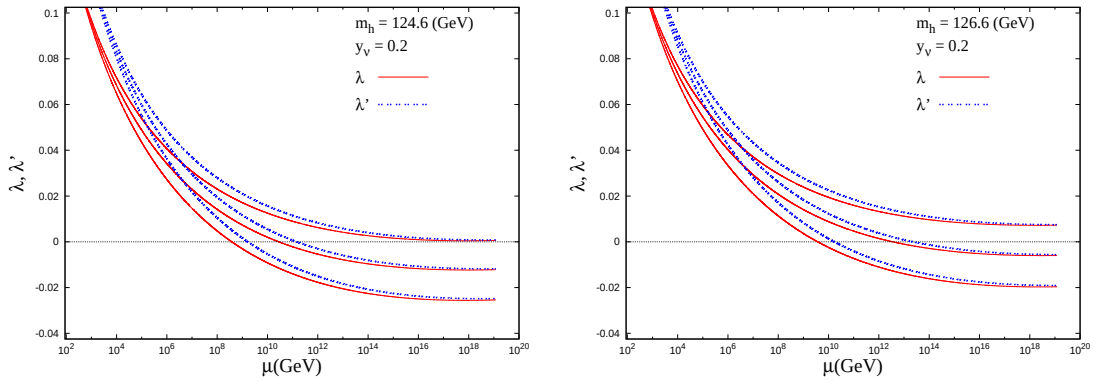

Figure 3.9: *Same as in Fig. 3.8 with the inclusion of* y_ν (*representative value*).

parameter space of m_t and α_s, both $\tilde{\lambda} \geq 0$ and $\lambda \geq 0$ can be maintained upto Planck scale. This is shown in Fig. 3.8. In Fig. 3.9 we plotted the variation of λ and $\tilde{\lambda}$ with representative values of y_ν.

Also it was discussed in [224] that combining the NNLO corrections in QCD in determining the inclusive top quark pair production cross-section with the Tevatron measurement, one gets the pole mass for the top-quark as 173.2 ± 2.8 GeV. This makes a 126 GeV Higgs boson compatible with the stability of the electroweak vacuum. Thus we believe that a clear mandate regarding the instability of the electroweak vacuum in SM has not yet been reached.

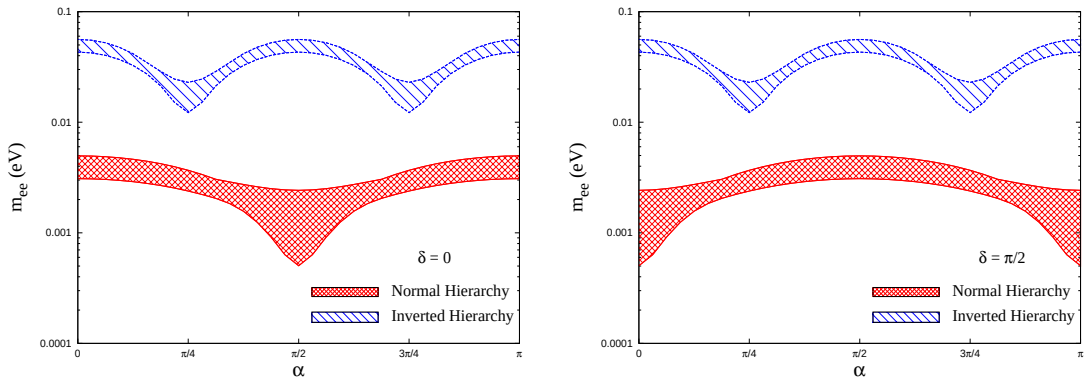

Figure 3.10: The effective mass governing $0\nu\beta\beta$ as a function of the Majorana phase α for NH (dark (red) shaded curve) and IH (light (green) shaded curve). The left panel is for $\delta = 0$ while the right panel is for $\delta = \pi/2$.

3.3.5 $0\nu\beta\beta$ decay in MLSM

The half life for neutrino-less double beta decay in presence of heavy singlets is given in Eq. (2.4.19). For convenience let us write it down once again

$$T^{-1}_{(1/2)} = G\frac{|\mathcal{M}_\nu|^2}{m_e^2}\left|U^2_{L_e\,i}\, m_i + < p^2 > \frac{V^2_{e\,i}}{M_i}\right|^2 , \tag{3.3.29}$$

The first term in Eq. (3.3.29) is the usual contribution from the left-handed neutrinos. The second term denotes the contribution of the singlet neutrinos. The matrix V is defined in Eq. (2.3.7). Taking the most general form of the matrix m'_D as

$$m'_D = \begin{pmatrix} m_{d1} & m_{d2} & m_{d3} \\ m_{s1} & m_{s2} & m_{s3} \end{pmatrix} \tag{3.3.30}$$

and the diagonalizing matrix of U_R and M as defined in Eq. (2.3.31) and (2.3.30) respectively, we obtain,

$$V_{e1} = \frac{i}{\sqrt{2}\ M_R}(m^*_{s1} - m^*_{d1}), \qquad V_{e2} = \frac{1}{\sqrt{2}\ M_R}(m^*_{s1} + m^*_{d1}) \tag{3.3.31}$$

Then the contribution from the heavy part is $2 < p^2 > m^*_{s1}m^*_{d1}/M^3_R \sim 10^{-8}m_i$. Thus this contribution is negligible as compared to the contribution from the light sector which is $\sim m_i$. Therefore, $0\nu\beta\beta$ is due to the light neutrinos only

and the effective mass is defined as

$$m_{ee} = \left| U_{L_e\, i}^2\, m_i \right| \tag{3.3.32}$$

Since in this case the lightest mass is zero one can plot the conventional plots of effective mass as a function of the unknown CP phases for both hierarchies. This dependence is shown in Fig. 3.10.

For NH the effective mass m_{ee} in the limit of the smallest mass $m_1 \to 0$ is given as

$$|m_{ee}|_{NH} = \sqrt{\Delta m^2_{atm}}\ \left| \sqrt{r} s^2_{12} c^2_{13} e^{2i\alpha} + s^2_{13} e^{-2i\delta} \right| \tag{3.3.33}$$

The maximum is obtained for $(\alpha, \delta) = (0, 0)$ or $(\pi/2, \pi/2)$ while the minimum occurs for $(\alpha, \delta) = (0, \pi/2)$ or $(\pi/2, 0)$. This is reflected in Fig. 3.10 by the dark (red) shaded curve which represents the effective mass governing $0\nu\beta\beta$ as a function of the Majorana phase α. The shaded portion is due to the 3σ uncertainty in the oscillation parameters that appear in the expression of effective mass. The left panel is for $\delta = 0$ and the right panel is for $\delta = \pi/2$. The cancellation condition is

$$\sqrt{r}\ sin^2\theta_{12} = \tan^2\theta_{13} \tag{3.3.34}$$

which is not satisfied for the current 3σ ranges of parameters and therefore the effective mass does not vanish which is also seen from the figure. For IH the smallest mass is m_3 which is zero in this model and the effective mass is

$$|m_{ee}|_{IH} = \sqrt{\Delta m^2_{atm}}(c^2_{12} c^2_{13} e^{-2i\alpha} + s^2_{12} c^2_{13} e^{2i\alpha}) \tag{3.3.35}$$

For IH the effective mass is independent of the Dirac phase δ. The maximum of $|m_{ee}|$ occurs for $\alpha = 0, \pi/2, \pi$ and the corresponding expression is,

$$|m_{ee}|_{max} = c^2_{13} \sqrt{\Delta m^2_{atm}} \tag{3.3.36}$$

The minimum value is obtained for $\alpha = \pi/4, 3\pi/4$ as,

$$|m_\nu^{ee}|_{min} = c_{13}^2 cos\, 2\theta_{12} \sqrt{\Delta m_{atm}^2} \tag{3.3.37}$$

This is seen from Fig. 3.10 by the light (green) shaded curve. m_{ee} for IH is in the range accessible to future neutrinoless double beta decay experiments.

3.3.6 Collider Signatures of MLSM

As mentioned earlier, if the heavy singlet neutrinos have mass less than the Higgs boson mass, then the Higgs boson can have new decay modes [79]. For example, the Higgs boson can decay into $h \to \bar{\nu} N$. Now, the singlet neutrinos can decay into lW and νZ through the mixing between the heavy neutrinos and the light active neutrinos. At the LHC this will lead to final states such as $pp \to h \to \ell^+\ell^- + \not{E}_T$, where $\ell = e, \mu$. Note that these final states will depend on the Yukawa couplings and one can put bounds on these Yukawa couplings from the existing LHC data on these types of final states [79].

We have considered the singlet neutrino to be heavier than the Higgs boson. In this case one has to look at the 3-body decay modes of the Higgs boson through the virtual heavy neutrino to have similar final states. Obviously, in this case the constraints on the Yukawa couplings will be much less restrictive. In this model we have obtained upper bound on the Yukawa couplings y_ν from the vacuum stability condition and this can be used to test this model at the LHC by looking at the dilepton plus missing E_T final states.

One can also have trilepton plus missing E_T final states at the LHC from the production of these heavy neutrinos [80]. For example, at the LHC the heavy neutrinos can be produced through the s-channel $W^\pm$ exchange: $u\bar{d} \to \ell^+ N$ or $u\bar{d} \to \ell^+ S$. N or S can again decay into lW and νZ through $\nu - N$ or $\nu - S$ mixings. This will lead to trilepton plus missing E_T final states at the LHC. Now, the trilepton plus $\not{E}_T$ signal is a very clean signal for looking at physics beyond the standard model. In this model, the trilepton final states depend once again on the Yukawa couplings of this model. Using the upper bound on

y_ν obtained from vacuum stability condition, it would be possible to study the present model at the LHC through the trilepton channel.

Chapter 4

Renormalization Group Evolution of Higher Dimensional Operators

4.1 Introduction

Parameters of the Quantum Field Theory (QFT) get affected by higher order corrections. This results in a shift in the values of the parameters. In an experiment, the quantity that is being measured includes all possible higher order or loop corrections. Quantum loop effects come from the interaction with the virtual particles which can never be "turned off". Loop corrections typically lead to divergences. They change the value of the bare parameters in the Lagrangian. Thus the loop correction must be included for any consistent QFT calculation. Divergence of the loop correction always makes the parameter infinite but physical quantity which is being measured in experiment is always finite. This leads to the fact that the bare parameter of a theory is infinite in such a way that it cancels the divergence coming from the loop diagrams and gives a finite value of the physical quantity. This value is called the renormalized value of the corresponding parameter. In other words, one can absorb the divergence coming from the loop diagrams to the bare parameter. This way of calculating the renormalized value of a parameter is called renor-

malization procedure. In the literature there exist many different procedures to absorb the divergences of the loop diagrams to the bare parameters. These are called renormalization schemes.

Physical quantities depend on the scale at which they are being evaluated. However the experimental value of a particular quantity should be fixed at a particular energy scale irrespective of renormalization scheme which implies there must exists mapping between different renormalization schemes. The set of all such mappings (transformations) said to form the renormalization group.

In this Chapter, we discuss the Renormalization Group (RG) equations for dimension-6 operators. RG Evolution (RGE) of the dimension-5 operator in the context of seesaw mechanism is extensively studied in the literature [97–110]. RGE of the dimension-6 operator is not studied widely in literature. In [228] only part of the β-function of the dimension-6 operator is computed. Here we shall present a full computation of the β-function of the dimension-6 operator which is also responsible for the non-unitary correction to the light neutrino mixing, in the context of Type-I seesaw.

Before proceeding to discuss the RGE of dimension-6 operators, we shall briefly discuss the renormalization scheme chosen for the computation of the loop divergence of dimension-6 operator *i.e.* Minimal Subtraction (MS) scheme. We shall also briefly discuss the one loop beta function from the Callan-Symanzik equation.

4.2 Renormalization schemes

Renormalization consists of adding counterterms to the bare Lagrangian which cancel the loop divergence. In a renormalization scheme where renormalized mass of a particle is chosen to be at the pole of the propagator is called on-shell scheme. Thus renormalized mass represents the physical mass and hence this scheme is also physical scheme. Also the renormalized couplings are equal to the physical couplings in this scheme. However the counterterms

are mass dependent and thus makes computation cumbersome.

A different renormalization scheme called minimal subtraction (MS) scheme is often used. In this scheme one absorbs only the divergent part of the loop diagrams in the counter term and thus makes computation much simpler. To demonstrate this scheme further we consider the effect of incorporating one loop corrections to the non-unitary operator (2.2.7) *i.e. renormalization* of this operator. This requires wave function renormalization of l_L and ϕ doublet as well as the $c^{(6)}$ vertex renormalization. The wave function renormalization is defined as

$$\begin{aligned} (l_{Li})_B &= \left(Z_{l_L}^{\frac{1}{2}}\right)_{ij} l_{Lj} \\ \phi_B &= Z_\phi^{\frac{1}{2}} \phi \end{aligned} \tag{4.2.1}$$

The subscript B stands for a bare quantity. Fields on the right hand side are the renormalized quantities. Z's are the renormalization constants which contain the divergence arising from quantum corrections and can be written in terms of counterterm as

$$Z = 1 + \delta Z \tag{4.2.2}$$

where δZ is the counterterm that contains all the divergences. In the same spirit, the bare Lagrangian can be written as the sum of renormalized Lagrangian and the counter term Lagrangian

$$\mathcal{L}_B^{(6)} = \mathcal{L}^{(6)} + \mathscr{L}^{(6)} \tag{4.2.3}$$

with $\mathscr{L}^{(6)}$, given by

$$\mathscr{L}^{(6)} = \frac{1}{2}\Delta c_{ji}^{(6)} \left(\overline{l_{Lj}}\epsilon\phi^*\right) i\partial\!\!\!/ \left(\phi^T \epsilon^T l_{Li}\right) \tag{4.2.4}$$

$\Delta c^{(6)}$ is the counterterm, related to the bare and renormalized coupling as below

$$c_B^{(6)} = Z_\phi^{-\frac{1}{2}} Z_{l_L}^{-\frac{1}{2}} \left(c^{(6)} + \Delta c^{(6)}\right) Z_{l_L}^{-\frac{1}{2}} Z_\phi^{-\frac{1}{2}} \tag{4.2.5}$$

Similarly as before, $\Delta c^{(6)}$ contains all the divergence coming from the loop correction the $c^{(6)}$ vertex.

Dimensional regularization

Loop integrals encountered in a practical calculation are typically divergent. To make sense out of them one needs to regularize them in some way. We shall use dimensional regularization [229, 230]. In this procedure the loop integrals are computed in d dimension, where $d = 4 - \epsilon$ and at end take the limit $\epsilon \to 0$. Consequently the loop integral becomes

$$\int \frac{\mathrm{d}^4 q}{(2\pi)^4} \longrightarrow \mu^\epsilon \int \frac{\mathrm{d}^d q}{(2\pi)^d} \tag{4.2.6}$$

where μ is the renormalization scale. In general the renormalized quantities depends on the renormalization scale. The Eq. (4.2.5) changes in d dimension as follows

$$c_B^{(6)} = Z_\phi^{-\frac{1}{2}} Z_{l_L}^{-\frac{1}{2}} \left(c^{(6)} + \Delta c^{(6)}\right) \mu^\epsilon Z_{l_L}^{-\frac{1}{2}} Z_\phi^{-\frac{1}{2}} \tag{4.2.7}$$

In the MS scheme, the renormalization constant, for any field labeled i, is defined as

$$Z_i = 1 + \sum_{j \geq 1} \delta Z_{i,j} \frac{1}{\epsilon^j} \tag{4.2.8}$$

where $\delta Z_{i,j}$ are coefficients of $\frac{1}{\epsilon^j}$ in the divergent part of a loop diagram.

In the literature there exist a variant of MS scheme called $\overline{\text{MS}}$. In this scheme a finite constant is absorbed in the counterterm in addition to the

divergent part. This is defined as follows

$$\frac{1}{\bar{\epsilon}} \equiv \frac{1}{\epsilon} - \gamma_E + \ln(4\pi) \tag{4.2.9}$$

where γ_E is the Euler constant, $\gamma_E \simeq 0.5772\cdots$. There are also DR and $\overline{\text{DR}}$ schemes which are used in SUSY theories [231, 232].

4.2.1 Counterterm in one loop correction

In the MS scheme, the counterterm is determined by compensating the divergence arising from all possible one loop 1 particle irreducible diagrams. Pictorially it is shown below for $c^{(6)}$

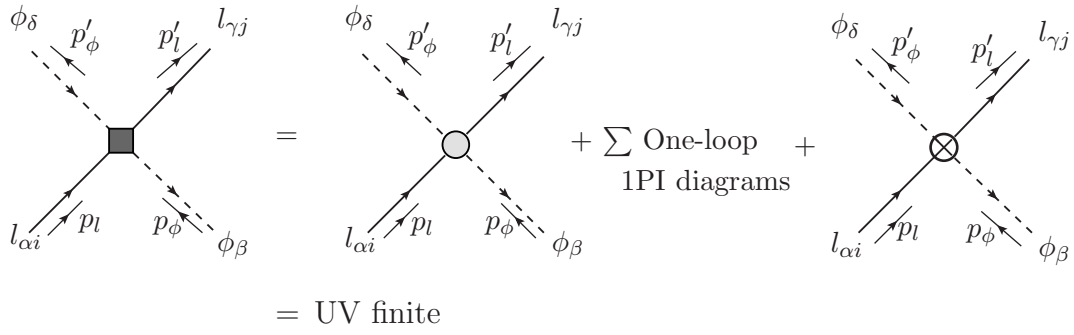

Figure 4.1: *One loop renormalized $c^{(6)}$ vertex (on the left hand side). First diagram on the right hand side is the tree level $c^{(6)}$ vertex. Diagram on the extreme right is the counterterm vertex which eventually cancels the divergence.*

the above figure can be expressed in words as:

$$\text{Divergent part of all diagrams} \quad + \quad \text{the counterterm} = 0 \tag{4.2.10}$$

Same procedure is followed to calculate the counterterms of l_L and ϕ form the self energy diagrams.

4.3 Renormalization group equations

Renormalized quantities exhibit a dependence on the renormalization scale, μ, which is a artifact of the calculational procedure. However, the bare quantity is independent of μ *i.e.* variation of the bare Green's function of a theory with respect to the variation of μ (total derivative) should vanish. n-point Green's function is defined as

$$\mathcal{G}_B^{(n)}\left(\{x_i\}\right) = \langle 0|\mathcal{T}\phi_B(x_1)\cdots\phi_B(x_n)|0\rangle \tag{4.3.1}$$

for any field ϕ. $|0\rangle$ is the ground state of the interacting theory. According to Eq. (4.2.1), the above expression becomes

$$\begin{aligned}\mathcal{G}_B^{(n)}\left(\{x_i\}\right) &= Z^{\frac{n}{2}}\langle 0|\mathcal{T}\phi(x_1)\cdots\phi(x_n)|0\rangle \\ &= Z^{\frac{n}{2}}\mathcal{G}^{(n)}\left(\{x_i\}\right)\end{aligned} \tag{4.3.2}$$

Renormalization implies

$$\mu\frac{d}{d\mu}\mathcal{G}_B^{(n)}\left(\{x_i\}\right) = 0 \tag{4.3.3}$$

This is the renormalization group equation. In general the Green's function depends on μ, couplings, masses, gauge parameters, space time dimension. With this and using the chain rule one obtains the Callan-Symanzik equation, given by [230, 233, 234]

$$\left[\mu\frac{\partial}{\partial\mu} + \beta\frac{\partial}{\partial g} - \gamma_m m\frac{\partial}{\partial m} - \gamma_\xi\xi\frac{\partial}{\partial\xi} + \frac{n}{2}\gamma\right]\mathcal{G}^{(n)} = 0 \tag{4.3.4}$$

$$\beta = \mu\frac{dg}{d\mu} \tag{4.3.5}$$

$$\gamma_m = -\frac{1}{m}\mu\frac{dm}{d\mu} \tag{4.3.6}$$

$$\gamma_\xi = -\frac{1}{\xi}\mu\frac{d\xi}{d\mu} \tag{4.3.7}$$

$$\gamma \;=\; \frac{1}{Z_\phi}\mu\frac{dZ_\phi}{d\mu} \tag{4.3.8}$$

$g\,, m\,, \xi\,, Z_\phi$ stand for couplings, masses, gauge fixing parameters, field strength renormalization constant respectively. β is known as the beta function and governs the running behavior of the couplings. We shall explore the beta functions further.

In the MS renormalization scheme where the counterterm absorbs the divergent part only, the beta function of coupling Q at one loop is given by [101].

$$\begin{aligned}\beta_Q \;=\;& D_Q\left\langle\frac{d\delta Q_{,1}}{dQ}\middle|Q\right\rangle+\sum_A D_{V_A}\left\langle\frac{d\delta Q_{,1}}{dV_A}\middle|V_A\right\rangle-D_Q\,\delta Q_{,1}\\&+\sum_{i\in I}n_i\left[D_Q\left\langle\frac{d\delta Z_{\phi_i,1}}{dQ}\middle|Q\right\rangle+\sum_A D_{V_A}\left\langle\frac{d\delta Z_{\phi_i,1}}{dV_A}\middle|V_A\right\rangle\right]Q\\&+Q\sum_{j\in J}n_j\left[D_Q\left\langle\frac{d\delta Z_{\phi_j,1}}{dQ}\middle|Q\right\rangle+\sum_A D_{V_A}\left\langle\frac{d\delta Z_{\phi_j,1}}{dV_A}\middle|V_A\right\rangle\right]\end{aligned} \tag{4.3.9}$$

$\langle|\rangle$ denotes scalar product. The bare and the renormalized quantities are related by

$$Q_B \;=\; \left(\prod_{i\in I}Z_{\phi_i}^{n_i}\right)[Q+\Delta Q]\,\mu^{D_Q\epsilon}\left(\prod_{j\in J}Z_{\phi_j}^{n_j}\right) \tag{4.3.10}$$

Z_{ϕ_i} are the wave function renormalization constants. D_Q is constant. $\delta Q_{,1}\,, Z_{\phi_i,1}$ are to be understood as in Eq. (4.2.8).

4.4 RGE of dimension-6 operator

We have discussed the origin of dimension-6 operator in Chapter 2. The effective Lagrangian (2.2.7) which becomes significant at a scale $\mathcal{O}$ (TeV), start receiving quantum corrections at loop level. In this section we shall present the one loop correction to the lepton and Higgs self energy as well as the $c^{(6)}$ vertex. Here we shall give the one loop diagrams and compute the UV

divergence. From these, the counterterms are obtained and the beta function at one loop is calculated.

4.4.1 One loop correction of the lepton doublet l_L

The one loop self energy diagram of l_L consists of the following diagrams

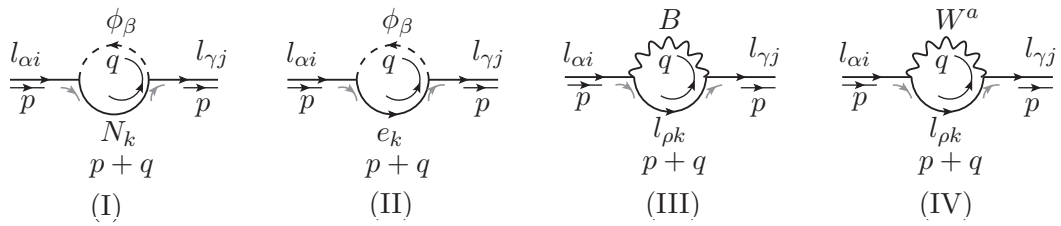

Figure 4.2: *One loop self energy diagrams of l_L.*

Divergent part of these diagrams can be found in [235]. For completeness we tabulated these divergence in Appendix D.2. Taking the divergent part of the above diagrams and following Eq. (4.2.10) we find the expression for the counterterm as

$$\Delta Z_{l_L,1} = -\frac{1}{16\pi^2}\left[Y_\nu^\dagger Y_\nu + Y_e^\dagger Y_e + \frac{1}{2}\xi_B g_1^2 + \frac{3}{2}\xi_W g_2^2\right] \tag{4.4.1}$$

In the above expression, Y_e is the Yukawa coupling coming from the $l-e-\phi$ vertex. g_1, g_2 are $U(1)_Y$ and $SU(2)_L$ gauge coupling constant. ξ_B, ξ_W are the gauge fixing parameters for the $U(1)_Y$ and $SU(2)_L$ gauge fields respectively. $Y_\nu^\dagger Y_\nu$ term contributes till the heavy field gets integrated out from the theory.

4.4.2 One loop correction of the Higgs doublet ϕ

The one loop self energy diagram of ϕ consists of the following diagrams

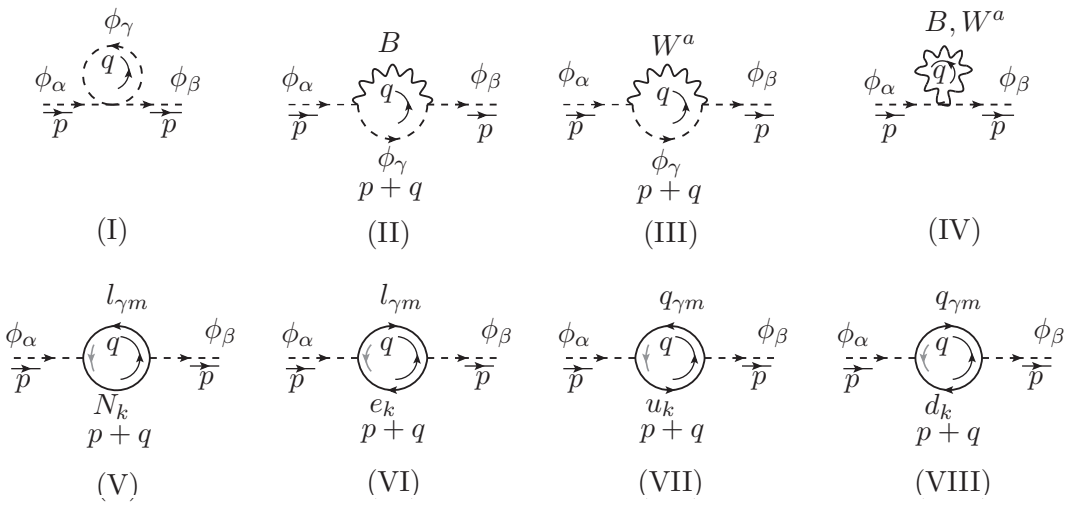

Figure 4.3: *One loop self energy diagrams of ϕ.*

It is noteworthy that the fourth diagram (IV) vanishes in dimensional regularization, hence does not contribute. Divergent part of the other diagrams are tabulated in Appendix D.2, also computed in [235]. Following the similar procedure as above we find

$$\Delta Z_{\phi,1} = -\frac{1}{16\pi^2}\left[2T - \frac{1}{2}(3-\xi_B)\,g_1^2 - \frac{3}{2}(3-\xi_W)\,g_2^2\right] \tag{4.4.2}$$

where, in general,

$$T_1 = \mathrm{Tr}\left[Y_\nu^\dagger Y_\nu + Y_e^\dagger Y_e + 3\,Y_u^\dagger Y_u + 3\,Y_d^\dagger Y_d\right] \tag{4.4.3}$$

Y_u, Y_d are the Yukawa coupling arising from the $q-u-\phi$, $q-d-\phi$ vertices respectively. Below the mass scale M, the heavy field N gets decoupled from the theory. In that case, diagram V will not contribute to the self energy of ϕ, consequently one needs to omit the term $Y_\nu^\dagger Y_\nu$ from the expression of the T. Here we do not write down the Higgs mass counterterm which is relevant for the anomalous mass dimension of Higgs. Here we are interested only in the beta function of the $c^{(6)}$ parameter.

4.4.3 One loop correction of $c^{(6)}$ up to $\mathcal{O}(1/M^2)$

Below we give all the one loop diagrams which contribute up to $\mathcal{O}(1/M^2)$ towards the correction of $c^{(6)}$. We proceed with the kind of vertex in Fig. 2.3*.

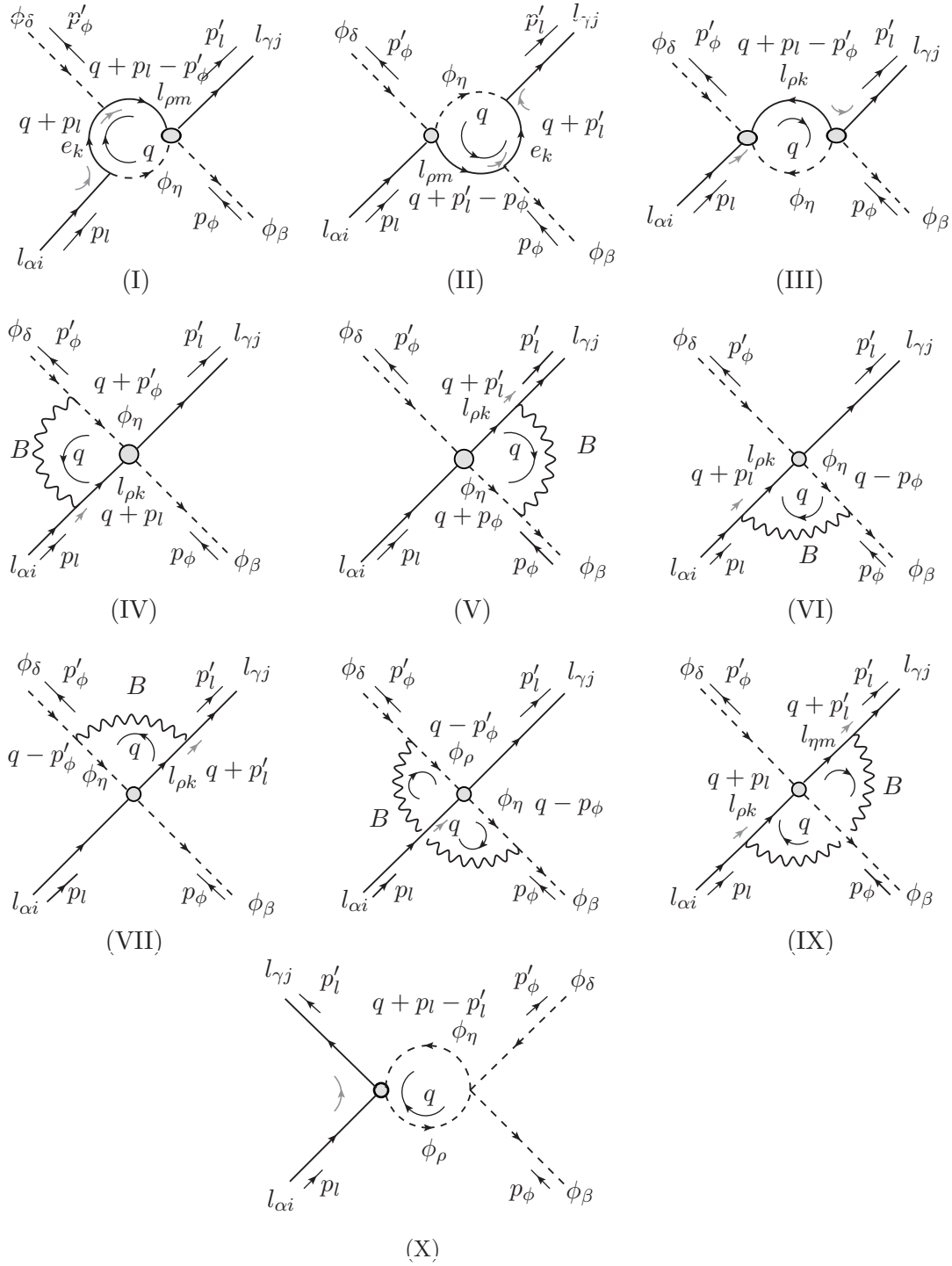

Figure 4.4: *Diagrams for one loop correction of* $c^{(6)}$.

*Either of the diagrams (in Fig. 2.2, 2.3) leads to same β-function.

One loop correction of $c^{*(5)}c^{(5)}$ which is of the order of $\mathcal{O}\left(1/M^2\right)$ contributes towards the correction of $c^{(6)}$ (diagram III). There will be six additional gauge boson diagrams with B replaced by W^a.

4.4.3.1 Calculation of UV divergence

Below we shall present the UV divergent part of these diagrams. We begin with the first diagram.

I

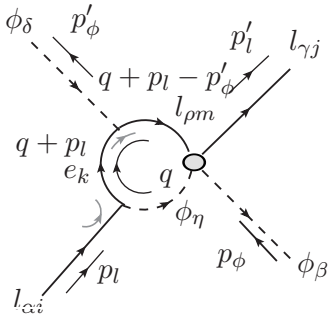

$$
\begin{aligned}
i\mathcal{M} &= \frac{i}{2}\mu^\epsilon c^{(6)}_{jm}\epsilon_{\gamma\beta}\epsilon_{\rho\eta}\left(\not{p}_l-\not{p}'_\phi\right)P_L\int\frac{d^4q}{(2\pi)^4}\frac{i\left(\not{q}+\not{p}_l-\not{p}'_\phi\right)}{\left(q+p_l-p'_\phi\right)^2}(-i)\mu^{\epsilon/2}\left(Y_e^*\right)_{km}\delta_{\rho\delta}P_R \\
&\qquad\qquad \frac{i\left(\not{q}+\not{p}_l\right)}{\left(q+p_l\right)^2}(-i)\mu^{\epsilon/2}\left(Y_e\right)_{ki}\delta_{\alpha\eta}P_L\frac{i}{q^2-m^2} \\
&= \frac{\mu^\epsilon}{2}\left(c^{(6)}Y_e^\dagger Y_e\right)_{ji}\epsilon_{\gamma\beta}\epsilon_{\alpha\delta}\left(\not{p}_l-\not{p}'_\phi\right)\mu^\epsilon \\
&\qquad\qquad \int\frac{d^4q}{(2\pi)^4}\left[\frac{q^2-m^2+m^2}{\left(q^2-m^2\right)\left(q+p_l\right)^2\left(q+p_l-p'_\phi\right)^2}+\cdots\right]P_L \\
&= \frac{i}{16\pi^2}\mu^\epsilon\left(c^{(6)}Y_e^\dagger Y_e\right)_{ji}\epsilon_{\gamma\beta}\epsilon_{\alpha\delta}\left(\not{p}_l-\not{p}'_\phi\right)P_L\frac{1}{\epsilon}\ +\ \text{UV finite} \qquad (4.4.4)
\end{aligned}
$$

II

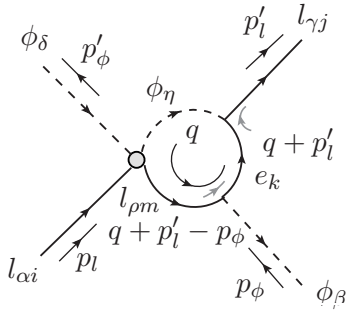

Diagram II can be calculated in a similar manner. The corresponding UV divergent part is given by

$$i\mathcal{M} = \frac{i}{16\pi^2}\mu^\epsilon \left(Y_e^\dagger Y_e\, c^{(6)}\right)_{ji} \epsilon_{\gamma\beta}\epsilon_{\alpha\delta} \left(\not{p}_l - \not{p}'_\phi\right) P_L \frac{1}{\epsilon} + \text{UV finite} \quad (4.4.5)$$

III

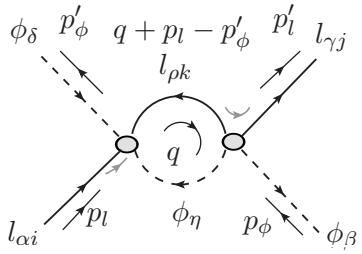

$$\begin{aligned} i\mathcal{M} &= \frac{i}{2}\mu^\epsilon c^{*(5)}_{jk} \left(\epsilon_{\gamma\beta}\epsilon_{\rho\eta} + \epsilon_{\gamma\eta}\epsilon_{\rho\beta}\right) P_R \int \frac{d^4q}{(2\pi)^4} \frac{i\left(\not{q} + \not{p}'_l - \not{p}_\phi\right)}{\left(q + p'_l - p_\phi\right)^2} \\ &\qquad \frac{i}{2}\mu^\epsilon c^{(5)}_{ki} \left(\epsilon_{\rho\eta}\epsilon_{\alpha\delta} + \epsilon_{\rho\delta}\epsilon_{\alpha\eta}\right) P_L \frac{i}{q^2 - m^2} \\ &= \frac{\mu^\epsilon}{4}\left(c^{*(5)}c^{(5)}\right)_{ji} \left(2\,\epsilon_{\gamma\beta}\epsilon_{\alpha\delta} + 2\,\epsilon_{\gamma\beta}\epsilon_{\alpha\delta} + \delta_{\beta\delta}\delta_{\gamma\alpha}\right)\mu^\epsilon \\ &\qquad \int \frac{d^4q}{(2\pi)^4} \frac{\left(\not{q} + \not{p}'_l - \not{p}_\phi\right)}{\left(q^2 - m^2\right)\left(q + p'_l - p_\phi\right)^2} P_L \\ &= \frac{i}{16\pi^2}\mu^\epsilon \left(c^{*(5)}c^{(5)}\right)_{ji} \left(\epsilon_{\gamma\beta}\epsilon_{\alpha\delta} + \frac{1}{4}\,\delta_{\beta\delta}\delta_{\gamma\alpha}\right) \left(\not{p}_l - \not{p}'_\phi\right) P_L \frac{1}{\epsilon} \\ &\qquad + \text{UV finite} \end{aligned} \quad (4.4.6)$$

where we have used $\not{p}'_l - \not{p}_\phi = \not{p}_l - \not{p}'_\phi$. Let us note down one identity here

$$\begin{aligned} \epsilon_{\gamma\beta}\epsilon_{\alpha\delta} &= \delta_{\gamma\alpha}\delta_{\beta\delta} - \delta_{\beta\alpha}\delta_{\gamma\delta} \\ \Rightarrow \delta_{\gamma\alpha}\delta_{\beta\delta} &= \epsilon_{\gamma\beta}\epsilon_{\alpha\delta} + \delta_{\beta\alpha}\delta_{\gamma\delta} \end{aligned} \tag{4.4.7}$$

Using this identity we can change $\delta_{\gamma\alpha}\delta_{\beta\delta}$ part of any loop contribution to $\epsilon_{\gamma\beta}\epsilon_{\alpha\delta}$. The other part *i.e.* $\delta_{\beta\alpha}\delta_{\gamma\delta}$ is orthogonal to the non-unitary operator and hence irrelevant in the present context [228].

IV

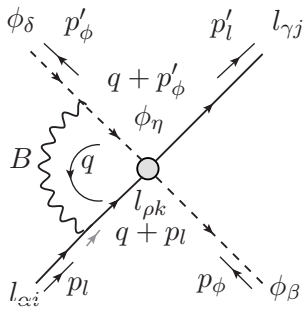

$$\begin{aligned} i\mathcal{M} &= \frac{i}{2}\mu^\epsilon c^{(6)}_{jk}\epsilon_{\gamma\beta}\epsilon_{\rho\eta}\left(\not{p}_l - \not{p}'_\phi\right) P_L \int \frac{d^4q}{(2\pi)^4} \frac{i\left(\not{q} + \not{p}_l\right)}{(q+p_l)^2} i\mu^{\epsilon/2}\frac{g_1}{2}\delta_{\alpha\rho}\delta_{ik}\gamma^\mu P_L \\ &\quad i\frac{-g_{\mu\nu} + (1-\xi_B)\frac{q_\mu q_\nu}{q^2}}{q^2}(-i)\mu^{\epsilon/2}\frac{g_1}{2}\delta_{\delta\eta}\left(-q - 2p'_\phi\right)^\nu \frac{i}{\left(q+p'_\phi\right)^2 - m^2} \\ &= \left(-\frac{g_1^2}{4}\right)\frac{\mu^\epsilon}{2}c^{(6)}_{ji}\epsilon_{\gamma\beta}\epsilon_{\alpha\delta}\left(\not{p}_l - \not{p}'_\phi\right)\mu^\epsilon \int \frac{d^4q}{(2\pi)^4}\left[\frac{\left(\not{q} + \not{p}_l\right)\left(-\xi_B\not{q} - 2\not{p}'_\phi\right)}{q^2\left(q+p_l\right)^2\left[\left(q+p'_\phi\right)^2 - m^2\right]}\right. \\ &\qquad \left. + 2\left(1-\xi_B\right)\frac{\left(\not{q} + \not{p}_l\right)\not{q}\left(q\cdot p'_\phi\right)}{q^2q^2\left(q+p_l\right)^2\left[\left(q+p'_\phi\right)^2 - m^2\right]}\right] P_L \\ &= \left(-\frac{g_1^2}{4}\right)\frac{\mu^\epsilon}{2}c^{(6)}_{ji}\epsilon_{\gamma\beta}\epsilon_{\alpha\delta}\left(\not{p}_l - \not{p}'_\phi\right)\mu^\epsilon \int \frac{d^4q}{(2\pi)^4} \\ &\qquad \left[\frac{-\xi_B\, q^2 - 2\not{q}\not{p}'_\phi - \xi_B\not{p}_l\not{q} - 2\not{p}_l\not{p}'_\phi}{q^2\left(q+p_l\right)^2\left[\left(q+p'_\phi\right)^2 - m^2\right]} + \cdots\right] P_L \\ &= \frac{i}{16\pi^2}\mu^\epsilon\frac{g_1^2}{4}c^{(6)}_{ji}\epsilon_{\gamma\beta}\epsilon_{\alpha\delta}\left(\not{p}_l - \not{p}'_\phi\right)P_L\xi_B\frac{1}{\epsilon} \;+\; \text{UV finite} \end{aligned} \tag{4.4.8}$$

There is a similar diagram with B_μ replaced by W^a_μ. Contribution of this diagram can be calculated as follows:
g_1, $\delta_{\alpha\rho}$, $\delta_{\delta\eta}$ and ξ_B are replaced by g_2, $\sigma^a_{\alpha\rho}$, $\sigma^a_{\delta\eta}$ and ξ_W respectively. There is one additional $-ive$ sign because $l-l-W$ vertex differs by a minus sign from that of $l-l-B$ vertex. Using the following identity we get

$$\begin{aligned} -\epsilon_{\gamma\beta}\epsilon_{\rho\eta}\sigma^a_{\rho\alpha}\sigma^a_{\eta\delta} &= -\epsilon_{\gamma\beta}\epsilon_{\rho\eta}\left(2\delta_{\rho\delta}\delta_{\alpha\eta}-\delta_{\rho\alpha}\delta_{\eta\delta}\right) \\ &= -2\epsilon_{\gamma\beta}\epsilon_{\delta\alpha}+\epsilon_{\gamma\beta}\epsilon_{\alpha\delta} \\ &= 3\epsilon_{\gamma\beta}\epsilon_{\alpha\delta} \end{aligned} \tag{4.4.9}$$

$-ive$ sign in the extreme left is the additional $-ive$ sign mentioned above. So we see that contribution of W^a_μ is three times B_μ with g_1 and ξ_B replaced by g_2 and ξ_W respectively.

V

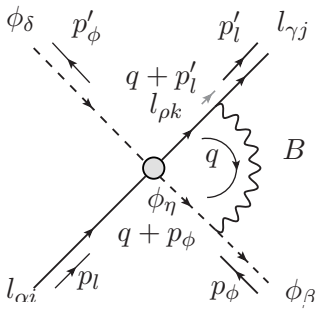

Diagram V can be calculated in a similar manner. Corresponding UV divergent part is given by

$$i\mathcal{M} \simeq \frac{i}{16\pi^2}\mu^\epsilon\frac{g_1^2}{4}c^{(6)}_{ji}\epsilon_{\gamma\beta}\epsilon_{\alpha\delta}\left(\not{p}_l-\not{p}'_\phi\right)P_L\xi_B\frac{1}{\epsilon} \tag{4.4.10}$$

Corresponding W boson diagram is simply three times the B boson diagram with g_1 and ξ_B replaced by g_2 and ξ_W respectively, similar to the previous diagram.

VI

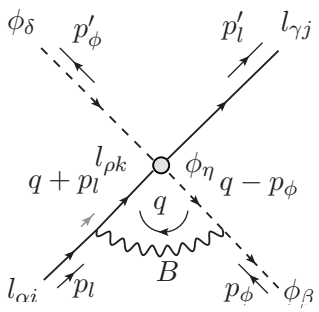

$$
\begin{aligned}
i\mathcal{M} &= \frac{i}{2}\mu^\epsilon c^{(6)}_{jk}\epsilon_{\gamma\eta}\epsilon_{\rho\delta}\int\frac{d^4q}{(2\pi)^4}\left(\not{q}+\not{p}_l-\not{p}'_\phi\right)P_L\frac{i\left(\not{q}+\not{p}_l\right)}{(q+p_l)^2}i\mu^{\epsilon/2}\,\frac{g_1}{2}\delta_{\rho\alpha}\delta_{ki}\gamma^\mu P_L \\
&\quad i\frac{-g_{\mu\nu}+(1-\xi_B)\frac{q_\mu q_\nu}{q^2}}{q^2}(-i)\mu^{\epsilon/2}\,\frac{g_1}{2}\delta_{\beta\eta}\,(q-2p_\phi)^\nu\,\frac{i}{(q-p_\phi)^2-m^2} \\
&= \left(\frac{g_1^2}{4}\right)\frac{\mu^\epsilon}{2}c^{(6)}_{ji}\epsilon_{\gamma\beta}\epsilon_{\alpha\delta}\mu^\epsilon\int\frac{d^4q}{(2\pi)^4}\left[\frac{\left(\not{q}+\not{p}_l-\not{p}'_\phi\right)\left(\not{q}+\not{p}_l\right)\left(-\xi_B\not{q}+2\not{p}_\phi\right)}{q^2\,(q+p_l)^2\left[(q-p_\phi)^2-m^2\right]}\right. \\
&\qquad\left. -2\,(1-\xi_B)\,\frac{\left(\not{q}+\not{p}_l-\not{p}'_\phi\right)\left(\not{q}+\not{p}_l\right)\not{q}\,(q\cdot p_\phi)}{q^2q^2\,(q+p_l)^2\left[(q-p_\phi)^2-m^2\right]}\right]P_L \\
&= \left(\frac{g_1^2}{4}\right)\frac{\mu^\epsilon}{2}c^{(6)}_{ji}\epsilon_{\gamma\beta}\epsilon_{\alpha\delta}\mu^\epsilon\int\frac{d^4q}{(2\pi)^4}\left[\frac{-\xi_B\left(\not{q}+\not{p}_l-\not{p}'_\phi\right)+2\not{p}_\phi}{(q+p_l)^2\left[(q-p_\phi)^2-m^2\right]}+\right. \\
&\quad \frac{-\xi_B\not{q}\not{p}_l\not{q}}{q^2\,(q+p_l)^2\left[(q-p_\phi)^2-m^2\right]}+\cdots-\frac{2\,(1-\xi_B)\not{q}\,(q\cdot p_\phi)}{q^2\,(q+p_l)^2\left[(q-p_\phi)^2-m^2\right]}+\cdots\Bigg]P_L \\
&= \frac{i}{16\pi^2}\mu^\epsilon\frac{g_1^2}{4}c^{(6)}_{ji}\epsilon_{\gamma\beta}\epsilon_{\alpha\delta}\left[\frac{3}{2}\not{p}_\phi+\xi_B\not{p}'_\phi\right]P_L\frac{1}{\epsilon}\;+\;\text{UV finite} \qquad (4.4.11)
\end{aligned}
$$

For the corresponding W boson diagram, we have

$$
\begin{aligned}
-\epsilon_{\gamma\eta}\epsilon_{\rho\delta}\sigma^a_{\rho\alpha}\sigma^a_{\beta\eta} &= -\epsilon_{\gamma\beta}\epsilon_{\rho\eta}\left(2\delta_{\rho\eta}\delta_{\alpha\beta}-\delta_{\rho\alpha}\delta_{\beta\eta}\right) \\
&= 2\,\delta_{\gamma\delta}\delta_{\alpha\beta}+\epsilon_{\gamma\beta}\epsilon_{\alpha\delta} \qquad (4.4.12)
\end{aligned}
$$

As mentioned earlier, $\delta_{\gamma\delta}\delta_{\alpha\beta}$ is orthogonal to the non-unitary operator. So the contribution of the W boson diagram is simply the B boson diagram with g_1 and ξ_B replaced by g_2 and ξ_W respectively.

VII

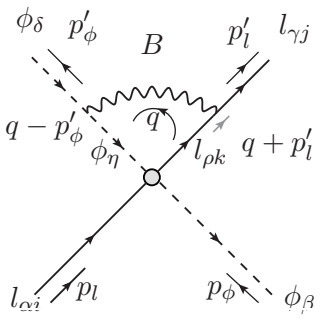

Diagram VII can be calculated in a similar manner. Corresponding UV divergent part is given by

$$i\mathcal{M} = \frac{i}{16\pi^2}\mu^\epsilon \frac{g_1^2}{4} c_{ji}^{(6)} \epsilon_{\gamma\beta}\epsilon_{\alpha\delta} \left[\left(\frac{3}{2}+\xi_B\right)\not{p}'_\phi + \xi_B \not{p}'_l - \xi_B \not{p}_l\right] P_L \frac{1}{\epsilon} + \text{UV finite} \quad (4.4.13)$$

contribution of the W boson diagram is same as the B boson diagram with g_1 and ξ_B replaced by g_2 and ξ_W respectively.

VIII

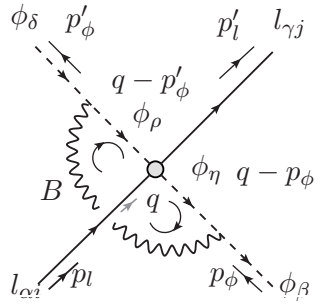

$$
\begin{aligned}
i\mathcal{M} &= \frac{i}{2}\mu^{\epsilon} c^{(6)}_{ji}\epsilon_{\gamma\rho}\epsilon_{\alpha\eta}\int\frac{d^4q}{(2\pi)^4}\left(\not{q}+\not{p}_l-\not{p}'_\phi\right)P_L\frac{i}{(q-p_\phi)^2-m^2}(-i)\mu^{\epsilon/2}\,\frac{g_1}{2}\delta_{\beta\rho}\times \\
&\quad (q-2p_\phi)^\mu\; i\frac{-g_{\mu\nu}+(1-\xi_B)\,\frac{q_\mu q_\nu}{q^2}}{q^2}(-i)\mu^{\epsilon/2}\,\frac{g_1}{2}\delta_{\eta\delta}\left(q-2p'_\phi\right)^\nu\frac{i}{\left(q-p'_\phi\right)^2-m^2} \\
&= \left(-\frac{g_1^2}{4}\right)\frac{\mu^\epsilon}{2}c^{(6)}_{ji}\epsilon_{\gamma\beta}\epsilon_{\alpha\delta}\mu^\epsilon\int\frac{d^4q}{(2\pi)^4}\left[\frac{\not{q}\left(-\xi_B\,q^2+2\,\xi_B\,q\cdot\left(p_\phi+p'_\phi\right)\right)}{q^2\left[(q-p_\phi)^2-m^2\right]\left[\left(q-p'_\phi\right)^2-m^2\right]}\right. \\
&\qquad\qquad \left.-\frac{\xi_B\left(\not{p}_l-\not{p}'_\phi\right)q^2}{q^2\left[(q-p_\phi)^2-m^2\right]\left[\left(q-p'_\phi\right)^2-m^2\right]}\right]P_L \\
&= \left(-\frac{g_1^2}{4}\right)\frac{\mu^\epsilon}{2}c^{(6)}_{ji}\epsilon_{\gamma\beta}\epsilon_{\alpha\delta}\mu^\epsilon\int\frac{d^4q}{(2\pi)^4}\left[\frac{-\xi_B\not{q}}{\left[(q-p_\phi)^2-m^2\right]\left[\left(q-p'_\phi\right)^2-m^2\right]}+\right. \\
&\quad \left.\frac{2\,\xi_B\,\gamma^\mu\,q_\mu\,q_\nu\left(p_\phi+p'_\phi\right)^\nu}{\left[(q-p_\phi)^2-m^2\right]\left[\left(q-p'_\phi\right)^2-m^2\right]}-\frac{\xi_B\left(\not{p}_l-\not{p}'_\phi\right)}{\left[(q-p_\phi)^2-m^2\right]\left[\left(q-p'_\phi\right)^2-m^2\right]}\right]P_L \\
&= \frac{i}{16\pi^2}\mu^\epsilon\frac{g_1^2}{4}c^{(6)}_{ji}\epsilon_{\gamma\beta}\epsilon_{\alpha\delta}\xi_B\left(\not{p}_l-\not{p}'_\phi\right)P_L\frac{1}{\epsilon}\;+\;\text{UV finite} \qquad (4.4.14)
\end{aligned}
$$

For the contribution of the W boson diagram, we have

$$
\begin{aligned}
-\;\epsilon_{\gamma\rho}\epsilon_{\alpha\eta}\sigma^a_{\beta\rho}\sigma^a_{\eta\delta} &= -\,\epsilon_{\gamma\rho}\epsilon_{\alpha\eta}\left(2\delta_{\beta\delta}\delta_{\rho\eta}-\delta_{\beta\rho}\delta_{\eta\delta}\right) \\
&= -\,2\delta_{\gamma\alpha}\delta_{\beta\delta}+\epsilon_{\gamma\beta}\epsilon_{\alpha\delta} \qquad (4.4.15)
\end{aligned}
$$

So the W boson diagram is same as the B boson diagram with g_1 and ξ_B replaced by g_2 and ξ_W respectively.

IX

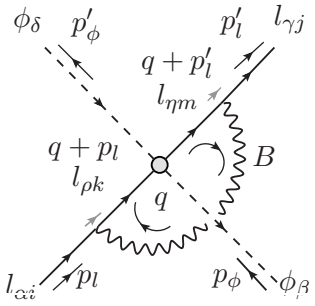

$$
\begin{aligned}
i\mathcal{M} &= i\mu^{\epsilon/2}\frac{g_1}{2}\delta_{\gamma\eta}\delta_{jm}\gamma^\mu P_L\int\frac{d^4q}{(2\pi)^4}\frac{i\left(\not q+\not p_l'\right)}{\left(q+p_l'\right)^2}\frac{i}{2}\mu^\epsilon c^{(6)}_{mk}\epsilon_{\eta\beta}\epsilon_{\rho\delta}\left(\not q+\not p_l-\not p_\phi'\right)P_L \\
&\qquad \frac{i\left(\not q+\not p_l\right)}{\left(q+p_l\right)^2}\,i\mu^{\epsilon/2}\frac{g_1}{2}\delta_{\rho\alpha}\delta_{ki}\,\gamma^\nu P_L\,i\frac{-g_{\mu\nu}+(1-\xi_B)\frac{q_\mu q_\nu}{q^2}}{q^2} \\
&= \left(-\frac{g_1^2}{4}\right)\frac{\mu^\epsilon}{2}c^{(6)}_{ji}\epsilon_{\gamma\beta}\epsilon_{\alpha\delta}\mu^\epsilon\int\frac{d^4q}{(2\pi)^4}\left[2\frac{\left(\not q+\not p_l\right)\left(\not q+\not p_l-\not p_\phi'\right)\left(\not q+\not p_l'\right)}{q^2\left(q+p_l'\right)^2\left(q+p_l\right)^2}\right. \\
&\qquad \left.+(1-\xi_B)\frac{\left(q^2+\not q\not p_l'\right)\left[\left(q+p_l\right)^2-\not p_\phi'\left(\not q+\not p_l\right)\right]\not q}{q^2q^2\left(q+p_l'\right)^2\left(q+p_l\right)^2}\right]P_L
\end{aligned}
$$

Now

$$
\begin{aligned}
\left(\not q+\not p_l\right)\left(\not q+\not p_l-\not p_\phi'\right)\left(\not q+\not p_l'\right) &= \left(q+p_l\right)^2\not q-\not q\not p_\phi'\not q-\not p_l\not p_\phi'\not q+ \\
&\quad \left(q+p_l\right)^2\not p_l'-\left(\not q+\not p_l\right)\not p_\phi'\not p_l' \\
\left(q^2+\not q\not p_l'\right)\left[\left(q+p_l\right)^2-\not p_\phi'\left(\not q+\not p_l\right)\right]\not q &= q^2\left(q+p_l\right)^2\not q-q^2\not p_\phi'q^2-q^2\not p_\phi'\not p_l\not q+ \\
&\quad \left(q+p_l'\right)^2\not q\not p_l'\not q-\not q\not p_l'\not p_\phi q^2-\not q\not p_l'\not p_\phi\not p_l\not q
\end{aligned}
$$

With these the above expression becomes

$$
\begin{aligned}
i\mathcal{M} &= \left(-\frac{g_1^2}{4}\right)\frac{\mu^\epsilon}{2}c^{(6)}_{ji}\epsilon_{\gamma\beta}\epsilon_{\alpha\delta}\mu^\epsilon\int\frac{d^4q}{(2\pi)^4}\left[2\frac{\left(\not q+\not p_l\right)}{q^2\left(q+p_l'\right)^2}-2\frac{\not q\not p_\phi'\not q}{q^2\left(q+p_l'\right)^2\left(q+p_l\right)^2}\right. \\
&\qquad \left.+\frac{(1-\xi_B)\not q}{q^2\left(q+p_l'\right)^2}-\frac{(1-\xi_B)\not p_\phi'}{\left(q+p_l'\right)^2\left(q+p_l\right)^2}+\frac{(1-\xi_B)\not q\not p_l'\not q}{q^2q^2\left(q+p_l'\right)^2}+\cdots\right]P_L \\
&= \frac{i}{16\pi^2}\mu^\epsilon\left(-\frac{g_1^2}{4}\right)c^{(6)}_{ji}\epsilon_{\gamma\beta}\epsilon_{\alpha\delta}\xi_B\left(\not p_l'+\not p_\phi'\right)P_L\frac{1}{\epsilon}\;+\;\text{UV finite} \qquad (4.4.16)
\end{aligned}
$$

Corresponding W boson diagram is same as the B boson diagram with g_1 and ξ_B replaced by g_2 and ξ_W respectively.

X

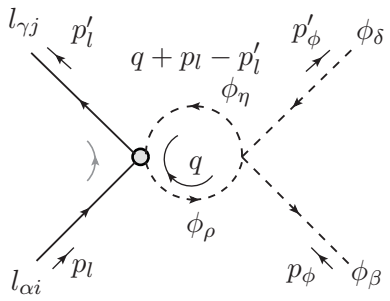

$$
\begin{aligned}
i\mathcal{M} &= \frac{1}{2}\frac{i}{2}\mu^\epsilon c_{ji}^{(6)}\epsilon_{\gamma\rho}\epsilon_{\alpha\eta}\int\frac{d^4q}{(2\pi)^4}\left(-\not{q}+\not{p}'_l\right)P_L\frac{i}{q^2-m^2}(-i)\mu^\epsilon\frac{\lambda}{2}\left(\delta_{\eta\rho}\delta_{\beta\delta}+\delta_{\eta\delta}\delta_{\beta\rho}\right) \\
&\qquad\qquad \frac{i}{\left(q+p_l-p'_l\right)^2-m^2} \\
&= \mu^\epsilon\frac{\lambda}{8}c_{ji}^{(6)}\left(\delta_{\gamma\alpha}\delta_{\beta\delta}+\epsilon_{\gamma\beta}\epsilon_{\alpha\delta}\right)\mu^\epsilon\int\frac{d^4q}{(2\pi)^4}\frac{\left(\not{q}-\not{p}'_l\right)}{\left(q^2-m^2\right)\left[\left(q+p_l-p'_l\right)^2-m^2\right]}P_L \\
&= -\frac{i}{16\pi^2}\mu^\epsilon\frac{\lambda}{8}c_{ji}^{(6)}\left(\delta_{\gamma\alpha}\delta_{\beta\delta}+\epsilon_{\gamma\beta}\epsilon_{\alpha\delta}\right)\left(\not{p}_l+\not{p}'_l\right)P_L\frac{1}{\epsilon}\ +\ \text{UV finite} \qquad (4.4.17)
\end{aligned}
$$

Additional factor of $1/2$ in the front is the symmetry factor. This divergence vanishes for on-shell condition of the external fermions.

4.4.3.2 Counterterm of $c^{(6)}$

Here we calculate the renormalization constant $\Delta c^{(6)}$. Using Eq. (4.2.10), we get

$$
\text{Divergent part of all diagrams} + \frac{i}{2}\mu^\epsilon\Delta c^{(6)}\epsilon_{\gamma\beta}\epsilon_{\alpha\delta}\left(\not{p}_l-\not{p}'_\phi\right)P_L=0 \quad (4.4.18)
$$

which gives us

$$\begin{aligned}
&\frac{i}{16\pi^2}\mu^\epsilon\left[\left(c^{(6)}Y_e^\dagger Y_e + Y_e^\dagger Y_e\, c^{(6)} + \frac{5}{4}c^{*(5)}c^{(5)} + 3\cdot\frac{g_1^2}{4}c^{(6)}\xi_B\right)\left(\not{p}_l - \not{p}'_\phi\right)\right.\\
&+\frac{g_1^2}{4}c^{(6)}\left(\frac{3}{2}\not{p}_\phi + \xi_B\not{p}'_\phi - \xi_B\not{p}_l + \xi_B\not{p}'_l + \xi_B\not{p}'_\phi + \frac{3}{2}\not{p}'_\phi - \xi_B\not{p}'_l - \xi_B\not{p}'_\phi\right)\\
&-\frac{\lambda}{4}c^{(6)}\left(\not{p}_l + \not{p}'_l\right) + 7\cdot\frac{g_2^2}{4}c^{(6)}\xi_W\left(\not{p}_l - \not{p}'_\phi\right) + \frac{g_2^2}{4}c^{(6)}\left(\frac{3}{2}\not{p}_\phi + \xi_W\not{p}'_\phi\right.\\
&\left.\left.-\xi_W\not{p}_l + \xi_W\not{p}'_l + \xi_W\not{p}'_\phi + \frac{3}{2}\not{p}'_\phi - \xi_W\not{p}'_l - \xi_W\not{p}'_\phi\right)\right]\epsilon_{\gamma\beta}\epsilon_{\alpha\delta}P_L\frac{1}{\epsilon}\\
&+\frac{i}{2}\mu^\epsilon\Delta c^{(6)}\epsilon_{\gamma\beta}\epsilon_{\alpha\delta}\left(\not{p}_l - \not{p}'_\phi\right)P_L = 0\\
\Rightarrow\quad &\frac{i}{16\pi^2}\left[\left(c^{(6)}Y_e^\dagger Y_e + Y_e^\dagger Y_e\, c^{(6)} + \frac{5}{4}c^{*(5)}c^{(5)} + \frac{g_1^2}{4}c^{(6)}2\xi_B + \frac{g_2^2}{4}c^{(6)}6\xi_W\right)\times\right.\\
&\left(\not{p}_l - \not{p}'_\phi\right) + \frac{g_1^2+g_2^2}{4}c^{(6)}\frac{3}{2}\left(\not{p}_\phi + \not{p}'_\phi\right) - \frac{\lambda}{4}c^{(6)}\left(\not{p}_l + \not{p}'_l\right)\Big]\epsilon_{\gamma\beta}\epsilon_{\alpha\delta}P_L\frac{1}{\epsilon}\\
&+\frac{i}{2}\Delta c^{(6)}\epsilon_{\gamma\beta}\epsilon_{\alpha\delta}\left(\not{p}_l - \not{p}'_\phi\right)P_L = 0
\end{aligned}\tag{4.4.19}$$

Following Eq. (4.2.8), we expand $\Delta c^{(6)}$ as

$$\Delta c^{(6)} = \Delta c^{(6)}_{,1}\frac{1}{\epsilon} + \cdots \tag{4.4.20}$$

Before proceeding further, we impose the on-shell condition for external fermions. All the terms associated with $\not{p}_l$ and $\not{p}'_l$ will vanish and one would obtain the expression for $\Delta c^{(6)}_{,1}$ as below

$$\begin{aligned}
\Delta c^{(6)}_{,1} \;=\; &-\frac{1}{16\pi^2}\left[2\left(c^{(6)}Y_e^\dagger Y_e + Y_e^\dagger Y_e\, c^{(6)}\right) + \frac{5}{2}c^{*(5)}c^{(5)}\right.\\
&\left.+\left(\xi_B - \frac{3}{2}\right)g_1^2c^{(6)} + 3\left(\xi_W - \frac{1}{2}\right)g_2^2c^{(6)}\right]
\end{aligned}\tag{4.4.21}$$

4.4.4 β-function of $c^{(6)}$

Now we are ready to compute the beta function of the non-unitary parameter from the general expression given in Eq. (4.3.9). In our case

$$Q = c^{(6)}, \qquad V_A \in \left\{Y_e, Y_e^\dagger, Y_u, Y_U^\dagger, Y_d, Y_d^\dagger, c^{(5)}, c^{*(5)}, g_1, g_2, \lambda\right\} \tag{4.4.22}$$

$$c_B^{(6)} = Z_\phi^{-\frac{1}{2}} Z_{l_L}^{-\frac{1}{2}} \left(c^{(6)} + \Delta c^{(6)}\right) \mu^\epsilon Z_{l_L}^{-\frac{1}{2}} Z_\phi^{-\frac{1}{2}}$$

To one loop order, Z_{l_L}, Z_ϕ and $c^{(6)}$ from (4.4.1), (4.4.2), (4.4.21) read

$$\Delta Z_{l_L,1} = -\frac{1}{16\pi^2}\left[Y_e^\dagger Y_e + \frac{1}{2}\xi_B g_1^2 + \frac{3}{2}\xi_B g_2^2\right] \tag{4.4.23}$$

$$\Delta Z_{\phi,1} = -\frac{1}{16\pi^2}\left[2T_1 - \frac{1}{2}\left(3-\xi_B\right)g_1^2 - \frac{3}{2}\left(3-\xi_B\right)g_2^2\right] \tag{4.4.24}$$

$$\begin{aligned}\Delta c_{,1}^{(6)} = -\frac{1}{16\pi^2}\Bigg[&2\left(c^{(6)}Y_e^\dagger Y_e + Y_e^\dagger Y_e\, c^{(6)}\right) + \frac{5}{2}c^{*(5)}c^{(5)} \\ &+ \left(\xi_B - \frac{3}{2}\right)g_1^2 c^{(6)} + 3\left(\xi_W - \frac{1}{2}\right)g_2^2 c^{(6)}\Bigg]\end{aligned} \tag{4.4.25}$$

As we discussed earlier, $c^{(6)}$ gets generated below the mass scale M, when the heavy particle gets integrated out effectively implying that the term $Y_\nu Y_\nu^\dagger$ can be dropped from the above expressions. Also the expression for T_1 becomes

$$T_1 = \mathrm{Tr}\left[Y_e^\dagger Y_e + 3\,Y_u^\dagger Y_u + 3\,Y_d^\dagger Y_d\right] \tag{4.4.26}$$

with $D_{c^{(6)}} = 1$ and $n_1 = n_2 = n_3 = n_4 = -\frac{1}{2}$. We get

$$\begin{aligned}D_{c^{(6)}}\left\langle \frac{d\delta c_{,1}^{(6)}}{dc^{(6)}}\middle| c^{(6)}\right\rangle &= -\frac{1}{16\pi^2}\Bigg[2\left(c^{(6)}Y_e^\dagger Y_e + Y_e^\dagger Y_e\, c^{(6)}\right) + \left(\xi_B - \frac{3}{2}\right)g_1^2 c^{(6)} \\ &\qquad + 3\left(\xi_W - \frac{1}{2}\right)g_2^2 c^{(6)}\Bigg] \\ D_{V_A}\left\langle \frac{d\delta c_{,1}^{(6)}}{dV_A}\middle| V_A\right\rangle &= -\frac{1}{16\pi^2}\frac{1}{2}\cdot 2\Bigg[2\left(c^{(6)}Y_e^\dagger Y_e + Y_e^\dagger Y_e\, c^{(6)}\right) + 2\cdot\frac{5}{2}c^{*(5)}c^{(5)} \\ &\qquad + \left(\xi_B - \frac{3}{2}\right)g_1^2 c^{(6)} + 3\left(\xi_W - \frac{1}{2}\right)g_2^2 c^{(6)}\Bigg]\end{aligned}$$

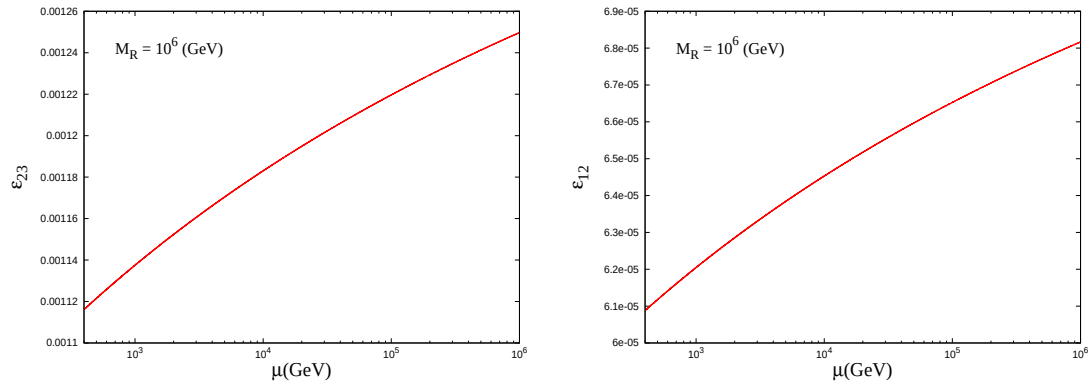

Figure 4.5: *Variation of non-unitary parameter* (ϵ) *with renormalization scale.*

$$\sum_{i=1}^{2} n_i \left[\sum_A D_{V_A} \left\langle \frac{d\delta Z_{\phi_i,1}}{dV_A}\middle| V_A \right\rangle\right] c^{(6)} = \left(-\frac{1}{2}\right)\left(-\frac{1}{16\pi^2}\right)\left[2T_1 - \frac{1}{2}\left(\frac{9}{2}-\xi_B\right)g_1^2 - \frac{3}{2}\left(\frac{7}{2}-\xi_W\right)g_2^2 + Y_e^\dagger Y_e + \frac{1}{2}\left(\xi_B-\frac{3}{2}\right)g_1^2 + \frac{3}{2}\left(\xi_W-\frac{1}{2}\right)g_2^2\right] c^{(6)}$$

$$c^{(6)}\sum_{j=1}^{2} n_j \left[\sum_A D_{V_A} \left\langle \frac{d\delta Z_{\phi_j,1}}{dV_A}\middle| V_A \right\rangle\right] = \left(-\frac{1}{2}\right)\left(-\frac{1}{16\pi^2}\right) c^{(6)}\left[2T_1 - \frac{1}{2}\times \left(\frac{9}{2}-\xi_B\right)g_1^2 - \frac{3}{2}\left(\frac{7}{2}-\xi_W\right)g_2^2 + Y_e^\dagger Y_e + \frac{1}{2}\left(\xi_B-\frac{3}{2}\right)g_1^2 + \frac{3}{2}\left(\xi_W-\frac{1}{2}\right)g_2^2\right]$$

$$\sum_{i=1}^{2} n_i D_{c^{(6)}} \left\langle \frac{d\delta Z_{\phi_i,1}}{dc^{(6)}}\middle| c^{(6)} \right\rangle = 0 = \sum_{j=1}^{2} n_j D_{c^{(6)}} \left\langle \frac{d\delta Z_{\phi_j,1}}{dc^{(6)}}\middle| c^{(6)} \right\rangle$$

Combining the above expressions we obtain the β-function for the non-unitary parameter, $c^{(6)}$, given by [236]

$$\beta_{c^{(6)}}^{1-loop} = -\frac{1}{16\pi^2}\left[\frac{3}{2}\left(c^{(6)}Y_e^\dagger Y_e + Y_e^\dagger Y_e\, c^{(6)}\right) - 2\,T_1 c^{(6)} + \frac{5}{2}\,c^{*(5)}c^{(5)} + 3\,g_2^2\,c^{(6)}\right] \tag{4.4.27}$$

This is the one loop β-function of the non-unitary parameter which governs the RGE of $c^{(6)}$. It is almost similar to the β-function of dimension-5 parameter,

widely known as κ in the literature [97–105, 110, 207], apart from $c^{*(5)}c^{(5)}$ term. The term $c^{*(5)}c^{(5)}$ is additional here[†]. Numerical consequence of the above equation is shown in Fig. 4.5. Values increases with scale governed mainly due to top Yukawa coupling. Running is very low but might have consequences in the precision study of neutrino antineutrino oscillation or $\nu_\mu - \nu_\tau$ oscillations.

[†]Coefficient of this term differs from an earlier paper [228].

Chapter 5

Summary and Conclusions

In this thesis we have studied several aspects of seesaw mechanism, particularly in the context of Type-I seesaw mechanism and minimal linear seesaw mechanism.

First we have investigated the implications of Dirac mass matrices (m_D) with 5 zeros for seesaw phenomenology. For the Majorana mass matrices (M_R) we consider both diagonal and non-diagonal forms. The diagonal form contains three zeros. However we noted that more minimal forms of M_R containing 4 zeros are possible. Three non-singular forms of M_R exist, which correspond to $L_\mu - L_\tau$, $L_e - L_\tau$ and $L_e - L_\mu$ symmetry. However, with 5 zero textures in m_D they can be shown to be incompatible with neutrino data. We have classified the allowed textures and discussed their implications for leptogenesis and lepton flavour violation. For m_D with 5 zeros and diagonal M_R there are 12 allowed textures

(i) 6 patterns with a vanishing $e\mu$ entry;

(ii) 6 patterns with a vanishing $e\tau$ entry;

All these 12 cases have one zero mass eigenvalue. The phenomenology of the cases (i) and (ii) is quite similar: θ_{13} is necessarily non-zero and sizable (at 3σ between 0.05 and 0.14 for the normal hierarchy and larger than 0.005 in the inverted hierarchy) and δ is in general non-trivial. Both normal and inverted hierarchy is possible. Leptogenesis is possible for all 12 patterns and the same

phase is responsible for leptogenesis as well as low energy CP violation in neutrino oscillations.

We have also considered the manifestations of seesaw mechanism for LFV by considering supersymmetric seesaw with minimal super gravity conditions as the only source for LFV. For the patterns with $(m_\nu)_{e\mu} = 0$ the BR($\mu \to e\gamma$) turns out to be zero. The BR($\tau \to e\gamma$) and BR($\tau \to \mu\gamma$) are proportional to $(m_\nu)_{e\tau}$ and $(m_\nu)_{\mu\tau}$, respectively, but depend on the unknown heavy neutrino masses and hence no definite predictions are possible for these. Similar conclusions hold true for patterns with $(m_\nu)_{e\tau} = 0$.

We also considered simultaneous presence of equality relations and texture zeros for Dirac and Majorana mass matrices in the minimal Type-I seesaw mechanism with 2 heavy right-handed neutrinos to reduce the number of parameters further. We study a large number of independent options and find that at the level of minimal number of free parameters only the 4 textures, presented in Table 3.3, and 4 others obtained by permuting the $2-3$ column of m_D presented in this table stand out to be almost consistent with global neutrino oscillation data. The latter 4 have the same predictions as the original ones and hence we have not presented these separately. One of the solutions in Table 3.3 are found to be consistent with normal mass hierarchy while three others with inverted mass hierarchy. Prediction of θ_{13} turned out be little outside the present 3σ range. We have argued that this situation can be remedied by assuming a small perturbation in the equalities in the mass matrix or elevate zeros. We also discuss the prediction of each solution for the oscillation parameters, $0\nu2\beta$ decay and the mass m_β probed by tritium β decay. It is noteworthy that the allowed values of m_β are below the sensitivity reach of KATRIN experiment. We also demonstrate in terms of the weak basis invariants if the solutions can give CP violation at low and high energy. We find that only one solution can have correlation between low and high energy CP violation. We discuss the implications of this solution for leptogenesis and explore the correlation between high and low energy CP violation.

Next we consider the phenomenology of the minimal linear seesaw model

consisting of three left-handed neutrinos and two singlet fields. The two singlet fields have opposite lepton numbers. Smallness of neutrino mass is ensured in this model by the tiny lepton number violating coupling (y_s) of one of the singlets with the left-handed neutrinos. Thus, the masses (M_R) of the heavy singlet neutrinos can be at the TeV scale even with the Dirac type coupling (y_ν) between the other singlet and the heavy state of $\mathcal{O}(1)$. This permits appreciable light-heavy mixing in the model which can have interesting phenomenological consequences. The model predicts one massless neutrino and hence there is only one Majorana phase. The great advantage of this model is that the Yukawa matrices can be fully reconstructed in terms of the oscillation parameters apart from the overall coupling strengths y_ν and y_s. We show that consideration of the vacuum stability of the scalar potential can constrain the coupling strength y_ν as $y_\nu \lesssim 0.3$ for 200 GeV $\lesssim M_R \lesssim 1$ TeV. However, it should be noted that this bound depends on the value of the strong coupling constant (α_s), the top quark mass (m_t) and the Higgs boson mass (m_h). Hence, this upper bound can be somewhat lowered depending on the experimental uncertainties on these quantities. The assumption of tiny lepton number violation implies $(y_s)_{max} \leq (y_\nu)_{min}$. This allows one to obtain an upper (lower) bound on y_s (y_ν) in conjunction with the constraints on neutrino masses from oscillation data. On the other hand the vacuum stability bound on y_ν, together with the measured values of neutrino mass squared differences gives a lower bound on y_s. Thus both the unknown overall coupling strengths of this model get constrained.

We also obtain the non-unitary correction to the PMNS mixing matrix. Bounds on y_ν/M_R can be obtained as a function of the CP phases α and δ from experimental constraints on lepton flavor violating processes. Combined constraints from vacuum stability and the lepton flavor violating process $\mu \to e\gamma$ rule out a significant portion of the parameter space in the (y_ν–M_R) plane for NH for masses of $M_R \lesssim 600$ GeV. On the other hand, contribution of the singlet neutrinos to the neutrinoless double beta decay process is insignificant. The model predicts interesting signatures at the LHC and can be tested using

the present and future data. However, a complete collider study merits a separate analysis.

We have also discussed the origin of non-unitarity at high energy for type-I seesaw. Below the mass scale of the heavy particle, the dimension-6 Dirac type effective operator leads to the non-unitarity of the lepton mixing matrix. We have calculated the one loop correction and derived the β-function which governs RG evolution of the non-unitary operator. Since non-unitarity becomes significant in TeV scale models, running is low as compared to the operators originated at a higher scale. But in fine tuned situation this running may give significant modification to the result. RGE of non-unitary operator may also become relevant for precision measurement of neutrino mixings.

Appendix A

The equalities in the Dirac mass matrix

In this appendix, we show the detailed classification of the Dirac mass matrix m_D. Since m_D has six entries, we can impose equalities on m_D up to five.

A.1 1 equality

We shall start with 1 equality in m_D. By imposing 1 equality among 6 matrix elements, the 6 elements are divided into 5 groups, that is, for instance $(m_D)_{11} = (m_D)_{12}$, and other 4 matrix elements. This situation can be symbolized by $(2, 1, 1, 1, 1)$, where each entry means the "slot" of the independent parameter. Since we impose 1 equality among 6 elements, the number of the independent parameters is reduced to 5. Therefore we have 5 entries in $(2, 1, 1, 1, 1)$. The number of each entry in the first bracket denotes the number of the matrix elements included in each group. The sum of the entries must be equal to 6.

The $(2, 1, 1, 1, 1)$ case includes ${}^6\mathrm{C}_2 = 15$ patterns of different textures. The

"representatives" are

$$(m_D)_{11} = (m_D)_{21} \quad \rightarrow \quad 3 \text{ patterns} \tag{A.1.1}$$

$$(m_D)_{11} = (m_D)_{12} \quad \rightarrow \quad 6 \text{ patterns} \tag{A.1.2}$$

$$(m_D)_{11} = (m_D)_{22} \quad \rightarrow \quad 6 \text{ patterns} \tag{A.1.3}$$

Here "representative" means that the other patterns can be generated by the permutation of the rows and the columns from the above three matrices. In other words, the above three matrices are not related to each other by permutations of the rows and the column, so that they compose a set of "primary" matrices in this category.

A.2 2 equalities

Here we consider 2 equalities in m_D. Since we have 2 equalities, the matrix elements are divided into 4 groups. There are two types of distributions; (2,2,1,1) and (3,1,1,1).

(2,2,1,1) case In this case, there are ${}^6\mathrm{C}_2 \times {}^4\mathrm{C}_2 = 90$ mass matrices. If we regard the first two groups of (2,2,1,1) as identical, then the total number is reduced to $90/2 = 45$ patterns. The representatives are

$$(m_D)_{11} = (m_D)_{21}, \quad (m_D)_{12} = (m_D)_{22} \quad \rightarrow \quad 3 \text{ patterns} \tag{A.2.1}$$

$$(m_D)_{11} = (m_D)_{12}, \quad (m_D)_{21} = (m_D)_{22} \quad \rightarrow \quad 3 \text{ patterns} \tag{A.2.2}$$

$$(m_D)_{11} = (m_D)_{22}, \quad (m_D)_{12} = (m_D)_{21} \quad \rightarrow \quad 3 \text{ patterns} \tag{A.2.3}$$

$$(m_D)_{11} = (m_D)_{12}, \quad (m_D)_{22} = (m_D)_{23} \quad \rightarrow \quad 6 \text{ patterns} \tag{A.2.4}$$

$$(m_D)_{11} = (m_D)_{22}, \quad (m_D)_{12} = (m_D)_{23} \quad \rightarrow \quad 6 \text{ patterns} \tag{A.2.5}$$

$$(m_D)_{11} = (m_D)_{23}, \quad (m_D)_{12} = (m_D)_{22} \quad \rightarrow \quad 6 \text{ patterns} \tag{A.2.6}$$

$$(m_D)_{11} = (m_D)_{21}, \quad (m_D)_{22} = (m_D)_{23} \quad \rightarrow \quad 6 \text{ patterns} \tag{A.2.7}$$

$$(m_D)_{11} = (m_D)_{22}, \quad (m_D)_{21} = (m_D)_{23} \quad \rightarrow \quad 6 \text{ patterns} \tag{A.2.8}$$

$$(m_D)_{11} = (m_D)_{23}, \quad (m_D)_{21} = (m_D)_{22} \quad \rightarrow \quad 6 \text{ patterns} \tag{A.2.9}$$

All 45 patterns can be generated from these 9 patterns. It should be noted again that we regard the textures which is related by the label exchange of the first two entries of (2,2,1,1) as identical. The classification of the above 9 patterns is similar to the general possibilities for the 2 zero textures for m_D.

(3,1,1,1) case We have ${}^6\mathrm{C}_3 = 20$ general possibilities and three representatives in this category.

$$(m_D)_{11} = (m_D)_{12} = (m_D)_{21} \quad \rightarrow \quad 12 \text{ patterns} \tag{A.2.10}$$

$$(m_D)_{11} = (m_D)_{12} = (m_D)_{13} \quad \rightarrow \quad 2 \text{ patterns} \tag{A.2.11}$$

$$(m_D)_{11} = (m_D)_{22} = (m_D)_{23} \quad \rightarrow \quad 6 \text{ patterns} \tag{A.2.12}$$

All 20 patterns can be generated from these 3 patterns. An easy way to understand these 3 patterns comes from the analogy with the 3 zero textures in m_D.

A.3 3 equalities

Here we consider 3 equalities in m_D. Since we have 3 equalities, the matrix elements are divided into 3 groups. There are three types of distributions; (3,2,1), (4,1,1) and (2,2,2). Let us see in turn.

(3,2,1) case In this case, there are ${}^6\mathrm{C}_3 \times {}^3\mathrm{C}_2 = 60$ patterns of textures. The representatives are

$$(m_D)_{11} = (m_D)_{12} = (m_D)_{13},\ (m_D)_{21} = (m_D)_{22} \ \rightarrow \ 6 \text{ patterns} \tag{A.3.1}$$

$$(m_D)_{11} = (m_D)_{12} = (m_D)_{21},\ (m_D)_{13} = (m_D)_{22} \ \rightarrow \ 12 \text{ patterns} \tag{A.3.2}$$

$$(m_D)_{11} = (m_D)_{12} = (m_D)_{21},\ (m_D)_{13} = (m_D)_{23} \ \rightarrow \ 12 \text{ patterns} \tag{A.3.3}$$

$$(m_D)_{11} = (m_D)_{12} = (m_D)_{21},\ (m_D)_{22} = (m_D)_{23} \ \rightarrow \ 12 \text{ patterns} \tag{A.3.4}$$

$$(m_D)_{11} = (m_D)_{12} = (m_D)_{23},\ (m_D)_{13} = (m_D)_{21} \ \rightarrow \ 12 \text{ patterns} \tag{A.3.5}$$

$$(m_D)_{11} = (m_D)_{12} = (m_D)_{23},\ (m_D)_{21} = (m_D)_{22} \ \rightarrow \ 6 \text{ patterns} \tag{A.3.6}$$

All 60 textures are generated from the above 6 representatives.

(4,1,1) case There are ${}^6\mathrm{C}_4 = 15$ patterns of textures. The representatives are

$$(m_D)_{11} = (m_D)_{12} = (m_D)_{13} = (m_D)_{21} \quad \to \quad 6 \text{ patterns} \quad \text{(A.3.7)}$$
$$(m_D)_{11} = (m_D)_{12} = (m_D)_{21} = (m_D)_{22} \quad \to \quad 3 \text{ patterns} \quad \text{(A.3.8)}$$
$$(m_D)_{11} = (m_D)_{12} = (m_D)_{21} = (m_D)_{23} \quad \to \quad 6 \text{ patterns} \quad \text{(A.3.9)}$$

All 15 textures are generated from the above 3 representatives.

(2,2,2) case There are ${}^6\mathrm{C}_2 \times {}^4\mathrm{C}_2 = 90$ patterns in this category. It is helpful to remember the case of (2,2,1,1) in 2 equalities. This case is obtained by imposing equalities between the last two entries of (2,2,1,1). As in the case of (2,2,1,1), we should identify the three entries of (2,2,2). Then the total number is reduced to $90/3! = 15$ patterns. The representatives are given by

$$(m_D)_{11} = (m_D)_{21},\ (m_D)_{12} = (m_D)_{22},\ (m_D)_{13} = (m_D)_{23} \ \to \ 1 \text{ pattern} \quad \text{(A.3.10)}$$
$$(m_D)_{11} = (m_D)_{12},\ (m_D)_{21} = (m_D)_{22},\ (m_D)_{13} = (m_D)_{23} \ \to \ 3 \text{ patterns} \quad \text{(A.3.11)}$$
$$(m_D)_{11} = (m_D)_{22},\ (m_D)_{12} = (m_D)_{21},\ (m_D)_{13} = (m_D)_{23} \ \to \ 3 \text{ patterns} \quad \text{(A.3.12)}$$
$$(m_D)_{11} = (m_D)_{12},\ (m_D)_{13} = (m_D)_{21},\ (m_D)_{22} = (m_D)_{23} \ \to \ 6 \text{ patterns} \quad \text{(A.3.13)}$$
$$(m_D)_{11} = (m_D)_{22},\ (m_D)_{12} = (m_D)_{23},\ (m_D)_{13} = (m_D)_{21} \ \to \ 2 \text{ patterns} \quad \text{(A.3.14)}$$

All 15 textures are generated from the above 5 representatives by the exchange of the rows and the columns.

A.4 4 equalities

Here we consider 4 equalities in m_D. As in 3 equalities, there are three types of distributions; (5,1), (4,2) and (3,3). We study the three cases in turn.

(5,1) case In this case, there are ${}^6\mathrm{C}_5 = {}^6\mathrm{C}_1 = 6$ patterns. A representative is

$$(m_D)_{11} = (m_D)_{12} = (m_D)_{13} = (m_D)_{21} = (m_D)_{22} \quad \rightarrow \quad 6 \text{ patterns} \tag{A.4.1}$$

All 6 textures are generated from the above representative by the exchange of the rows and the columns.

(4,2) case There are ${}^6\mathrm{C}_4 = 15$ patterns of textures. The representatives are

$$(m_D)_{11} = (m_D)_{12} = (m_D)_{13} = (m_D)_{21},\ (m_D)_{22} = (m_D)_{23} \ \rightarrow\ 6 \text{ patterns} \tag{A.4.2}$$
$$(m_D)_{11} = (m_D)_{12} = (m_D)_{21} = (m_D)_{22},\ (m_D)_{13} = (m_D)_{23} \ \rightarrow\ 3 \text{ patterns} \tag{A.4.3}$$
$$(m_D)_{11} = (m_D)_{12} = (m_D)_{21} = (m_D)_{23},\ (m_D)_{13} = (m_D)_{22} \ \rightarrow\ 6 \text{ patterns} \tag{A.4.4}$$

All 15 textures are generated from the above 3 representatives by the exchange of the rows and the columns.

(3,3) case There are ${}^6\mathrm{C}_3 = 20$ patterns of textures in this case. However 20 patterns contain redundancy. We can reproduce all 20 patterns from fundamental 10 patterns by exchanging the two entries of (3,3). The 10 patterns can be obtained from the three representatives. They can be taken as

$$(m_D)_{11} = (m_D)_{12} = (m_D)_{13},\ (m_D)_{21} = (m_D)_{22} = (m_D)_{23} \ \rightarrow\ 1 \text{ pattern} \tag{A.4.5}$$
$$(m_D)_{11} = (m_D)_{12} = (m_D)_{21},\ (m_D)_{13} = (m_D)_{22} = (m_D)_{23} \ \rightarrow\ 6 \text{ patterns} \tag{A.4.6}$$
$$(m_D)_{11} = (m_D)_{12} = (m_D)_{23},\ (m_D)_{13} = (m_D)_{21} = (m_D)_{22} \ \rightarrow\ 3 \text{ patterns} \tag{A.4.7}$$

All 10 textures are generated from the above 3 representatives by the exchange of the rows and the columns.

A.5 5 equalities

In this case, all the matrix elements in m_D are equal and the resultant left-handed Majorana mass matrix is of democratic form. This provides two massless neutrinos together with a nonzero M_R. Thus we can exclude m_D with 5 equalities.

Appendix B

Beta functions and matching corrections

In this appendix, we present all the beta functions upto three loop and expressions for matching corrections. The beta functions upto i^{th} loop for any coupling constant, Q, can be expressed in general as

$$\mu\frac{dQ}{d\mu} = \sum_i \frac{{\beta_Q}^{(i)}}{(16\pi^2)^i}, \tag{B.0.1}$$

B.1 One loop β-functions

The one loop beta functions of different coupling constants in SM can be found in literature [146, 158, 237, 238].

$$\beta_{g_1}^{(1)} = \left[\frac{4}{3}n + \frac{1}{10}\right] g_1^3 \tag{B.1.1}$$

$$\beta_{g_2}^{(1)} = \left[\frac{4}{3}n - \frac{22}{3} + \frac{1}{6}\right] g_2^3 \tag{B.1.2}$$

$$\beta_{g_3}^{(1)} = \left[\frac{4}{3}n - 11\right] g_3^3 \tag{B.1.3}$$

$$\begin{aligned}\beta_{\lambda}^{(1)} &= 24\lambda^2 - 3\lambda\left(\frac{3}{5}g_1^2 + 3g_2^2\right) + \frac{3}{4}g_2^4 + \frac{3}{8}\left(\frac{3}{5}g_1^2 + 3g_2^2\right)^2 \\ &\quad + 4\,T_1\lambda - 2Y_1\end{aligned} \tag{B.1.4}$$

$$\beta_{Y_e}^{(1)} = Y_e\left[\frac{3}{2}\left({Y_e}^\dagger Y_e - {Y_\nu}^\dagger Y_\nu\right) + T_1 - \frac{9}{4}\left(g_1^2 + g_2^2\right)\right] \tag{B.1.5}$$

$$\beta_{Y_u}^{(1)} = Y_u\left[\frac{3}{2}\left(Y_u{}^\dagger Y_u - Y_d{}^\dagger Y_d\right) + T_1 - \frac{17}{20}g_1^2 - \frac{9}{4}g_2^2 - 8g_3^2\right] \quad \text{(B.1.6)}$$

$$\beta_{Y_d}^{(1)} = Y_d\left[\frac{3}{2}\left(Y_d{}^\dagger Y_d - Y_u{}^\dagger Y_u\right) + T_1 - \frac{1}{4}g_1^2 - \frac{9}{4}g_2^2 - 8g_3^2\right] \quad \text{(B.1.7)}$$

$$\beta_{Y_\nu}^{(1)} = Y_\nu\left[\frac{3}{2}\left(Y_\nu{}^\dagger Y_\nu - Y_e{}^\dagger Y_e\right) + T_1 - \frac{9}{20}g_1^2 - \frac{9}{4}g_2^2\right] \quad \text{(B.1.8)}$$

where $$T_1 = \mathrm{Tr}\left[3Y_u{}^\dagger Y_u + 3Y_d{}^\dagger Y_d + Y_e{}^\dagger Y_e + Y_\nu{}^\dagger Y_\nu\right] \quad \text{(B.1.9)}$$

$$Y_1 = \mathrm{Tr}\left[3(Y_u{}^\dagger Y_u)^2 + 3(Y_d{}^\dagger Y_d)^2 + (Y_e{}^\dagger Y_e)^2 + (Y_\nu{}^\dagger Y_\nu)^2\right] \quad \text{(B.1.10)}$$

B.2 Two loop β-functions

The two loop beta functions in SM are taken from [146–150].

$$\beta_{g_1}^{(2)} = g_1^3\left[\left(\frac{9}{50}+\frac{19}{15}n\right)g_1^2 + \left(\frac{9}{10}+\frac{3}{5}n\right)g_2^2 + \frac{44}{15}n\,g_3^2 - \frac{17}{10}\mathrm{Tr}\left(\mathrm{Y_u}{}^\dagger\mathrm{Y_u}\right) - \frac{1}{2}\mathrm{Tr}\left(\mathrm{Y_d}{}^\dagger\mathrm{Y_d}\right) - \frac{3}{2}\mathrm{Tr}\left(\mathrm{Y_e}{}^\dagger\mathrm{Y_e}\right)\right] \quad \text{(B.2.1)}$$

$$\beta_{g_2}^{(2)} = g_2^3\left[\left(\frac{3}{10}+\frac{n}{15}\right)g_1^2 + \left(\frac{49}{3}n-\frac{259}{6}\right)g_2^2 + 4\,n\,g_3^2 - \frac{3}{2}\mathrm{Tr}\left(\mathrm{Y_u}{}^\dagger\mathrm{Y_u}\right) - \frac{3}{2}\mathrm{Tr}\left(\mathrm{Y_d}{}^\dagger\mathrm{Y_d}\right) - \frac{1}{2}\mathrm{Tr}\left(\mathrm{Y_e}{}^\dagger\mathrm{Y_e}\right)\right] \quad \text{(B.2.2)}$$

$$\beta_{g_3}^{(2)} = g_3^3\left[\frac{11}{30}n\,g_1^2 + \frac{3}{2}n\,g_2^2 + \left(\frac{76}{3}n-102\right)g_3^2 - 2\,\mathrm{Tr}\left(\mathrm{Y_u}{}^\dagger\mathrm{Y_u}\right) - 2\,\mathrm{Tr}\left(\mathrm{Y_d}{}^\dagger\mathrm{Y_d}\right)\right] \quad \text{(B.2.3)}$$

$$\begin{aligned}\beta_\lambda^{(2)} = {} & -312\,\lambda^3 + 36\left(3g_2^2+\frac{3}{5}g_1^2\right)\lambda^2 - \left[\left(\frac{313}{8}-10n\right)g_2^4 - \frac{117}{20}g_1^2g_2^2 - \left(\frac{687}{200}+2n\right)g_1^4\right]\lambda + \frac{1}{2}\left(\frac{497}{8}-8n\right)g_2^6 - \frac{1}{2}\left(\frac{97}{40}+\frac{8}{5}n\right)g_2^4g_1^2 \\ & - \frac{1}{2}\left(\frac{717}{200}+\frac{8}{5}n\right)g_2^2g_1^4 - \frac{1}{2}\left(\frac{531}{1000}+\frac{24}{25}n\right)g_1^6 - 32\,g_3^3\,\mathrm{Tr}\left[\left(Y_u{}^\dagger Y_u\right)^2 + \left(Y_d{}^\dagger Y_d\right)^2\right] - \frac{8}{10}\,g_1^2\,\mathrm{Tr}\left[2\left(Y_u{}^\dagger Y_u\right)^2 - \left(Y_d{}^\dagger Y_d\right)^2 + 3\left(Y_e{}^\dagger Y_e\right)^2\right] \\ & + \frac{1}{2}\,g_1^2\left[\left(\frac{63}{5}g_2^2-\frac{171}{50}g_1^2\right)\mathrm{Tr}\left(Y_u{}^\dagger Y_u\right) + \left(\frac{27}{5}g_2^2+\frac{9}{10}g_1^2\right)\mathrm{Tr}\left(Y_d{}^\dagger Y_d\right) + \left(\frac{33}{5}g_2^2-\frac{9}{2}g_1^2\right)\mathrm{Tr}\left(Y_e{}^\dagger Y_e\right)\right] - \frac{3}{4}\,g_2^4\,T_2 + 10\,\lambda\,Y_4 - 48\,\lambda^2\,T_2 - \lambda\,Y_2 \\ & - 42\,\lambda\,\mathrm{Tr}\left(Y_u{}^\dagger Y_u Y_d{}^\dagger Y_d\right) + 10\,Y_6 - 6\,\mathrm{Tr}\left[Y_u{}^\dagger Y_u\left(Y_u{}^\dagger Y_u + Y_d{}^\dagger Y_d\right)Y_d{}^\dagger Y_d\right]\end{aligned} \quad \text{(B.2.4)}$$

where

$$
\begin{aligned}
T_2 &= \mathrm{Tr}\left[3Y_u{}^\dagger Y_u + 3Y_d{}^\dagger Y_d + Y_e{}^\dagger Y_e\right] && \text{(B.2.5)}\\
Y_2 &= \mathrm{Tr}\left[3(Y_u{}^\dagger Y_u)^2 + 3(Y_d{}^\dagger Y_d)^2 + (Y_e{}^\dagger Y_e)^2\right] && \text{(B.2.6)}\\
Y_4 &= \left(\frac{17}{20}g_1^2 + \frac{9}{4}g_2^2 + 8\,g_3^2\right)\mathrm{Tr}\left(Y_u{}^\dagger Y_u\right) + \left(\frac{1}{4}g_1^2 + \frac{9}{4}g_2^2 + 8\,g_3^2\right)\mathrm{Tr}\left(Y_d{}^\dagger Y_d\right)\\
&\quad + \frac{3}{4}\left(g_1^2 + g_2^2\right)\mathrm{Tr}\left(Y_e{}^\dagger Y_e\right) && \text{(B.2.7)}\\
Y_6 &= \mathrm{Tr}\left[3(Y_u{}^\dagger Y_u)^3 + 3(Y_d{}^\dagger Y_d)^3 + (Y_e{}^\dagger Y_e)^3\right] && \text{(B.2.8)}
\end{aligned}
$$

n is the effective number of generation. $n = 5/2$ for $\mu < m_t$ and $n = 3$ for $\mu > m_t$.

$$
\begin{aligned}
\beta_{Y_e}^{(2)} &= Y_e\left[\frac{3}{2}\left(Y_e{}^\dagger Y_e\right)^2 + \left(\frac{387}{80}g_1^2 + \frac{135}{16}g_2^2 - 12\lambda - \frac{9}{4}T_2\right)Y_e{}^\dagger Y_e - \chi_4 + 6\lambda^2\right.\\
&\quad \left. + \frac{5}{2}Y_4 + \left(\frac{51}{200} + \frac{11}{5}n\right)g_1^4 + \frac{27}{20}g_1^2 g_2^2 - \left(\frac{35}{4} - n\right)g_2^4\right] && \text{(B.2.9)}\\
\beta_{Y_u}^{(2)} &= Y_u\left[Y_u{}^\dagger Y_u\left(\frac{3}{2}Y_u{}^\dagger Y_u - Y_d{}^\dagger Y_d\right) - \frac{1}{4}Y_d{}^\dagger Y_d\left(Y_u{}^\dagger Y_u - 11\,Y_d{}^\dagger Y_d\right) + \left(\frac{223}{80}g_1^2\right.\right.\\
&\quad \left. + \frac{135}{16}g_2^2 + 16g_3^2 - 12\lambda - \frac{9}{4}T_2\right)Y_u{}^\dagger Y_u - \left(\frac{43}{80}g_1^2 - \frac{9}{16}g_2^2 + 16g_3^2\right.\\
&\quad \left.\left. - \frac{5}{4}T_2\right)Y_d{}^\dagger Y_d - \chi_4 + 6\lambda^2 + \frac{5}{2}Y_4 + \left(\frac{9}{200} + \frac{29}{45}n\right)g_1^4 - \frac{9}{20}g_1^2 g_2^2\right.\\
&\quad \left. + \frac{19}{15}g_1^2 g_3^2 - \left(\frac{35}{4} - n\right)g_2^4 + 9\,g_2^2 g_3^2 - \left(\frac{404}{3} - \frac{80}{9}n\right)g_3^4\right] && \text{(B.2.10)}\\
\beta_{Y_d}^{(2)} &= Y_d\left[Y_d{}^\dagger Y_d\left(\frac{3}{2}Y_d{}^\dagger Y_d - Y_u{}^\dagger Y_u\right) - \frac{1}{4}Y_u{}^\dagger Y_u\left(Y_d{}^\dagger Y_d - 11\,Y_u{}^\dagger Y_u\right) + \left(\frac{187}{80}g_1^2\right.\right.\\
&\quad \left. + \frac{135}{16}g_2^2 + 16g_3^2 - 12\lambda - \frac{9}{4}T_2\right)Y_d{}^\dagger Y_d - \left(\frac{79}{80}g_1^2 - \frac{9}{16}g_2^2 + 16g_3^2\right.\\
&\quad \left.\left. - \frac{5}{4}T_2\right)Y_u{}^\dagger Y_u - \chi_4 + 6\lambda^2 + \frac{5}{2}Y_4 - \left(\frac{29}{200} + \frac{1}{45}n\right)g_1^4 - \frac{27}{20}g_1^2 g_2^2\right.\\
&\quad \left. + \frac{31}{15}g_1^2 g_3^2 - \left(\frac{35}{4} - n\right)g_2^4 + 9\,g_2^2 g_3^2 - \left(\frac{404}{3} - \frac{80}{9}n\right)g_3^4\right] && \text{(B.2.11)}
\end{aligned}
$$

where χ_4 is given as below

$$
\chi_4 = \frac{9}{4}\left(Y_2 - \frac{1}{3}\mathrm{Tr}\left[Y_u{}^\dagger Y_u Y_d{}^\dagger Y_d + Y_d{}^\dagger Y_d Y_u{}^\dagger Y_u\right]\right) \qquad \text{(B.2.12)}
$$

B.3 Three loop β-functions

The 3 loop β-functions of SM g_1, g_2, g_3, λ and Y_t are taken from [226, 227]

$$\begin{aligned}
\beta_{g_1}^{(3)} &= g_1^3\left[\left(\frac{489}{8000}-\frac{58}{75}n-\frac{209}{135}n^2\right)g_1^4+\left(\frac{783}{800}-\frac{7}{100}n\right)g_1^2g_2^2-\frac{n}{5}g_2^2g_3^2\right.\\
&\quad-\frac{137n}{225}g_1^2g_3^2+\left(\frac{3401}{320}+\frac{83}{30}n-\frac{11}{15}n^2\right)g_2^4+\left(\frac{275}{9}n\right.\\
&\quad\left.-\frac{484}{135}n^2\right)g_3^4+n_tY_t^2\left(\left(\frac{339}{80}+\frac{303}{40}n_t\right)Y_t^2-\frac{2827}{800}g_1^2-\frac{471}{32}g_2^2\right.\\
&\quad\left.\left.-\frac{29}{5}g_3^2\right)+\left(\frac{27}{50}g_1^2+\frac{9}{10}g_2^2-\frac{9}{5}\lambda\right)\lambda\right] \qquad \text{(B.3.1)}\\
\beta_{g_2}^{(3)} &= g_2^3\left[\left(\frac{163}{1600}-\frac{7}{15}n-\frac{11}{45}n^2\right)g_1^4+\left(\frac{561}{160}+\frac{13}{20}n\right)g_1^2g_2^2-\frac{n}{15}g_1^2g_3^2\right.\\
&\quad+\left(-\frac{667111}{1728}+\frac{6412}{27}n-\frac{415}{27}n^2\right)g_2^4+13\,n\,g_2^2g_3^2\\
&\quad+\left(\frac{125}{3}n-\frac{44}{9}n^2\right)g_3^4+n_tY_t^2\left(\left(\frac{57}{16}+\frac{45}{8}n_t\right)Y_t^2-\frac{593}{160}g_1^2\right.\\
&\quad\left.\left.-\frac{729}{32}g_2^2-7\,g_3^2\right)+\left(\frac{3}{10}g_1^2+\frac{3}{2}g_2^2-3\,\lambda\right)\lambda\right] \qquad \text{(B.3.2)}\\
\beta_{g_3}^{(3)} &= g_3^3\left[\left(-\frac{13}{120}n-\frac{121}{270}n^2\right)g_1^4-\frac{n}{40}g_1^2g_2^2+\frac{77n}{45}g_1^2g_3^2+7\,n\,g_2^2g_3^2\right.\\
&\quad+\left(\frac{241}{24}n-\frac{11}{6}n^2\right)g_2^4+\left(-\frac{2857}{2}+\frac{5033}{9}n-\frac{650}{27}n^2\right)g_3^4\\
&\quad\left.+\,n_tY_t^2\left(\left(\frac{9}{2}+\frac{21}{2}n_t\right)Y_t^2-\frac{101}{40}g_1^2-\frac{93}{8}g_2^2-40\,g_3^2\right)\right] \qquad \text{(B.3.3)}\\
\beta_{\lambda}^{(3)} &= 2\left[\lambda^4\left(3588+2016\,\zeta_3\right)+291\,d_RY_t^2\lambda^3+Y_t^4\lambda^2\left(\frac{789}{2}d_R+252\,\zeta_3\,d_R\right.\right.\\
&\quad\left.-36\,d_R^2\right)+Y_t^6\lambda\left(-\frac{1881}{8}d_R-66\,\zeta_3\,d_R+80\,d_R^2\right)+Y_t^8\left(\frac{13}{2}d_R\right.\\
&\quad\left.-12\,\zeta_3\,d_R-\frac{195}{8}d_R^2\right)+g_3^2\,Y_t^2\lambda^2\left(-306\,C_F\,d_R+288\,\zeta_3\,C_F\,d_R\right)\\
&\quad+g_3^2\,Y_t^4\lambda\left(\frac{895}{4}C_F\,d_R-324\,\zeta_3\,C_F\,d_R\right)+g_3^2\,Y_t^6\left(-\frac{19}{2}C_F\,d_R\right.\\
&\quad\left.+60\,\zeta_3\,C_F\,d_R\right)+g_3^4\,Y_t^2\lambda\left(-\frac{119}{2}C_F^2\,d_R+77\,C_A\,C_F\,d_R\right.\\
&\quad\left.-32\,n\,T_F\,C_F\,d_R+72\,\zeta_3\,C_F^2d_R-36\,\zeta_3\,C_A\,C_F\,d_R\right)+\,g_3^4\,Y_t^4\left(\frac{131}{2}C_F^2d_R\right.\\
&\quad+48\,T_F\,C_F\,d_R-\frac{109}{2}C_A\,C_F\,d_R+20\,n\,T_F\,C_F\,d_R-48\,\zeta_3\,C_F^2\,d_R\\
&\quad\left.+24\,\zeta_3\,C_A\,C_F\,d_R\right)\Big] \qquad \text{(B.3.4)}
\end{aligned}$$

$$\begin{aligned}\beta_{Y_t}^{(3)} &= 2\,Y_t\left[-18\,\lambda^3+Y_t^2\lambda^2\left(\frac{285}{8}-\frac{45}{4}d_R\right)+Y_t^4\lambda\left(\frac{63}{2}+\frac{45}{2}d_R\right)+Y_t^6\left(+\frac{9}{4}\,\zeta_3\right.\right.\\ &-\frac{345}{32}+\frac{107}{32}\,d_R+\frac{3}{2}\,\zeta_3\,d_R+\frac{39}{16}\,d_R^2\Big)+6\,C_F\,g_3^2\,Y_t^2\lambda-g_3^2\,Y_t^4\left(\frac{57}{2}C_F\right.\\ &+\frac{81}{8}C_F\,d_R\Big)+g_3^4\,Y_t^2\left(\frac{471}{16}C_F^2-\frac{119}{8}C_F^2\,d_R+25\,T_F\,C_F+\frac{717}{16}C_AC_F\right.\\ &+\frac{77}{4}C_AC_F\,d_R-\frac{33}{2}nT_FC_F-8\,nT_FC_F\,d_R-27\,\zeta_3\,C_F^2+18\,\zeta_3\,C_F^2\,d_R\\ &-\frac{27}{2}\zeta_3\,C_AC_F-9\,\zeta_3\,C_AC_F\,d_R\Big)+g_3^6\left(-\frac{129}{2}C_F^3+\frac{129}{4}C_AC_F^2\right.\\ &-\frac{11413}{108}C_A^2C_F+92\,n\,T_FC_F^2+\frac{1112}{27}n\,C_AT_FC_F+\frac{560}{27}n^2\,T_F^2\,C_F\\ &\left.\left.-96\,\zeta_3\,n\,T_FC_F^2+96\,\zeta_3\,n\,C_AT_FC_F\right)\right]\end{aligned}\tag{B.3.5}$$

n_t is the number of heavy up-type quark. $n_t = 1$ in our case. C_A, C_F, T_F, d_R are constants of the $SU(3)$ representation in the quark sector. $C_A = 3$, $C_F = 4/3$, $T_F = 1/2$, $d_R = 3$.

B.4 $\overline{\text{MS}}$ coupling constants and pole mass matching

The matching correction between $\overline{\text{MS}}$ λ and Higgs pole mass is given by* [157]

$$\delta_h^{(1)}(m_t) = \frac{m_Z^2}{16\pi^2v^2}\left[xf_1(x)+f_0(x)+x^{-1}f_{-1}(x)\right]\tag{B.4.1}$$

where $x = m_h^2/m_z^2$. f_1, f_0, f_{-1} are given by

$$\begin{aligned}f_1(x) &= 6\ln(x_1)+\frac{3}{2}\ln(x)-\frac{1}{2}\,Y\left(\frac{1}{x}\right)-Y\left(\frac{c_w^2}{x}\right)-\ln\left(c_w^2\right)\\ &+\frac{9}{2}\left[\frac{25}{9}-\frac{\pi}{\sqrt{3}}\right]\end{aligned}\tag{B.4.2}$$

*This expression is also given in [91] with a factor $32\pi^2$ instead of $16\pi^2$. But we were informed from the authors that it was a typo and the factor $16\pi^2$ in the original paper was correct.

$$
\begin{aligned}
f_0(x) &= -6\ln(x_2)\left[1+2\,c_w^2-2\,x_2\right]+\frac{3\,c_w^2\,x}{x-c_w^2}\ln\left(\frac{x}{c_w^2}\right)+2\,Y\left(\frac{1}{x}\right)\\
&\quad+\left[\frac{3\,c_w^2}{1-c_w^2}+12\,c_w^2\right]\ln\left(c_w^2\right)-\frac{15}{2}\left[1+2\,c_w^2\right]\\
&\quad-3\,x_2\left[2\,Y\left(\frac{x_2}{x}\right)+4\ln(x_2)-5\right]+4\,c_w^2\,Y\left(\frac{c_w^2}{x}\right) \qquad \text{(B.4.3)}\\
f_{-1}(x) &= 6\ln(x_2)\left[1+2\,c_w^4-4\,x_2^2\right]-6\,Y\left(\frac{1}{x}\right)-12\,c_w^4\left[Y\left(\frac{c_w^2}{x}\right)+\ln\left(c_w^2\right)\right]\\
&\quad+24\,x_2^2\left[\ln\left(x_2\right)-2+Y\left(\frac{x_2}{x}\right)\right]+8\left[1+2\,c_w^4\right] \qquad \text{(B.4.4)}
\end{aligned}
$$

$x_1 = m_t^2/m_h^2$, $x_2 = m_t^2/m_z^2$. $c_w = \cos\theta_w$, where θ_w is the Weinberg mixing angle. Y is given by

$$
Y(x) = \begin{cases} 2\sqrt{|1-4\,x|}\,\tan^{-1}\left(\frac{1}{\sqrt{|1-4\,x|}}\right) & \text{for} \quad x > \frac{1}{4} \\ \sqrt{|1-4\,x|}\,\ln\left(\frac{1+\sqrt{|1-4\,x|}}{1-\sqrt{|1-4\,x|}}\right) & \text{for} \quad x < \frac{1}{4} \end{cases} \qquad \text{(B.4.5)}
$$

The two loop correction has been taken from [222]

$$
\delta_h^{(2)}\left(m_t\right) = \delta_{h,\mathrm{Yuk}}^{(2)}\left(m_t\right) + \delta_{h,\mathrm{QCD}}^{(2)}\left(m_t\right) \qquad \text{(B.4.6)}
$$

$$
\begin{aligned}
\delta_{h,\mathrm{Yuk}}^{(2)}\left(m_t\right) &= \frac{m_t^4}{\left(16\pi^2 v^2\right)^2}\,x_1\left[N_c^2\left\{-16B_0\left(m_t\,,m_t\,,m_h\right)+\frac{1}{x_1}\Bigg(1+\right.\right.\\
&\quad\left.4B_0\left(m_t\,,m_t\,,m_h\right)\Bigg)\right\}+N_c\left\{16+\frac{8}{3}\pi^2+32B_0\left(m_t\,,m_h\,,m_t\right)\right.\\
&\quad-\frac{1}{x_1}\left(\frac{929}{6}+\frac{16}{3}\pi^2+48B_0\left(m_h\,,m_h\,,m_h\right)-16L_H\right.\\
&\quad\left.+\frac{76}{3}B_0\left(m_t\,,m_h\,,m_t\right)\right)+\frac{1}{x_1^2}\left(\frac{17629}{270}+\frac{8}{3}\pi^2-\frac{2}{3}L_H\right.\\
&\quad\left.+27B_0\left(m_h\,,m_h\,,m_h\right)+\frac{13}{3}B_0\left(m_t\,,m_h\,,m_t\right)\right)+\frac{1}{x_1^3}\left(\frac{1181}{900}\right.\\
&\quad\left.\left.-\frac{\pi^2}{2}+\frac{61}{30}B_0\left(m_h\,,m_h\,,m_h\right)+\frac{59}{90}L_H-\frac{2}{35}B_0\left(m_t\,,m_h\,,m_t\right)\right)\right\}\\
&\quad+\frac{1}{x_1^3}\left\{\frac{131}{6}\pi^2+\left(\frac{729}{2}-\frac{135}{4}\sqrt{3}\,\pi\right)S_2-111L_H+36L_H^2\right.\\
&\quad\left.+\sqrt{3}\,\pi\left(18\,L_H-\frac{225}{4}\right)+\frac{75+72\,\zeta_3}{4}\right\}\Bigg] \qquad \text{(B.4.7)}
\end{aligned}
$$

where $N_c = 3$, $L_H = \ln(1/x_1)$, $S_2 = 0.260434138\cdots$, $\zeta_3 = 1.2020569\cdots$ and B_0's are given by (for $m_t > m_h$)

$$B_0(m_t, m_t, m_h) = 2 - 2\sqrt{4x_1 - 1}\,\tan^{-1}\left(\frac{1}{\sqrt{4x_1-1}}\right) \tag{B.4.8}$$

$$B_0(m_h, m_h, m_h) = 2 - \frac{\pi}{\sqrt{3}} \tag{B.4.9}$$

$$B_0(m_t, m_h, m_t) = 2 - \frac{1}{2x_1}\ln\left(\frac{1}{x_1}\right) - \frac{\sqrt{4x_1-1}}{x_1}\left[\tan^{-1}\left(\frac{2x_1-1}{\sqrt{4x_1-1}}\right) + \tan^{-1}\left(\frac{1}{\sqrt{4x_1-1}}\right)\right] \tag{B.4.10}$$

$$\delta^{(2)}_{h,\rm QCD}(m_t) = \frac{m_t^2}{(16\pi^2)^2 v^2} 4\pi N_c C_F \alpha_s(m_t)\left[35 - \frac{2\pi^2}{3} - 64\,x_1 + \frac{1}{x_1}\left(\frac{61}{135} + \frac{1}{x_1}\frac{1233}{6300} + \frac{1}{x_1^2}\frac{43123}{1323000}\right)\right] \tag{B.4.11}$$

where $C_F = 4/3$. The matching correction between $\overline{\rm MS}$ Y_t and top pole mass is given by

$$\delta_t(m_t) = \delta_t^{\rm QCD}(m_t) + \delta_t^{\rm QED+W}(m_t) + \delta_t^{\rm QCD,QED}(m_t) \tag{B.4.12}$$

$\delta_t^{\rm QCD}$ is taken upto three loop [155] and $\delta_t^{\rm QED+W}$ is taken upto one loop [156,239]

$$\delta_t^{\rm QCD}(m_t) = -\frac{4}{3\pi}\alpha_s(m_t) - \frac{9.1253}{\pi^2}\alpha_s^2(m_t) - \frac{80.4046}{\pi^3}\alpha_s^3(m_t) \tag{B.4.13}$$

$$\delta_t^{\rm QED+W}(m_t) = -\frac{4}{9\pi}\alpha_{em}(m_t) + \frac{m_t^2}{16\pi^2 v^2}\left[\frac{11}{2} - \frac{1}{4x_1} - \frac{1}{2x_1^2}(4\,x_1-1)^{3/2}\times \cos^{-1}\left(\frac{1}{2\sqrt{x_1}}\right) + \frac{1}{2x_1}\left(\frac{1}{2x_1} - 3\right)\ln\left(\frac{1}{x_1}\right)\right] - 6.9\times 10^{-3} + 1.73\times 10^{-3}\ln\left(\frac{m_h}{300\,\rm GeV}\right) - 5.82\times 10^{-3}\ln\left(\frac{m_t}{175\,\rm GeV}\right) \tag{B.4.14}$$

for $m_h^2 < 4m_t^2$.

$\delta_t^{\rm QCD,QED}$ is the $\mathcal{O}\left(\alpha\,\alpha_s\right)$ correction which is comparable to $\delta_t^{\rm QCD}$. It is given by [225]

$$\begin{aligned}
\delta_t^{\rm QCD,QED} &= -\frac{\alpha\,\alpha_s}{16\pi^2}\frac{C_F}{1-c_w^2}\left[-78.591+\frac{6}{m_{hw}}\ln\left(\frac{1}{m_{tw}}\right)+3\,\frac{m_{zw}}{x}\ln\left(\frac{1}{x_2}\right)\right.\\
&-\frac{2}{m_{hw}}-x_1\,m_{tw}\left(\frac{11}{8\,x_1}\frac{1+Y_H^2}{Y_H}+\frac{1}{x_2^2}-6\right)+\zeta_2\,m_{tw}\left(\frac{3}{2Y_H}\right.\\
&\left.+\frac{9}{2}Y_H+\frac{3}{4}Y_H^2\right)+m_{tw}\frac{\left(1-Y_H\right)^2}{Y_H^2}\ln\left(Y_H\right)\left\{\ln\left(1-Y_H\right)\right.\\
&\left.+\frac{1}{2}\ln\left(1+Y_H\right)\right\}\left\{\left(1-Y_H^2\right)-\frac{1}{2}\left(1+Y_H^2\right)\ln\left(Y_H\right)\right\}-\frac{1}{8}\,m_{tw}\times\\
&\frac{2+8Y_H-10Y_H^2-3Y_H^3}{Y_H}\ln^2\left(Y_H\right)+\frac{1}{8}\,m_{tw}\left(1+Y_H\right)\left(11Y_H-39\right)\times\\
&\ln\left(Y_H\right)-\frac{1}{8}\,m_{hw}\frac{11-50Y_H+11Y_H^2}{Y_H}\ln\left(1+Y_H\right)-\frac{3}{2}\,m_{tw}\,\zeta_2\times\\
&\ln\left(1+Y_H\right)\frac{\left(1-Y_H\right)^2\left(1+Y_H^2\right)}{Y_H^2}+m_{tw}\frac{\left(1-Y_H\right)\left(1+Y_H\right)}{Y_H^2}\times\\
&\left\{\frac{5-28Y_H+5Y_H^2}{4}\,{\rm Li}_2\left(-Y_H\right)+\left(1-Y_H\right)^2{\rm Li}_2\left(Y_H\right)\right\}\\
&+m_{tw}\frac{\left(1-Y_H\right)^2\left(1+Y_H^2\right)}{Y_H^2}\left\{\frac{3}{2}\Big(2\,{\rm Li}_3\left(Y_H\right)+{\rm Li}_3\left(-Y_H\right)\Big)\right.\\
&\left.\left.-\ln\left(Y_H\right)\Big(2\,{\rm Li}_2\left(Y_H\right)+{\rm Li}_2\left(-Y_H\right)\Big)\right\}\right] \qquad \text{(B.4.15)}
\end{aligned}$$

where $\zeta_2=\pi^2/6$, $m_{hw}=m_h^2/m_w^2$, $m_{tw}=m_t^2/m_w^2$, $m_{zw}=m_z^2/m_w^2$. Y_H is given as below

$$Y_H = \frac{1-\sqrt{1-4x_1}}{1+\sqrt{1-4x_1}} \qquad \text{(B.4.16)}$$

${\rm Li}_n(z)$ is Poly-Logarithm function given by

$${\rm Li}_n(z) = \int_0^z \frac{{\rm Li}_{n-1}(t)}{t}dt \qquad \text{(B.4.17)}$$

with ${\rm Li}_0(z)$ given by

$${\rm Li}_0(z) = \frac{z}{1-z} \qquad \text{(B.4.18)}$$

Appendix C

Feynman Rules

In this Appendix, we give the relevant Feynman rules, those are used to compute the UV divergence in Chapter 4. Arrows on the particle line indicate charge flow. Arrows by the side of particle lines indicate momentum flow. Grey arrows indicate orientation, introduced in [240].

propagators:

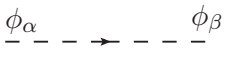

$$\frac{i}{p^2-m^2+i\varepsilon}\delta_{\beta\alpha}$$

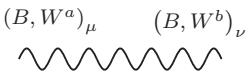

$$i\frac{-g_{\mu\nu}+(1-\xi_{B,W})\frac{p_\mu p_\nu}{p^2}}{p^2+i\varepsilon}\delta_{ab}\delta_{\beta\alpha}$$

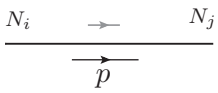

$$\frac{i\left(\not{p}+M_j\right)}{p^2-M_j^2+i\varepsilon}\delta_{ji}$$

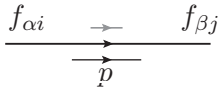

$$\frac{i\not{p}}{p^2+i\varepsilon}\delta_{ji}\delta_{\beta\alpha}$$

when momentum is opposite to the orientation, p should be replaced by $-p$. f denotes Dirac fermions. In case of singlet, the $SU(2)$ indices (*i.e.* α, β) should be omitted.

ϕ^4 interaction:

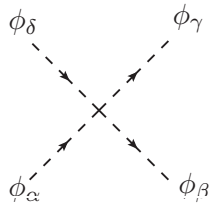

$$-\tfrac{i}{2}\,\mu^\epsilon \lambda\,(\delta_{\beta\alpha}\delta_{\gamma\delta} + \delta_{\beta\delta}\delta_{\gamma\alpha})$$

gauge boson interaction:

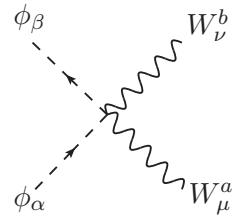

$$\tfrac{i}{2}\,\mu^\epsilon g_2^2 g^{\mu\nu}\delta_{\alpha\beta}\delta_{ab}$$

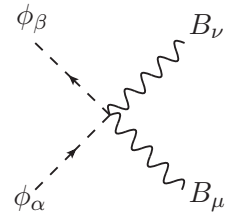

$$\tfrac{i}{2}\,\mu^\epsilon g_1^2 g^{\mu\nu}\delta_{\alpha\beta}$$

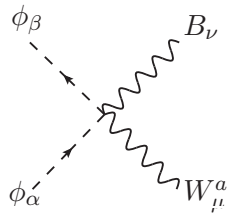

$$\tfrac{i}{2}\,\mu^\epsilon g_1 g_2 g^{\mu\nu}\sigma^a_{\alpha\beta}$$

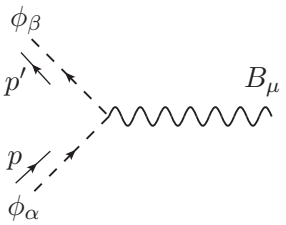

$$-\tfrac{i}{2}\,\mu^{\epsilon/2} g_1 \left(p_\mu + p'_\mu\right) \delta_{\beta\alpha}$$

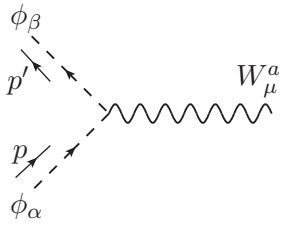

$$-\tfrac{i}{2}\,\mu^{\epsilon/2} g_1 \left(p_\mu + p'_\mu\right) \sigma^a_{\beta\alpha}$$

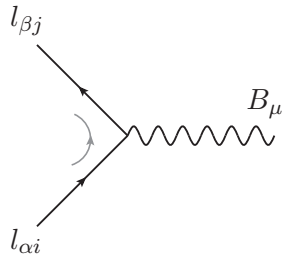

$$\tfrac{i}{2}\,\mu^{\epsilon/2}\, g_1 \delta_{\beta\alpha}\delta_{ji}\,\gamma_\mu P_L$$

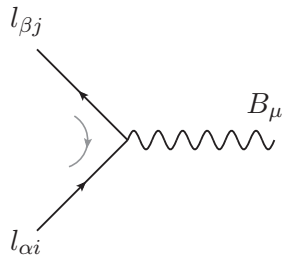

$$-\tfrac{i}{2}\,\mu^{\epsilon/2}\, g_1 \delta_{\beta\alpha}\delta_{ji}\,\gamma_\mu P_L$$

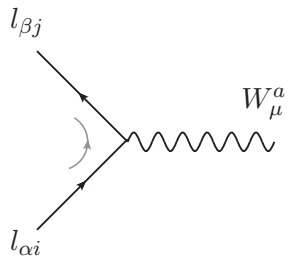

$$-\tfrac{i}{2}\,\mu^{\epsilon/2}\, g_2 \sigma^a_{\beta\alpha}\delta_{ji}\,\gamma_\mu P_L$$

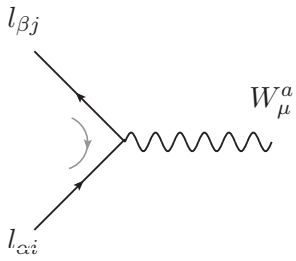

$$\tfrac{i}{2}\,\mu^{\epsilon/2}\, g_2 \sigma^a_{\beta\alpha}\delta_{ji}\,\gamma_\mu P_R$$

Yukawa interaction:

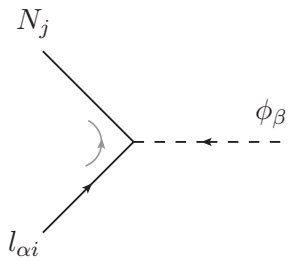

$$-i\,\mu^{\epsilon/2}\,(Y_\nu)_{ji}\,\epsilon_{\alpha\beta}P_L$$

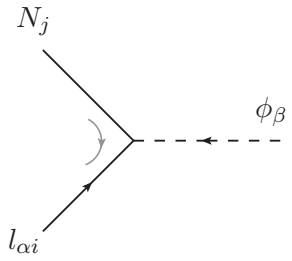

$$-i\,\mu^{\epsilon/2}\,(Y_\nu)_{ji}\,\epsilon_{\alpha\beta}P_L$$

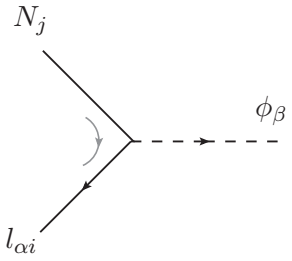

$$-i\,\mu^{\epsilon/2}\,(Y_\nu^*)_{ji}\,\epsilon_{\alpha\beta}P_R$$

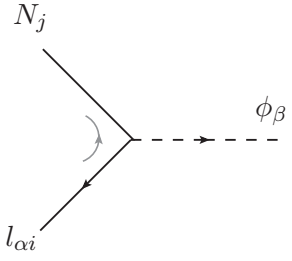

$$-i\,\mu^{\epsilon/2}\,(Y_\nu^*)_{ji}\,\epsilon_{\alpha\beta}P_R$$

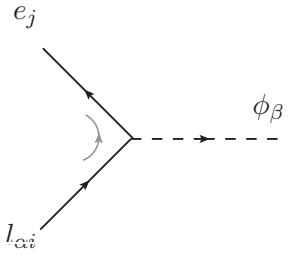

$$-i\,\mu^{\epsilon/2}\,(Y_e)_{ji}\,\delta_{\alpha\beta}P_L$$

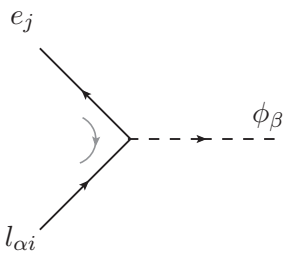

$$-i\,\mu^{\epsilon/2}\,(Y_e)_{ji}\,\delta_{\alpha\beta}P_L$$

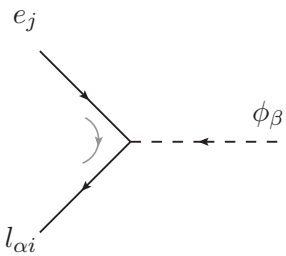

$$-i\,\mu^{\epsilon/2}\,(Y_e^*)_{ji}\,\delta_{\alpha\beta}P_R$$

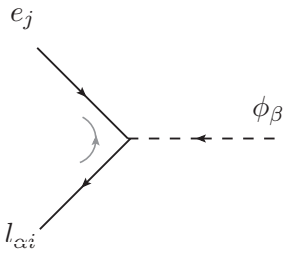

$$-i\,\mu^{\epsilon/2}\,(Y_e^*)_{ji}\,\delta_{\alpha\beta}P_R$$

dimension-5 effective vertex, $c^{(5)}$:

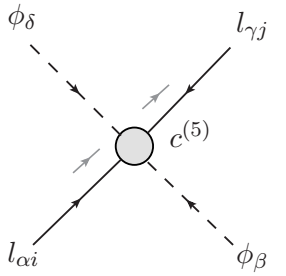

$$\tfrac{i}{2}\,\mu^{\epsilon}c_{ji}^{(5)}\,(\epsilon_{\gamma\delta}\epsilon_{\alpha\beta}+\epsilon_{\gamma\beta}\epsilon_{\alpha\delta})\,P_L$$

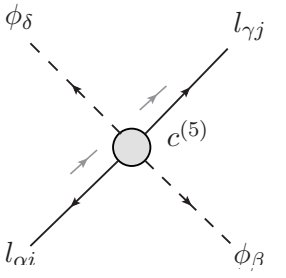

$$\tfrac{i}{2}\,\mu^{\epsilon}c_{ji}^{*(5)}\,(\epsilon_{\gamma\delta}\epsilon_{\alpha\beta}+\epsilon_{\gamma\beta}\epsilon_{\alpha\delta})\,P_R$$

dimension-6 effective vertex, $c^{(6)}$:

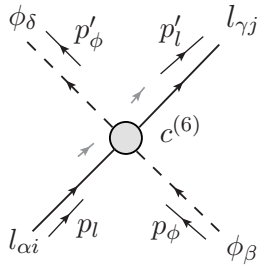

$$\tfrac{i}{2}\,\mu^\epsilon c^{(6)}_{ji}\epsilon_{\gamma\delta}\epsilon_{\alpha\beta}\left(\not{p}_l+\not{p}_\phi\right)P_L$$

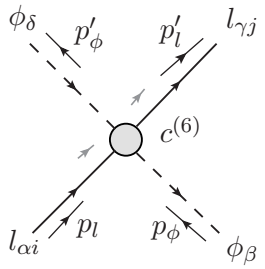

$$\tfrac{i}{2}\,\mu^\epsilon c^{(6)}_{ji}\epsilon_{\gamma\beta}\epsilon_{\alpha\delta}\left(\not{p}_l-\not{p}'_\phi\right)P_L$$

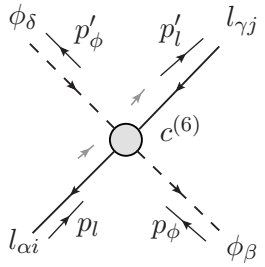

$$\tfrac{i}{2}\,\mu^\epsilon c^{*(6)}_{ji}\epsilon_{\gamma\delta}\epsilon_{\alpha\beta}\left(\not{p}_l+\not{p}_\phi\right)P_R$$

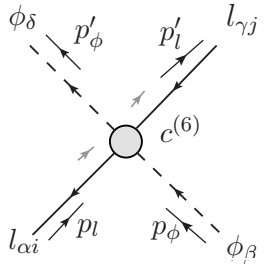

$$\tfrac{i}{2}\,\mu^\epsilon c^{*(6)}_{ji}\epsilon_{\gamma\beta}\epsilon_{\alpha\delta}\left(\not{p}_l-\not{p}'_\phi\right)P_R$$

counterterm of l_L and ϕ:

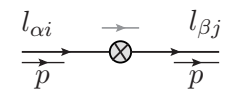

$$i\not{p}\,\left(\Delta Z_{l_L}\right)_{ij}P_L\,\delta_{\beta\alpha}$$

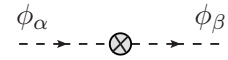

$$i\left(p^2\,\Delta Z_\phi-\Delta m^2\right)\delta_{\beta\alpha}$$

$c^{(6)}$ counterterm:

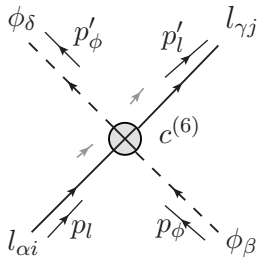

$$\tfrac{i}{2}\,\mu^\epsilon \Delta c^{(6)}_{ji} \epsilon_{\gamma\delta}\epsilon_{\alpha\beta} \left(\not{p}_l + \not{p}_\phi\right) P_L$$

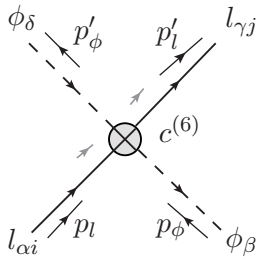

$$\tfrac{i}{2}\,\mu^\epsilon \Delta c^{(6)}_{ji} \epsilon_{\gamma\beta}\epsilon_{\alpha\delta} \left(\not{p}_l - \not{p}'_\phi\right) P_L$$

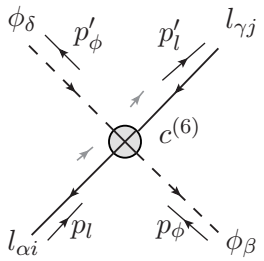

$$\tfrac{i}{2}\,\mu^\epsilon \Delta c^{*(6)}_{ji} \epsilon_{\gamma\delta}\epsilon_{\alpha\beta} \left(\not{p}_l + \not{p}_\phi\right) P_R$$

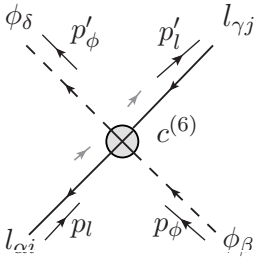

$$\tfrac{i}{2}\,\mu^\epsilon \Delta c^{*(6)}_{ji} \epsilon_{\gamma\beta}\epsilon_{\alpha\delta} \left(\not{p}_l - \not{p}'_\phi\right) P_R$$

Appendix D

Divergent part of loop integrals

In this appendix we note down some standard form of loop integrals due to Passarino and Veltman [241, 242]. The one loop amplitude of the $c^{(6)}$ vertex can be recasted into any of these forms. As for RGE, only UV divergent part is needed, we tabulate only the UV divergent part in Table D.1.

D.1 Integrals in d dimension

We define the integrals in $d = 4 - \epsilon$ dimension, where $\epsilon \to 0$. One-point function is given by

$$A_0\left(m^2\right) = \mu^\epsilon \int \frac{\mathrm{d}^d q}{(2\pi)^d} \frac{1}{q^2 - m^2} \tag{D.1.1}$$

The two point functions are given by

$$B_0\left(p^2, m_1^2, m_2^2\right) = \mu^\epsilon \int \frac{\mathrm{d}^d q}{(2\pi)^d} \frac{1}{\left[q^2 - m_1^2\right]\left[(q+p)^2 - m_2^2\right]} \tag{D.1.2}$$

$$B_\mu\left(p^2, m_1^2, m_2^2\right) = \mu^\epsilon \int \frac{\mathrm{d}^d q}{(2\pi)^d} \frac{q_\mu}{\left[q^2 - m_1^2\right]\left[(q+p)^2 - m_2^2\right]} \tag{D.1.3}$$

$$B_{\mu\nu}\left(p^2, m_1^2, m_2^2\right) = \mu^\epsilon \int \frac{\mathrm{d}^d q}{(2\pi)^d} \frac{q_\mu\, q_\nu}{\left[q^2 - m_1^2\right]\left[(q+p)^2 - m_2^2\right]} \tag{D.1.4}$$

B_μ and $B_{\mu\nu}$ can be expressed in terms of external momentum as

$$B_\mu\left(p^2, m_1^2, m_2^2\right) = p_\mu B_1\left(p^2, m_1^2, m_2^2\right) \tag{D.1.5}$$

$$B_{\mu\nu}\left(p^2, m_1^2, m_2^2\right) = g_{\mu\nu}\, B_{00}\left(p^2, m_1^2, m_2^2\right) + p_\mu\, p_\nu\, B_{11}\left(p^2, m_1^2, m_2^2\right) \tag{D.1.6}$$

B_{00} and B_{11} can be decomposed and expressed in terms of A_0 and B_0.

The three point functions are given by

$$C_0 = \mu^\epsilon \int \frac{\mathrm{d}^d q}{(2\pi)^d} \frac{1}{\left[q^2 - m_1^2\right]\left[(q+p)^2 - m_2^2\right]\left[(q+k)^2 - m_3^2\right]} \tag{D.1.7}$$

$$C_\mu = \mu^\epsilon \int \frac{\mathrm{d}^d q}{(2\pi)^d} \frac{q_\mu}{\left[q^2 - m_1^2\right]\left[(q+p)^2 - m_2^2\right]\left[(q+k)^2 - m_3^2\right]} \tag{D.1.8}$$

$$C_{\mu\nu} = \mu^\epsilon \int \frac{\mathrm{d}^d q}{(2\pi)^d} \frac{q_\mu\, q_\nu}{\left[q^2 - m_1^2\right]\left[(q+p)^2 - m_2^2\right]\left[(q+k)^2 - m_3^2\right]} \tag{D.1.9}$$

$$C_{\mu\nu\eta} = \mu^\epsilon \int \frac{\mathrm{d}^d q}{(2\pi)^d} \frac{q_\mu\, q_\nu\, q_\eta}{\left[q^2 - m_1^2\right]\left[(q+p)^2 - m_2^2\right]\left[(q+k)^2 - m_3^2\right]} \tag{D.1.10}$$

where the argument of C is read

$$C = C\left(p^2, (p-k)^2, k^2, m_1^2, m_2^2, m_3^2\right) \tag{D.1.11}$$

Similar to the two point functions, the tensorial form of the three point functions can be taken out with coefficients purely dependent on the squared momenta and masses.

$$C_\mu = p_\mu C_1 + k_\mu C_2 \tag{D.1.12}$$

$$C_{\mu\nu} = g_{\mu\nu}\, C_{00} + p_\mu\, p_\nu\, C_{11} + k_\mu\, k_\nu\, C_{22} + (\, p_\mu\, k_\nu + k_\mu\, p_\nu)\, C_{12} \tag{D.1.13}$$

$$\begin{aligned} C_{\mu\nu\eta} = {} & (g_{\mu\nu}\, p_\eta + g_{\nu\eta}\, p_\mu + g_{\eta\mu}\, p_\nu)\, C_{001} + (g_{\mu\nu}\, k_\eta + g_{\nu\eta}\, k_\mu + g_{\eta\mu}\, k_\nu)\, C_{002} \\ & + p_\mu\, p_\nu\, p_\eta\, C_{111} + k_\mu\, k_\nu\, k_\eta\, C_{222} + (\, p_\mu\, p_\nu\, k_\eta + p_\mu\, k_\nu\, p_\eta \\ & + k_\mu\, p_\nu\, p_\eta)\, C_{112} + (k_\mu\, k_\nu\, p_\eta + k_\mu\, p_\nu\, k_\eta + p_\mu\, k_\nu\, k_\eta)\, C_{122} \end{aligned} \tag{D.1.14}$$

Again non-tensorial coefficients can be further decomposed in forms of A_0 , B_0 and C_0 .

Four-point functions can be written down in a similar manner. We do not give those as it is not necessary for the calculation of Chapter 4. Below we give the divergent part of the functions mentioned above

Functions	Divergent part
A_0	$\frac{i}{16\pi^2}\, m^2\, \frac{2}{\epsilon}$
B_0	$\frac{i}{16\pi^2}\, \frac{2}{\epsilon}$
B_1	$-\frac{i}{16\pi^2}\, \frac{1}{\epsilon}$
B_{00}	$-\frac{i}{16\pi^2}\, (p^2 - 3\, m_1^2 - 3\, m_2^2)\, \frac{1}{6\,\epsilon}$
B_{11}	$\frac{i}{16\pi^2}\, \frac{2}{3\,\epsilon}$
C_{00}	$\frac{i}{16\pi^2}\, \frac{1}{2\,\epsilon}$
$C_{001}\,, C_{002}$	$-\frac{i}{16\pi^2}\, \frac{1}{6\,\epsilon}$

Table D.1: *Divergent part of Passarino Veltman functions.*

D.2 UV divergence of the self-energy digrams

Here we give the divergent part of different self-energy diagrams

Self energy diagrams of l_L, Fig. 4.2:

$$\text{(I)} \qquad \frac{i}{16\pi^2}\left(Y_\nu Y_\nu^\dagger\right)_{ji}\delta_{\gamma\alpha}\,\not{p}\,P_L\,\frac{1}{\epsilon} \;+\; \text{UV finite} \tag{D.2.1}$$

$$\text{(II)} \qquad \frac{i}{16\pi^2}\left(Y_e Y_e^\dagger\right)_{ji}\delta_{\gamma\alpha}\,\not{p}\,P_L\,\frac{1}{\epsilon} \;+\; \text{UV finite} \tag{D.2.2}$$

$$\text{(III)} \qquad \frac{i}{16\pi^2}\,\frac{g_1^2}{2}\,\delta_{ji}\,\delta_{\gamma\alpha}\,\xi_B\,\not{p}\,P_L\frac{1}{-\epsilon} \;+\; \text{UV finite} \tag{D.2.3}$$

$$\text{(IV)} \qquad \frac{i}{16\pi^2}\,\frac{3}{2}\,g_2^2\,\delta_{ji}\,\delta_{\gamma\alpha}\,\xi_W\,\not{p}\,P_L\,\frac{1}{\epsilon} \;+\; \text{UV finite} \tag{D.2.4}$$

Self energy diagrams of ϕ, Fig. 4.3:

$$\text{(I)} \qquad \frac{i}{16\pi^2}\, 3\,\lambda\, m^2\, \delta_{\beta\alpha}\, \frac{1}{\epsilon} \;+\; \text{UV finite} \tag{D.2.5}$$

$$\text{(II)} \qquad \frac{i}{16\pi^2}\, \frac{g_1^2}{2}\, \delta_{\beta\alpha}\, \left[(-3+\xi_B)\, p^2 - \xi_B\, m^2\right] \frac{1}{\epsilon} \;+\; \text{UV finite} \tag{D.2.6}$$

$$\text{(III)} \qquad \frac{i}{16\pi^2}\, \frac{3}{2}\, g_2^2\, \delta_{\beta\alpha}\, \left[(-3+\xi_W)\, p^2 - \xi_W\, m^2\right] \frac{1}{\epsilon} \;+\; \text{UV finite} \tag{D.2.7}$$

$$\text{(V)} \qquad \frac{i}{16\pi^2}\, 2\, (Y_\nu)_{jk}\, \left(Y_\nu^\dagger\right)_{ki}\, \delta_{\beta\alpha}\, \left[p^2 - 2M_k^2\right] \frac{1}{\epsilon} \;+\; \text{UV finite} \tag{D.2.8}$$

$$\text{(VI)} \qquad \frac{i}{16\pi^2}\, 2\, \mathrm{Tr}\left(Y_e Y_e^\dagger\right)\, \delta_{\beta\alpha}\, p^2\, \frac{1}{\epsilon} \;+\; \text{UV finite} \tag{D.2.9}$$

$$\text{(VII)} \qquad \frac{i}{16\pi^2}\, 6\, \mathrm{Tr}\left(Y_u Y_u^\dagger\right)\, \delta_{\beta\alpha}\, p^2\, \frac{1}{\epsilon} \;+\; \text{UV finite} \tag{D.2.10}$$

$$\text{(VIII)} \qquad \frac{i}{16\pi^2}\, 6\, \mathrm{Tr}\left(Y_d Y_d^\dagger\right)\, \delta_{\beta\alpha}\, p^2\, \frac{1}{\epsilon} \;+\; \text{UV finite} \tag{D.2.11}$$

Bibliography

[1] T. Lee and C.-N. Yang, Phys.Rev. **104**, 254 (1956)

[2] C. Wu, E. Ambler, R. Hayward, D. Hoppes, and R. Hudson, Phys.Rev. **105**, 1413 (1957)

[3] M. Goldhaber, L. Grodzins, and A. Sunyar, Phys.Rev. **109**, 1015 (1958)

[4] J. Beringer *et al.* (Particle Data Group), Phys.Rev. **D86**, 010001 (2012)

[5] S. Chatrchyan *et al.* (CMS Collaboration), Phys.Lett. **B716**, 30 (2012), arXiv:1207.7235 [hep-ex]

[6] G. Aad *et al.* (ATLAS Collaboration), Phys.Lett. **B716**, 1 (2012), arXiv:1207.7214 [hep-ex]

[7] H. Georgi and S. Glashow, Phys.Rev.Lett. **32**, 438 (1974)

[8] H. Georgi, AIP Conf.Proc. **23**, 575 (1975)

[9] R. Mohapatra and J. Valle, Phys.Rev. **D34**, 1642 (1986)

[10] P. Langacker, Phys.Rept. **72**, 185 (1981)

[11] P. Langacker and M.-x. Luo, Phys.Rev. **D44**, 817 (1991)

[12] G. Senjanovic(2006), arXiv:hep-ph/0612312 [hep-ph]

[13] L. Susskind, Phys.Rev. **D20**, 2619 (1979)

[14] S. Dimopoulos and H. Georgi, Nucl.Phys. **B193**, 150 (1981)

[15] R. K. Kaul and P. Majumdar, Nucl.Phys. **B199**, 36 (1982)

[16] M. Drees, R. Godbole, and P. Roy, *Theory and phenomenology of sparticles: An account of four-dimensional N=1 supersymmetry in high energy physics* (World Scientific Publishing Co. Pte. Ltd., 2004)

[17] M. Drees(1996), arXiv:hep-ph/9611409 [hep-ph]

[18] S. Dimopoulos, S. Raby, and F. Wilczek, Phys.Rev. **D24**, 1681 (1981)

[19] V. D. Barger, M. Berger, and P. Ohmann, Phys.Rev. **D47**, 1093 (1993), arXiv:hep-ph/9209232 [hep-ph]

[20] N. Arkani-Hamed, S. Dimopoulos, and G. Dvali, Phys.Lett. **B429**, 263 (1998), arXiv:hep-ph/9803315 [hep-ph]

[21] L. Randall and R. Sundrum, Phys.Rev.Lett. **83**, 3370 (1999), arXiv:hep-ph/9905221 [hep-ph]

[22] Y. Fukuda *et al.* (Super-Kamiokande Collaboration), Phys.Rev.Lett. **81**, 1562 (1998), arXiv:hep-ex/9807003 [hep-ex]

[23] K. Eguchi *et al.* (KamLAND Collaboration), Phys.Rev.Lett. **90**, 021802 (2003), arXiv:hep-ex/0212021 [hep-ex]

[24] Q. Ahmad *et al.* (SNO Collaboration), Phys.Rev.Lett. **89**, 011301 (2002), arXiv:nucl-ex/0204008 [nucl-ex]

[25] Y. Ashie *et al.* (Super-Kamiokande Collaboration), Phys.Rev.Lett. **93**, 101801 (2004), arXiv:hep-ex/0404034 [hep-ex]

[26] D. Spergel *et al.* (WMAP Collaboration), Astrophys.J.Suppl. **170**, 377 (2007), arXiv:astro-ph/0603449 [astro-ph]

[27] M. Gavela, P. Hernandez, J. Orloff, and O. Pene, Mod.Phys.Lett. **A9**, 795 (1994), arXiv:hep-ph/9312215 [hep-ph]

[28] P. Huet and E. Sather, Phys.Rev. **D51**, 379 (1995), arXiv:hep-ph/9404302 [hep-ph]

[29] S. Abe *et al.* (KamLAND Collaboration), Phys.Rev.Lett. **100**, 221803 (2008), arXiv:0801.4589 [hep-ex]

[30] Y. Ashie *et al.* (Super-Kamiokande Collaboration), Phys.Rev. **D71**, 112005 (2005), arXiv:hep-ex/0501064 [hep-ex]

[31] K. Abe *et al.* (Super-Kamiokande Collaboration), Phys.Rev. **D83**, 052010 (2011), arXiv:1010.0118 [hep-ex]

[32] B. Aharmim *et al.* (SNO Collaboration)(2011), arXiv:1109.0763 [nucl-ex]

[33] P. Adamson *et al.* (MINOS Collaboration), Phys.Rev.Lett. **101**, 131802 (2008), arXiv:0806.2237 [hep-ex]

[34] K. Abe *et al.* (T2K Collaboration), Phys.Rev. **D85**, 031103 (2012), arXiv:1201.1386 [hep-ex]

[35] M. Gonzalez-Garcia and M. Maltoni, Phys.Rept. **460**, 1 (2008), arXiv:0704.1800 [hep-ph]

[36] D. Forero, M. Tortola, and J. Valle, Phys.Rev. **D86**, 073012 (2012), arXiv:1205.4018 [hep-ph]

[37] S. Choubey, A. Bandyopadhyay, S. Goswami, and D. Roy, 291(2002), arXiv:hep-ph/0209222 [hep-ph]

[38] S. Hannestad, Phys.Rev.Lett. **95**, 221301 (2005), arXiv:astro-ph/0505551 [astro-ph]

[39] S. Hannestad, Prog.Part.Nucl.Phys. **65**, 185 (2010), arXiv:1007.0658 [hep-ph]

[40] E. Komatsu *et al.* (WMAP Collaboration), Astrophys.J.Suppl. **180**, 330 (2009), arXiv:0803.0547 [astro-ph]

[41] S. A. Thomas, F. B. Abdalla, and O. Lahav, Phys.Rev.Lett. **105**, 031301 (2010), arXiv:0911.5291 [astro-ph.CO]

[42] S. Joudaki(2012), arXiv:1202.0005 [astro-ph.CO]

[43] S. Weinberg, Phys.Rev.Lett. **43**, 1566 (1979)

[44] S. Weinberg, Phys.Rev. **D22**, 1694 (1980)

[45] P. Minkowski, Phys.Lett. **B67**, 421 (1977)

[46] R. N. Mohapatra and G. Senjanovic, Phys.Rev.Lett. **44**, 912 (1980)

[47] B. Grzadkowski, M. Iskrzynski, M. Misiak, and J. Rosiek, JHEP **1010**, 085 (2010), arXiv:1008.4884 [hep-ph]

[48] W. Buchmuller and D. Wyler, Nucl.Phys. **B268**, 621 (1986)

[49] A. Broncano, M. Gavela, and E. E. Jenkins, Phys.Lett. **B552**, 177 (2003), arXiv:hep-ph/0210271 [hep-ph]

[50] A. Abada, C. Biggio, F. Bonnet, M. Gavela, and T. Hambye, JHEP **0712**, 061 (2007), arXiv:0707.4058 [hep-ph]

[51] W. Furry, Phys.Rev. **56**, 1184 (1939)

[52] S. Pascoli and S. Petcov, Phys.Rev. **D77**, 113003 (2008), arXiv:0711.4993 [hep-ph]

[53] A. Ibarra, E. Molinaro, and S. Petcov, Phys.Rev. **D84**, 013005 (2011), arXiv:1103.6217 [hep-ph]

[54] M. Mitra, G. Senjanovic, and F. Vissani, Nucl.Phys. **B856**, 26 (2012), arXiv:1108.0004 [hep-ph]

[55] J. Chakrabortty, H. Z. Devi, S. Goswami, and S. Patra, JHEP **1208**, 008 (2012), arXiv:1204.2527 [hep-ph]

[56] L. Covi, E. Roulet, and F. Vissani, Phys.Lett. **B384**, 169 (1996), arXiv:hep-ph/9605319 [hep-ph]

[57] J. A. Harvey and M. S. Turner, Phys.Rev. **D42**, 3344 (1990)

[58] F. R. Klinkhamer and N. Manton, Phys.Rev. **D30**, 2212 (1984)

[59] M. Fukugita and T. Yanagida, Phys.Lett. **B174**, 45 (1986)

[60] P. B. Arnold and L. D. McLerran, Phys.Rev. **D36**, 581 (1987)

[61] M. Luty, Phys.Rev. **D45**, 455 (1992)

[62] T. Cheng and L.-F. Li, Phys.Rev.Lett. **38**, 381 (1977)

[63] F. Wilczek and A. Zee, Phys.Rev.Lett. **38**, 531 (1977)

[64] B. Lee, S. Pakvasa, R. Shrock, and H. Sugawara, Phys.Rev.Lett. **38**, 937 (1977)

[65] T. Cheng and L. Li, *GAUGE THEORY OF ELEMENTARY PARTICLE PHYSICS* (CLARENDON PRESS · OXFORD, 1985)

[66] E. Ma and A. Pramudita, Phys.Rev. **D24**, 1410 (1981)

[67] P. Langacker and D. London, Phys.Rev. **D38**, 907 (1988)

[68] D. Tommasini, G. Barenboim, J. Bernabeu, and C. Jarlskog, Nucl.Phys. **B444**, 451 (1995), arXiv:hep-ph/9503228 [hep-ph]

[69] S. Davidson and A. Ibarra, JHEP **0109**, 013 (2001), arXiv:hep-ph/0104076 [hep-ph]

[70] J. R. Ellis and M. Raidal, Nucl.Phys. **B643**, 229 (2002), arXiv:hep-ph/0206174 [hep-ph]

[71] S. Pascoli, S. Petcov, and W. Rodejohann, Phys.Rev. **D68**, 093007 (2003), arXiv:hep-ph/0302054 [hep-ph]

[72] J. Casas and A. Ibarra, Nucl.Phys. **B618**, 171 (2001), arXiv:hep-ph/0103065 [hep-ph]

[73] H. Fritzsch, Phys.Lett. **B73**, 317 (1978)

[74] R. Adhikari and A. Raychaudhuri, Phys.Rev. **D84**, 033002 (2011), arXiv:1004.5111 [hep-ph]

[75] J. Kersten and A. Y. Smirnov, Phys.Rev. **D76**, 073005 (2007), arXiv:0705.3221 [hep-ph]

[76] A. Pilaftsis, Z.Phys. **C55**, 275 (1992), arXiv:hep-ph/9901206 [hep-ph]

[77] F. Deppisch and J. Valle, Phys.Rev. **D72**, 036001 (2005), arXiv:hep-ph/0406040 [hep-ph]

[78] P. Bandyopadhyay, E. J. Chun, H. Okada, and J.-C. Park(2012), arXiv:1209.4803 [hep-ph]

[79] P. Bhupal Dev, R. Franceschini, and R. Mohapatra, Phys.Rev. **D86**, 093010 (2012), arXiv:1207.2756 [hep-ph]

[80] A. Das and N. Okada(2012), arXiv:1207.3734 [hep-ph]

[81] M. Hirsch, S. Morisi, and J. Valle, Phys.Lett. **B679**, 454 (2009), arXiv:0905.3056 [hep-ph]

[82] H. Zhang and S. Zhou, Phys.Lett. **B685**, 297 (2010), arXiv:0912.2661 [hep-ph]

[83] P.-H. Gu and U. Sarkar, Phys.Lett. **B694**, 226 (2010), arXiv:1007.2323 [hep-ph]

[84] S. King, Phys.Lett. **B439**, 350 (1998), arXiv:hep-ph/9806440 [hep-ph]

[85] M. Raidal and A. Strumia, Phys.Lett. **B553**, 72 (2003), arXiv:hep-ph/0210021 [hep-ph]

[86] R. Barbieri, T. Hambye, and A. Romanino, JHEP **0303**, 017 (2003), arXiv:hep-ph/0302118 [hep-ph]

[87] A. Ibarra and G. G. Ross, Phys.Lett. **B591**, 285 (2004), arXiv:hep-ph/0312138 [hep-ph]

[88] J. Casas, V. Di Clemente, A. Ibarra, and M. Quiros, Phys.Rev. **D62**, 053005 (2000), arXiv:hep-ph/9904295 [hep-ph]

[89] I. Gogoladze, N. Okada, and Q. Shafi, Phys.Lett. **B668**, 121 (2008), arXiv:0805.2129 [hep-ph]

[90] M. Shaposhnikov and C. Wetterich, Phys.Lett. **B683**, 196 (2010), arXiv:0912.0208 [hep-th]

[91] M. Holthausen, K. S. Lim, and M. Lindner, JHEP **1202**, 037 (2012), arXiv:1112.2415 [hep-ph]

[92] N. Cabibbo, L. Maiani, G. Parisi, and R. Petronzio, Nucl.Phys. **B158**, 295 (1979)

[93] C. Ford, D. Jones, P. Stephenson, and M. Einhorn, Nucl.Phys. **B395**, 17 (1993), arXiv:hep-lat/9210033 [hep-lat]

[94] W. Rodejohann and H. Zhang, JHEP **1206**, 022 (2012), arXiv:1203.3825 [hep-ph]

[95] J. Chakrabortty, M. Das, and S. Mohanty(2012), arXiv:1207.2027 [hep--ph]

[96] S. Antusch, C. Biggio, E. Fernandez-Martinez, M. Gavela, and J. Lopez-Pavon, JHEP **0610**, 084 (2006), arXiv:hep-ph/0607020 [hep-ph]

[97] P. H. Chankowski and Z. Pluciennik, Phys.Lett. **B316**, 312 (1993), arXiv:hep-ph/9306333 [hep-ph]

[98] P. H. Chankowski and S. Pokorski, Int.J.Mod.Phys. **A17**, 575 (2002), arXiv:hep-ph/0110249 [hep-ph]

[99] K. Babu, C. N. Leung, and J. T. Pantaleone, Phys.Lett. **B319**, 191 (1993), arXiv:hep-ph/9309223 [hep-ph]

[100] J. R. Ellis and S. Lola, Phys.Lett. **B458**, 310 (1999), arXiv:hep-ph/9904279 [hep-ph]

[101] S. Antusch, M. Drees, J. Kersten, M. Lindner, and M. Ratz, Phys.Lett. **B519**, 238 (2001), arXiv:hep-ph/0108005 [hep-ph]

[102] M. S. Carena, J. R. Ellis, S. Lola, and C. Wagner, Eur.Phys.J. **C12**, 507 (2000), arXiv:hep-ph/9906362 [hep-ph]

[103] S. Antusch, J. Kersten, M. Lindner, and M. Ratz, Nucl.Phys. **B674**, 401 (2003), arXiv:hep-ph/0305273 [hep-ph]

[104] S. Antusch, M. Drees, J. Kersten, M. Lindner, and M. Ratz, Phys.Lett. **B525**, 130 (2002), arXiv:hep-ph/0110366 [hep-ph]

[105] M. A. Schmidt, Phys.Rev. **D76**, 073010 (2007), arXiv:0705.3841 [hep-ph]

[106] A. Dighe, S. Goswami, and W. Rodejohann, Phys.Rev. **D75**, 073023 (2007), arXiv:hep-ph/0612328 [hep-ph]

[107] A. Dighe, S. Goswami, and P. Roy, Phys.Rev. **D76**, 096005 (2007), arXiv:0704.3735 [hep-ph]

[108] A. Dighe, S. Goswami, and S. Ray, Phys.Rev. **D79**, 076006 (2009), arXiv:0810.5680 [hep-ph]

[109] S. Goswami, S. T. Petcov, S. Ray, and W. Rodejohann, Phys.Rev. **D80**, 053013 (2009), arXiv:0907.2869 [hep-ph]

[110] J. Chakrabortty, A. Dighe, S. Goswami, and S. Ray, Nucl.Phys. **B820**, 116 (2009), arXiv:0812.2776 [hep-ph]

[111] S. Antusch, S. Blanchet, M. Blennow, and E. Fernandez-Martinez, JHEP **1001**, 017 (2010), arXiv:0910.5957 [hep-ph]

[112] W. Rodejohann, Europhys.Lett. **88**, 51001 (2009), arXiv:0903.4590 [hep-ph]

[113] M. Magg and C. Wetterich, Phys.Lett. **B94**, 61 (1980)

[114] G. Lazarides, Q. Shafi, and C. Wetterich, Nucl.Phys. **B181**, 287 (1981)

[115] R. N. Mohapatra and G. Senjanovic, Phys.Rev. **D23**, 165 (1981)

[116] J. Schechter and J. Valle, Phys.Rev. **D22**, 2227 (1980)

[117] J. Schechter and J. Valle, Phys.Rev. **D25**, 774 (1982)

[118] R. Foot, H. Lew, X. He, and G. C. Joshi, Z.Phys. **C44**, 441 (1989)

[119] E. Ma and D. Roy, Nucl.Phys. **B644**, 290 (2002), arXiv:hep-ph/0206150 [hep-ph]

[120] B. Bajc and G. Senjanovic, JHEP **0708**, 014 (2007), arXiv:hep-ph/0612029 [hep-ph]

[121] W. Grimus and L. Lavoura, JHEP **0011**, 042 (2000), arXiv:hep-ph/0008179 [hep-ph]

[122] S. Pascoli, S. Petcov, and C. Yaguna, Phys.Lett. **B564**, 241 (2003), arXiv:hep-ph/0301095 [hep-ph]

[123] E. J. Chun and S. K. Kang, Phys.Rev. **D63**, 097902 (2001), arXiv:hep-ph/0001296 [hep-ph]

[124] T. Hambye and G. Senjanovic, Phys.Lett. **B582**, 73 (2004), arXiv:hep-ph/0307237 [hep-ph]

[125] E. Ma and U. Sarkar, Phys.Rev.Lett. **80**, 5716 (1998), arXiv:hep-ph/9802445 [hep-ph]

[126] E. Witten, Phys.Lett. **B91**, 81 (1980)

[127] J. Chakrabortty, S. Goswami, and A. Raychaudhuri, Phys.Lett. **B698**, 265 (2011), arXiv:1012.2715 [hep-ph]

[128] M. Malinsky, T. Ohlsson, Z.-z. Xing, and H. Zhang, Phys.Lett. **B679**, 242 (2009), arXiv:0905.2889 [hep-ph]

[129] L.-J. Hu, S. Dulat, and A. Ablat, Eur.Phys.J. **C71**, 1772 (2011)

[130] S. K. Kang and C. Kim, Phys.Lett. **B646**, 248 (2007), arXiv:hep-ph/0607072 [hep-ph]

[131] F. Bazzocchi, Phys.Rev. **D83**, 093009 (2011), arXiv:1011.6299 [hep-ph]

[132] P. B. Dev and A. Pilaftsis, Phys.Rev. **D86**, 113001 (2012), arXiv:1209.4051 [hep-ph]

[133] M. Gavela, T. Hambye, D. Hernandez, and P. Hernandez, JHEP **0909**, 038 (2009), arXiv:0906.1461 [hep-ph]

[134] C. Jarlskog, Phys.Rev.Lett. **55**, 1039 (1985)

[135] H. Nunokawa, S. J. Parke, and J. W. Valle, Prog.Part.Nucl.Phys. **60**, 338 (2008), arXiv:0710.0554 [hep-ph]

[136] J. Bernabeu, G. Branco, and M. Gronau, Phys.Lett. **B169**, 243 (1986)

[137] G. C. Branco, T. Morozumi, B. Nobre, and M. Rebelo, Nucl.Phys. **B617**, 475 (2001), arXiv:hep-ph/0107164 [hep-ph]

[138] G. C. Branco, M. Rebelo, and J. Silva-Marcos, Phys.Lett. **B633**, 345 (2006), arXiv:hep-ph/0510412 [hep-ph]

[139] M. Bando, S. Kaneko, M. Obara, and M. Tanimoto(2004), arXiv:hep-ph/0405071 [hep-ph]

[140] H. B. Nielsen and Y. Takanishi, Phys.Lett. **B507**, 241 (2001), arXiv:hep-ph/0101307 [hep-ph]

[141] F. Borzumati and A. Masiero, Phys.Rev.Lett. **57**, 961 (1986)

[142] J. Hisano, T. Moroi, K. Tobe, M. Yamaguchi, and T. Yanagida, Phys.Lett. **B357**, 579 (1995), arXiv:hep-ph/9501407 [hep-ph]

[143] J. Hisano, T. Moroi, K. Tobe, and M. Yamaguchi, Phys.Rev. **D53**, 2442 (1996), arXiv:hep-ph/9510309 [hep-ph]

[144] J. Adam *et al.* (MEG collaboration), Phys.Rev.Lett. **107**, 171801 (2011), arXiv:1107.5547 [hep-ex]

[145] V. Tello, M. Nemevsek, F. Nesti, G. Senjanovic, and F. Vissani, Phys.Rev.Lett. **106**, 151801 (2011), arXiv:1011.3522 [hep-ph]

[146] M. Einhorn and D. Jones, Phys.Rev. **D46**, 5206 (1992)

[147] M.-x. Luo and Y. Xiao, Phys.Rev.Lett. **90**, 011601 (2003), arXiv:hep-ph/0207271 [hep-ph]

[148] M. E. Machacek and M. T. Vaughn, Nucl.Phys. **B222**, 83 (1983)

[149] M. E. Machacek and M. T. Vaughn, Nucl.Phys. **B236**, 221 (1984)

[150] M. E. Machacek and M. T. Vaughn, Nucl.Phys. **B249**, 70 (1985)

[151] J. Casas, J. Espinosa, and M. Quiros, Phys.Lett. **B342**, 171 (1995), arXiv:hep-ph/9409458 [hep-ph]

[152] J. Casas, J. Espinosa, and M. Quiros, Phys.Lett. **B382**, 374 (1996), arXiv:hep-ph/9603227 [hep-ph]

[153] (2011), arXiv:1107.5255 [hep-ex]

[154] S. Bethke, Eur.Phys.J. **C64**, 689 (2009), arXiv:0908.1135 [hep-ph]

[155] K. Melnikov and T. v. Ritbergen, Phys.Lett. **B482**, 99 (2000), arXiv:hep-ph/9912391 [hep-ph]

[156] R. Hempfling and B. A. Kniehl, Phys.Rev. **D51**, 1386 (1995), arXiv:hep-ph/9408313 [hep-ph]

[157] A. Sirlin and R. Zucchini, Nucl.Phys. **B266**, 389 (1986)

[158] S. Antusch, J. Kersten, M. Lindner, and M. Ratz, Phys.Lett. **B538**, 87 (2002), arXiv:hep-ph/0203233 [hep-ph]

[159] G. Bhattacharyya, A. Raychaudhuri, and A. Sil, Phys.Rev. **D67**, 073004 (2003), arXiv:hep-ph/0211074 [hep-ph]

[160] P. H. Frampton, S. L. Glashow, and D. Marfatia, Phys.Lett. **B536**, 79 (2002), arXiv:hep-ph/0201008 [hep-ph]

[161] A. Kageyama, S. Kaneko, N. Shimoyama, and M. Tanimoto, Phys.Lett. **B538**, 96 (2002), arXiv:hep-ph/0204291 [hep-ph]

[162] Z.-z. Xing, Phys.Lett. **B530**, 159 (2002), arXiv:hep-ph/0201151 [hep-ph]

[163] Z.-z. Xing, Phys.Lett. **B539**, 85 (2002), arXiv:hep-ph/0205032 [hep-ph]

[164] B. R. Desai, D. Roy, and A. R. Vaucher, Mod.Phys.Lett. **A18**, 1355 (2003), arXiv:hep-ph/0209035 [hep-ph]

[165] C. Hagedorn, J. Kersten, and M. Lindner, Phys.Lett. **B597**, 63 (2004), arXiv:hep-ph/0406103 [hep-ph]

[166] S. Dev, S. Kumar, S. Verma, and S. Gupta, Phys.Rev. **D76**, 013002 (2007), arXiv:hep-ph/0612102 [hep-ph]

[167] S. Dev, S. Kumar, S. Verma, and S. Gupta, Phys.Lett. **B656**, 79 (2007), arXiv:0708.3321 [hep-ph]

[168] A. Dighe and N. Sahu(2009), arXiv:0812.0695 [hep-ph]

[169] H. Fritzsch, Z.-z. Xing, and S. Zhou, JHEP **1109**, 083 (2011), arXiv:1108.4534 [hep-ph]

[170] P. Ludl, S. Morisi, and E. Peinado, Nucl.Phys. **B857**, 411 (2012), arXiv:1109.3393 [hep-ph]

[171] Y.-L. Zhou, Phys.Rev. **D86**, 093011 (2012), arXiv:1205.2303 [hep-ph]

[172] D. Meloni and G. Blankenburg(2012), arXiv:1204.2706 [hep-ph]

[173] W. Grimus and P. Ludl(2012), arXiv:1208.4515 [hep-ph]

[174] A. Merle and W. Rodejohann, Phys.Rev. **D73**, 073012 (2006), arXiv:hep-ph/0603111 [hep-ph]

[175] E. Lashin and N. Chamoun, Phys.Rev. **D85**, 113011 (2012), arXiv:1108.4010 [hep-ph]

[176] K. Deepthi, S. Gollu, and R. Mohanta, Eur.Phys.J. **C72**, 1888 (2012), arXiv:1111.2781 [hep-ph]

[177] Z.-z. Xing and H. Zhang, Phys.Lett. **B569**, 30 (2003), arXiv:hep-ph/0304234 [hep-ph]

[178] Z.-z. Xing, Int.J.Mod.Phys. **A19**, 1 (2004), arXiv:hep-ph/0307359 [hep--ph]

[179] S. Zhou and Z.-z. Xing, Eur.Phys.J. **C38**, 495 (2005), arXiv:hep-ph/0404188 [hep-ph]

[180] Z.-z. Xing and S. Zhou, Phys.Lett. **B593**, 156 (2004), arXiv:hep-ph/0403261 [hep-ph]

[181] M. Randhawa, G. Ahuja, and M. Gupta, Phys.Lett. **B643**, 175 (2006), arXiv:hep-ph/0607074 [hep-ph]

[182] P. Ferreira and L. Lavoura, Mod.Phys.Lett. **A27**, 1250159 (2012), arXiv:1202.4024 [hep-ph]

[183] G. Leontaris, S. Lola, C. Scheich, and J. Vergados, Phys.Rev. **D53**, 6381 (1996), arXiv:hep-ph/9509351 [hep-ph]

[184] S. M. Barr and I. Dorsner, Nucl.Phys. **B585**, 79 (2000), arXiv:hep-ph/0003058 [hep-ph]

[185] P. Frampton, S. Glashow, and T. Yanagida, Phys.Lett. **B548**, 119 (2002), arXiv:hep-ph/0208157 [hep-ph]

[186] S. Chang, S. K. Kang, and K. Siyeon, Phys.Lett. **B597**, 78 (2004), arXiv:hep-ph/0404187 [hep-ph]

[187] A. Watanabe and K. Yoshioka, JHEP **0605**, 044 (2006), arXiv:hep-ph/0601152 [hep-ph]

[188] W.-l. Guo, Z.-z. Xing, and S. Zhou, Int.J.Mod.Phys. **E16**, 1 (2007), arXiv:hep-ph/0612033 [hep-ph]

[189] S. Goswami and A. Watanabe, Phys.Rev. **D79**, 033004 (2009), arXiv:0807.3438 [hep-ph]

[190] G. C. Branco, D. Emmanuel-Costa, M. Rebelo, and P. Roy, Phys.Rev. **D77**, 053011 (2008), arXiv:0712.0774 [hep-ph]

[191] S. Choubey, W. Rodejohann, and P. Roy, Nucl.Phys. **B808**, 272 (2009), arXiv:0807.4289 [hep-ph]

[192] R. Kuchimanchi and R. Mohapatra, Phys.Rev. **D66**, 051301 (2002), arXiv:hep-ph/0207110 [hep-ph]

[193] T. Endoh, S. Kaneko, S. Kang, T. Morozumi, and M. Tanimoto, Phys.Rev.Lett. **89**, 231601 (2002), arXiv:hep-ph/0209020 [hep-ph]

[194] S. King, Phys.Rev. **D67**, 113010 (2003), arXiv:hep-ph/0211228 [hep-ph]

[195] M. Frigerio and A. Y. Smirnov, Nucl.Phys. **B640**, 233 (2002), arXiv:hep-ph/0202247 [hep-ph]

[196] S. Kaneko, H. Sawanaka, and M. Tanimoto, JHEP **0508**, 073 (2005), arXiv:hep-ph/0504074 [hep-ph]

[197] C. Hagedorn and W. Rodejohann, JHEP **0507**, 034 (2005), arXiv:hep-ph/0503143 [hep-ph]

[198] G. Fogli, E. Lisi, A. Marrone, D. Montanino, A. Palazzo, *et al.*, Phys.Rev. **D86**, 013012 (2012), arXiv:1205.5254 [hep-ph]

[199] S. Goswami, S. Khan, and W. Rodejohann, Phys.Lett. **B680**, 255 (2009), arXiv:0905.2739 [hep-ph]

[200] F. An *et al.* (DAYA-BAY Collaboration), Phys.Rev.Lett. **108**, 171803 (2012), arXiv:1203.1669 [hep-ex]

[201] J. Ahn *et al.* (RENO collaboration), Phys.Rev.Lett. **108**, 191802 (2012), arXiv:1204.0626 [hep-ex]

[202] Y. Abe *et al.* (Double Chooz Collaboration), Phys.Rev. **D86**, 052008 (2012), arXiv:1207.6632 [hep-ex]

[203] G. Fogli, E. Lisi, A. Marrone, A. Palazzo, and A. Rotunno, Phys.Rev. **D84**, 053007 (2011), arXiv:1106.6028 [hep-ph]

[204] S. Goswami and W. Rodejohann, JHEP **0710**, 073 (2007), arXiv:0706.1462 [hep-ph]

[205] A. Osipowicz *et al.* (KATRIN Collaboration)(2001), arXiv:hep-ex/0109033 [hep-ex]

[206] F. Frankle (KATRIN Collaboration), PoS **EPS-HEP2009**, 271 (2009)

[207] S. Antusch, J. Kersten, M. Lindner, M. Ratz, and M. A. Schmidt, JHEP **0503**, 024 (2005), arXiv:hep-ph/0501272 [hep-ph]

[208] A. Dighe, S. Goswami, and P. Roy, Phys.Rev. **D73**, 071301 (2006), arXiv:hep-ph/0602062 [hep-ph]

[209] R. Barbieri, P. Creminelli, A. Strumia, and N. Tetradis, Nucl.Phys. **B575**, 61 (2000), arXiv:hep-ph/9911315 [hep-ph]

[210] A. Abada, S. Davidson, F.-X. Josse-Michaux, M. Losada, and A. Riotto, JCAP **0604**, 004 (2006), arXiv:hep-ph/0601083 [hep-ph]

[211] E. Nardi, Y. Nir, E. Roulet, and J. Racker, JHEP **0601**, 164 (2006), arXiv:hep-ph/0601084 [hep-ph]

[212] S. Khan, S. Goswami, and S. Roy(2012), arXiv:1212.3694 [hep-ph]

[213] D. Dinh, A. Ibarra, E. Molinaro, and S. Petcov, JHEP **1208**, 125 (2012), arXiv:1205.4671 [hep-ph]

[214] V. Cirigliano, B. Grinstein, G. Isidori, and M. B. Wise, Nucl.Phys. **B728**, 121 (2005), arXiv:hep-ph/0507001 [hep-ph]

[215] D. Forero, S. Morisi, M. Tortola, and J. Valle, JHEP **1109**, 142 (2011), arXiv:1107.6009 [hep-ph]

[216] A. Ilakovac and A. Pilaftsis, Nucl.Phys. **B437**, 491 (1995), arXiv:hep-ph/9403398 [hep-ph]

[217] V. De Romeri and M. Hirsch(2012), arXiv:1209.3891 [hep-ph]

[218] P. Achard *et al.* (L3 Collaboration), Phys.Lett. **B517**, 67 (2001), arXiv:hep-ex/0107014 [hep-ex]

[219] M. Akrawy *et al.* (OPAL Collaboration), Phys.Lett. **B247**, 448 (1990)

[220] O. Adriani *et al.* (L3 Collaboration), Phys.Lett. **B295**, 371 (1992)

[221] P. Abreu *et al.* (DELPHI Collaboration), Z.Phys. **C74**, 57 (1997)

[222] G. Degrassi, S. Di Vita, J. Elias-Miro, J. R. Espinosa, G. F. Giudice, *et al.*, JHEP **1208**, 098 (2012), arXiv:1205.6497 [hep-ph]

[223] F. Bezrukov, M. Y. Kalmykov, B. A. Kniehl, and M. Shaposhnikov, JHEP **1210**, 140 (2012), arXiv:1205.2893 [hep-ph]

[224] S. Alekhin, A. Djouadi, and S. Moch, Phys.Lett. **B716**, 214 (2012), arXiv:1207.0980 [hep-ph]

[225] F. Jegerlehner and M. Y. Kalmykov, Nucl.Phys. **B676**, 365 (2004), arXiv:hep-ph/0308216 [hep-ph]

[226] K. Chetyrkin and M. Zoller, JHEP **1206**, 033 (2012), arXiv:1205.2892 [hep-ph]

[227] L. N. Mihaila, J. Salomon, and M. Steinhauser, Phys.Rev.Lett. **108**, 151602 (2012), arXiv:1201.5868 [hep-ph]

[228] A. Broncano, M. Gavela, and E. E. Jenkins, Nucl.Phys. **B705**, 269 (2005), arXiv:hep-ph/0406019 [hep-ph]

[229] G. 't Hooft and M. Veltman, Nucl.Phys. **B44**, 189 (1972)

[230] M. E. Peskin and D. V. Schroeder, *An Introduction to quantum field theory* (Perseus Books Publishing, L.L.C., 1995)

[231] W. Siegel, Phys.Lett. **B84**, 193 (1979)

[232] D. Stockinger, JHEP **0503**, 076 (2005), arXiv:hep-ph/0503129 [hep-ph]

[233] C. G. Callan, Jr., Phys.Rev. **D2**, 1541 (1970)

[234] K. Symanzik, Commun.Math.Phys. **18**, 227 (1970)

[235] J. Kersten, *Renormalization Group Evolution of Neutrino Masses* (Diploma Thesis, 2001)

[236] S. Khan, Nucl.Phys. **B864**, 38 (2012), arXiv:1203.5043 [hep-ph]

[237] B. Grzadkowski and M. Lindner, Phys.Lett. **B193**, 71 (1987)

[238] S. Antusch, *The Running of Neutrino Masses, Lepton Mixings and CP Phases* (PhD thesis, 2003)

[239] B. Schrempp and M. Wimmer, Prog.Part.Nucl.Phys. **37**, 1 (1996), arXiv:hep-ph/9606386 [hep-ph]

[240] A. Denner, H. Eck, O. Hahn, and J. Kublbeck, Nucl.Phys. **B387**, 467 (1992)

[241] G. Passarino and M. Veltman, Nucl.Phys. **B160**, 151 (1979)

[242] A. Denner, Fortsch.Phys. **41**, 307 (1993), arXiv:0709.1075 [hep-ph]

LIST OF PUBLICATIONS

A. Publications related to the thesis work

1. **"Vacuum Stability constraints on the minimal singlet TeV Seesaw Model"**
   Subrata Khan, Srubabati Goswami, Sourov Roy
   [arXiv:1212.3694 [hep-ph]]. SPIRES entry

2. **"Renormalization Group Evolution of the Non-Unitary operator"**
   Subrata Khan
   Nucl. Phys. B **864** (2012) 38 [arXiv:1203.5043 [hep-ph]]. SPIRES entry

3. **"Minimal Textures in Seesaw Mass Matrices and their low and high Energy Phenomenology"**
   Srubabati Goswami, Subrata Khan and Werner Rodejohann
   Phys. Lett. B **680** (2009) 255 [arXiv:0905.2739 [hep-ph]]. SPIRES entry

4. **"Hybrid textures in minimal seesaw mass matrices"**
   Srubabati Goswami, Subrata Khan and Atsushi Watanabe
   Phys. Lett. B **693** (2010) 249 [arXiv:0811.4744 [hep-ph]]. SPIRES entry

B. Publications attached with the thesis

1. **"Renormalization Group Evolution of the Non-Unitary operator"**

   Subrata Khan

   Nucl. Phys. B **864** (2012) 38 [arXiv:1203.5043 [hep-ph]]. SPIRES entry

2. **"Minimal Textures in Seesaw Mass Matrices and their low and high Energy Phenomenology"**

   Srubabati Goswami, Subrata Khan and Werner Rodejohann

   Phys. Lett. B **680** (2009) 255 [arXiv:0905.2739 [hep-ph]]. SPIRES entry